THE UNIVERSITY OF CHICAGO

THE ROLES OF MICROBE-DERIVED TRANSFER RNA MODIFICATIONS IN EUKARYOTIC CELL PHYSIOLOGY

A DISSERTATION SUBMITTED TO

THE FACULTY OF THE DIVISION OF THE BIOLOGICAL SCIENCES

AND THE PRITZKER SCHOOL OF MEDICINE

IN CANDIDACY FOR THE DEGREE OF

DOCTOR OF PHILOSOPHY

GRADUATE PROGRAM IN BIOCHEMISTRY AND MOLECULAR BIOPHYSICS

BY

OLIVIA NATALIA PURA ZBIHLEY

CHICAGO, ILLINOIS

AUGUST 2025

© Copyright 2025 Olivia Natalia Pura Zbihley

ALL RIGHTS RESERVED

Dedicated to my dear husband, Dr. Andrew Zbihley, whose unwavering faith, love, and support moves even the biggest of mountains.

To my incredible parents, my biggest role models, who instilled in me a deep sense of curiosity and love for learning.

To my four-legged best friend, Rigatoni, who has been at my side (or at my feet) from the first day of graduate school.

“You must always have faith in people.

And most importantly, you must always have faith in yourself.”

Elle Woods, *Legally Blonde*

Table of Contents

List of Figures

List of Tables

Abbreviations

ANG	angiogenin
BMDC	bone marrow-derived dendritic cell
bp	base pair(s)
cDNA	complementary DNA
CPM	counts per million
cyt	cytosol(ic)
D	dihydrouridine
DC	dendritic cell
DE	differential expression/differentially expressed
DFBS	dialyzed fetal bovine serum
DNA	deoxyribonucleic acid
eGFP	enhanced green fluorescent protein
eIF	eukaryotic translation initiation factor
f^5C	5-formylcytidine
FACS	fluorescence-activated cell sorting
FBS	fetal bovine serum
FC	fold-change
G	guanine
galQ	galactosyl-queuosine
gluQ	glutamyl-queuosine
GM-CSF	granulocyte-macrophage colony-stimulating factor

GO	gene ontology
i-tRF	internal tRNA fragment
KD	knockdown
LPS	lipopolysaccharide
$m^2{}_2G$	N^2,N^2-methylguanosine
m^5C	5-methylcytidine
manQ	mannosyl-queuosine
MHC	major histocompatibility complex
mRNA	messenger RNA
MSR-seq	multiplexed small RNA sequencing
mt	mitochondria(l)
mt-tRNA	mitochondrial tRNA
ncRNA	non-coding RNA
nt	nucleotide(s)
PCR	polymerase chain reaction
PEG	polyethylene glycol
PI	propidium iodide
$preQ_1$	pre-queuosine 1
pre-tRNA	precursor tRNA
q	queuine
Q	queuosine
QNG1	Q-nucleotide N-glycosylase 1

QTRT1	queuine tRNA-ribosyltransferase catalytic subunit 1
QTRT2	queuine tRNA-ribosyltransferase accessory subunit 2
RNA	ribonucleic acid
rRNA	ribosomal RNA
RT	reverse transcription
RT-qPCR	real-time & reverse transcription polymerase chain reaction
sncRNA	small non-coding RNA
snRNA	small nuclear RNA
TGT	tRNA guanine transglycosylase
tiRNA	tRNA-derived stress induced RNA; tRNA half
TLR	Toll-like receptor
tRF	tRNA-derived fragment
TRMT1	tRNA methyltransferase 1
TRMT1L	tRNA methyltransferase 1 like
tRNA	transfer RNA
tsRNA	tRNA-derived small RNA
UTR	untranslated region
Y RNA	Ro-associated Y RNA

Acknowledgments

First and foremost, I would like to thank my advisor, Professor Tao Pan! Tao is a most spirited and creative scientist, whose passion for biology was a driving force for my own. Tao challenged me to grow as a researcher while still empowering me to pursue professional opportunities and personal passions. I'm immeasurably grateful for your kindness, optimism, and mentorship.

I have been extremely fortunate to work alongside incredible people throughout graduate school. I would especially like to acknowledge Dr. Wen Zhang, who was my mentor when I first joined the lab. Thank you for patiently answering my many, many questions over the last several years. Many thanks to Dr. Marcus Foo, Dr. Yichen Hou, Dr. Sihao Huang, Dr. Noah Peña, Dr. Adam Wylder, Mahdi Assari, Brandon Chew, Luke Frietze, Dominika Rudzka, Marek Sobczyk, Amin Tork, and Allamanda Tran – my wonderful lab mates, past and present – for your kindness and camaraderie. Because of you, I will sincerely miss my time in the Pan lab (and our delightful wine clubs).

Many thanks to my collaborators for their contributions to this work. The Schneekloth lab generously shared their $preQ_1$ probe compounds, without which Chapter 5 would not have been possible. Thank you to the Chevrier lab for providing space, mentorship, and mice that enabled the BMDC experiments. I'm especially grateful to Kate Johnson for the scientific and moral support.

Thank you to my committee members – Prof. Joe Piccirilli, Prof. Chuan He, and Assistant Prof. Weixin Tang – for their insights, feedback, and support. Their thoughtful input has been invaluable throughout all stages of my projects.

I would be remiss not to thank my friends, as well as my colleagues from Nucleate, Graduate Council, and Portal Innovations. Thank you for making my graduate school experience all the more fun and vibrant.

Of course, I am profoundly grateful for my family. Thank you to my parents, Anna and Derek Pura, for all the sacrifices they made that afforded me the opportunity to pursue higher education. There aren't enough words (even in this dissertation) to thank you for your unconditional love and support. Thank you to my siblings – Kayah, Patrick, and Adah Pura – for bringing so much joy and laughter into my life. To my parents and brothers in-law – John, Teri, Christian, and John Luke Zbihley – thank you for cheering me on from over 400 miles away.

Last, but certainly not least, I would like to thank my husband, Dr. Andrew Zbihley, for his unrelenting belief in me. I couldn't have done this without you.

Abstract

Across all kingdoms of life, transfer ribonucleic acid (tRNA) is essential for translation of mRNA into protein. These adaptor molecules, comprising 75-95 nucleotides, decode mRNA codons via base pairing and carry the amino acid dictated by the genetic code to the ribosome. The typical tRNA adopts a cloverleaf secondary structure and an L-shaped tertiary structure. This conserved conformation enables tRNA to engage with both the mRNA codon and the ribosome during translation. In eukaryotic cells, tRNAs are both the most abundant and the most extensively modified cellular RNA species. Indeed, eukaryotic tRNAs carry an average of 13 modifications per cytosolic tRNA and an average of 5 modifications per mitochondrial tRNA. Over 100 different tRNA modifications have been described to date. Though diverse in chemical structure and location, modifications are broadly important in maintaining tRNA stability and fine-tuning translational dynamics.

A modification of particular interest is queuosine (Q), a hypermodified guanosine analog found at position 34 in the anticodon of cytosolic and mitochondrial tRNAs for asparagine, aspartic acid, histidine, and tyrosine. While bacteria can synthesize queuosine-tRNA (Q-tRNA) *de novo*, eukaryotes must import extracellular queuine (the corresponding nucleobase of Q nucleotide) sourced from the environment (i.e., gut microbiome or diet). Q-modification is implicated in modulating decoding accuracy and decoding speed of synonymous NAC/U codons. However, despite being discovered decades ago, the full biological significance of queuosine is still being actively explored.

In Chapter 2, we investigate the role of Q-modification on mammalian cell physiology using proliferation experiments and multiplex small RNA-seq (MSR-seq). We report that Q-modification promotes proliferation in both HEK293T cells and murine bone marrow-derived dendritic cells (BMDCs). In both cell types, we identify a novel correlative relationship between the Q and $m^2{}_2G$ (N^2,N^2-methylguanosine) modifications. Our mRNA-seq results show a cell-type-specific transcriptomic response to Q-modification levels. Using the same data, we propose a codon-usage-based mechanism underlying the Q-dependent changes in transcription and proliferation.

In Chapter 3, we study how $preQ_1$, a metabolic precursor of bacterial Q-tRNA, impacts HEK293T cells and BMDCs. We find that $preQ_1$ generally attenuates cell proliferation in a cell-cycle-independent manner, a phenotype that can be rescued by co-treatment with queuine. By conducting mRNA-seq, we also identify global changes to the BMDC transcriptome in response to $preQ_1$ treatment.

In Chapter 4, we focus on BMDCs and their cell-specific functions. Using flow cytometry, we demonstrate that both queuine and $preQ_1$ impact the expression of MHC-II, an immune response mediator.

Finally, in Chapter 5, we characterize two photoactivatable $preQ_1$ analog probes in mammalian cell culture. We find that the probes exhibit queuine-like bioactivity and are covalently inserted into Q-modifiable tRNAs. Moreover, we present preliminary RT-qPCR results revealing a potential role for $preQ_1$ and queuine in regulating mammalian histone mRNA levels. Together, this work sheds light on the functions of Q and its derivatives, underscoring their importance in eukaryotic cell physiology.

Chapter 1 – Introduction

1.1 Overview of Transfer RNA

Discovery and Characterization of tRNA

The discovery of transfer RNA (tRNA) was a pivotal moment in molecular biology that emerged from efforts to decipher the genetic code. In the 1950s, Francis Crick posed the "adaptor hypothesis", which postulated the existence of an "adaptor" molecule mediating the translation of nucleotide codons into amino acids.[1] The search for such an adaptor culminated in 1958, when Paul Zamecnik and Mahlon Hoagland identified the then-called "soluble RNA" responsible for carrying amino acids to the ribosome during protein synthesis.[2] In 1965, Robert W. Holley et al. determined the chemical structure (i.e., sequence) of the 77 nucleotide (nt) yeast $tRNA^{Ala}$.[3] As a result, tRNA was both the first non-coding RNA (ncRNA) to be discovered and the first nucleic acid to be sequenced. This was followed by the 1974 report by Kim et al. of the 3D x-ray crystallography structure of yeast $tRNA^{Phe}$.[4] Importantly, this foundational study revealed that tRNAs are not linear strings of nucleic acids; rather, they take on complex secondary and tertiary structures (**Figure 1.1**) essential for their roles as translation adaptors.

Today, we know that all tRNAs share a conserved canonical conformation, despite their sequence variability. The typical tRNA is 75-95 nt in length and adopts a cloverleaf secondary structure (**Figure 1.1A**) with four stems and four loops.[5] These structural features include (1) the acceptor stem, a base-paired stem at the 5' and 3' ends terminating in the 5'-CCA-3' tail sequence; (2) the D arm, named for the presence

of dihydrouridine (D) in the D loop; (3) the anticodon arm, which contains the anticodon triplet at positions 34-36; and (4) the TΨC (T) arm, named for the conserved sequence of 5-methylcytidine (m^5C)–pseudouridine (Ψ)–cytidine (C) in the T loop.[6] Many tRNAs also contain a variable loop between the anticodon and T stems. The length of the variable loop differs across tRNA species, in some cases forming a fifth stem.[5] A complete tRNA folds into a conserved L-shaped conformation (**Figure 1.1B**). Whereas tRNA secondary structure is driven by Watson-Crick (A:U; G:C) and G:U wobble base-pairing, stability of the L-shaped tertiary structure relies primarily on non-Watson-Crick interactions, such as magnesium ion coordination and hydrogen bonding networks between the D and T loops.[7]

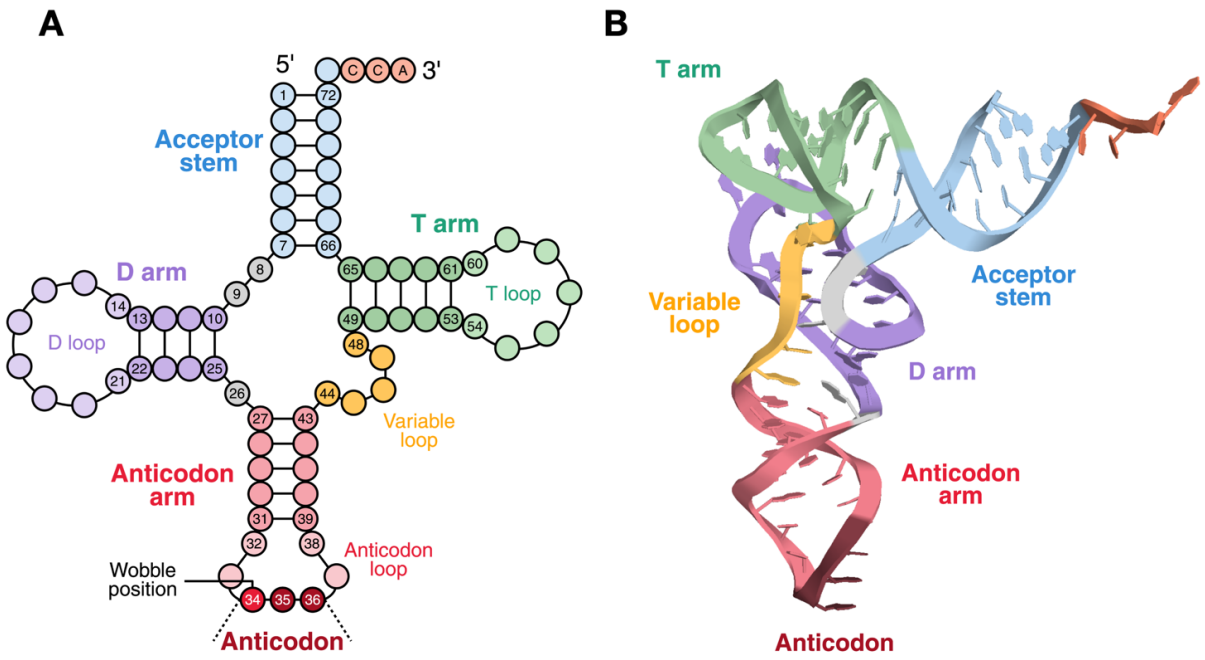

Figure 1.1: tRNA structure and standard residue nomenclature.

(A) tRNA cloverleaf showing conventional Watson-Crick base pairing in the stems, secondary structure features, and canonical position numbering.
(B) Tertiary structure of $tRNA^{Phe}$ (PDB ID: 4TNA) with regions colored as in (**A**).

tRNAs as Adaptors in Translation

Though the principle that structure dictates function is most associated with proteins, tRNA is a hallmark example of how this principle is applicable to nucleic acids, too. The L-shaped conformation enables the tRNA to act as a true adaptor molecule in translation, bridging the messenger RNA (mRNA) sequence to protein synthesis in the ribosome. First, the 3' end of tRNA is aminoacylated ("charged") with its cognate amino acid by the corresponding aminoacyl tRNA synthetase (aaRS). The aaRSs recognize both sequence and conformation of the tRNA to ensure fidelity between amino acid charging and tRNA anticodon triplet according to the genetic code.[9] The aminoacyl-tRNA (aa-tRNA) product is then delivered to the ribosome to take part in protein synthesis. While one end of the L (the acceptor stem with the 3' amino acid) protrudes into the peptidyl transferase center of the ribosome, the other end (the anticodon) simultaneously pairs with an mRNA codon triplet in the ribosome decoding center.[10] The cognate amino acid is then transferred to the growing peptide chain and the uncharged tRNA exits the ribosome. Translational accuracy is highly dependent on the L shape of tRNA, which is relatively sensitive to disruption – even subtle mutations or loss of modifications can destabilize tRNA structure and impair its function.[11,12] Given the cruciality of translation, it is unsurprising that tRNAs are among the most prevalent and highly-conserved RNA molecules.[13,14] In fact, humans cells each contain tens of millions of tRNA transcripts, making it the most abundant RNA (by copy number) among all cellular RNAs.[6]

In prokaryotes and eukaryotes, tRNAs facilitate the decoding of 61 codons into 20 proteinogenic amino acids. Eukaryotic genomes typically carry several hundred genes encoding tRNAs, resulting in extraordinary diversity among tRNAs in these organisms. So far, there are nearly 120,000 predicted tRNA genes across 155 available eukaryote genomes.[13] This multiplicity of tRNAs is organized into isoacceptor families and isodecoder variants.[15] Isoacceptors are tRNAs which carry the same amino acid but have different anticodon sequences (e.g., $tRNA^{Arg}ACG$ and $tRNA^{Arg}CCT$). Isodecoders, which exist within an isoacceptor family, are tRNAs which share the same anticodon but differ in other tRNA body nucleotides (e.g., $tRNA^{Arg}ACG$-1-1 and $tRNA^{Arg}ACG$-2-1). Both isoacceptor and isodecoder genes produce tRNAs that are functionally redundant in terms of genetic code translation.

The degeneracy of the genetic code and diversity of tRNAs are not just artifacts of evolution. Rather, they enable translational regulation through codon usage bias, or the preferential use of one synonymous codon over another. This phenomenon is ubiquitous across genomes, though codon usage varies by species and even between genes within an organism.[16,17] Synonymous codons differ in their translational efficiency, driven in part by the cellular availability of the corresponding tRNA isoacceptor family.[18] Codon usage plays multiple roles in regulating gene expression and protein folding through translation-dependent and translation-independent mechanisms. A prominent example is the mRNA “ramp” in *Saccharomyces cerevisiae* – a region at the 5’ end of mRNA comprising ~50 codons with lower translational efficiency – which slows ribosomes and functions as a late stage of translation initiation.[18] In 2010, another

example of codon usage bias was identified in *S. cerevisiae* by Cannarrozzi et al., who reported that repeated amino acids in a protein sequence are often encoded by the same codon, presumably to enhance translational efficiency.[19]

Despite the immense diversity of tRNA genes, most genomes contain fewer distinct tRNA isoacceptor families than there are codons. For example, the human reference genome encodes 429 high-confidence tRNA genes belonging to 49 isoacceptor families, which must read all 61 codons.[20] This gap is overcome by the phenomenon of wobble base pairing, first proposed by Francis Crick in 1956.[21] In an mRNA codon, the first two bases (corresponding to positions 36 and 35 in the tRNA anticodon) must adhere to canonical Watson-Crick base-pairing rules. However, the third codon base can engage in non-canonical "wobble" pairing with the tRNA base at position 34 ("wobble position"; **Figure 1.1A**).[22] This flexibility allows a single tRNA molecule to recognize and bind to multiple synonymous codons (e.g., GAA and GAG for Glu). Moreover, wobble pairing dynamics can be fine-tuned by tRNA anticodon loop modifications, particularly those at the wobble position, creating another important tRNA-based mechanism for translational regulation.[23] These and other tRNA modifications are discussed further in **1.2**.

Mitochondrial tRNAs

Cells of higher eukaryotes also contain a unique pool of mitochondrial tRNAs (mt-tRNAs) in addition to the cytosolic tRNAs encoded by the nuclear genome. The mammalian mitochondrial decoding rules deviate slightly from the canonical nuclear

genetic code: AUA for Met, UGA for Trp, and AGA/G for stop codons. Mitochondria contain hundreds to thousands of copies of mitochondrial DNA (mtDNA) which encode the mt-tRNA genes, a relic of their evolutionary origin as bacteria that were endocytosed by ancestral eukaryotic cells.[24] In humans, mtDNA is a circular, double-stranded DNA comprising 16,569 base pairs and encoding 22 mt-tRNAs for the 60 resultant sense codons.[25] To achieve decoding using only this minimum set of tRNAs, an unmodified uridine at the wobble position (U34) can read any of the four bases at the third codon position, a phenomenon known as four-way wobbling or superwobbling.[26] Consequently, a single tRNA can decode four codons that differ only in their third codon base. There are three notable exceptions to this rule. Firstly, mt-tRNA^{Met} contains a modified f^{5}C (5-formylcytidine) in the wobble position. The f^{5}C34 modification is unique to mammalian mitochondria and is required for decoding the non-canonical AUA and canonical AUG codons for Met.[27] Additionally, when amino acids are encoded by only two purine-ending codons, a modified uridine residue is required to prevent pairing with pyrimidines. Consequently, 5-taurinomethyluridine (τm^{5}U) is present at position 34 of mt-tRNAs for Leu and Trp, while its 2-thiouridine derivative (τm^{5}s^{2}U) is present at the same position in the mt-tRNAs for Lys, Glu, and Gln.

Human mt-tRNAs are shorter than nuclear-encoded tRNAs, ranging from 59-75 nt in length. This results in notable structural changes such as smaller stem and loop regions or even missing domains.[28] For example, the 59-nt mt-tRNA^{Ser}GCU entirely lacks the D arm.[29] Mitochondrial tRNAs are also less stable than their cytosolic counterparts, owing to their relatively A/U-rich sequences, and contain fewer modifications.[30] Indeed,

many pathologies are associated with mutations that exacerbate mt-tRNA instability, including mutations impacting modifications required for mt-tRNA folding.[31-34]

1.2 tRNA-derived Small RNA (tsRNA)

Biogenesis and Classification of tsRNAs

Although tRNAs are primarily recognized for their canonical role as amino acid carriers, it was relatively recently discovered that tRNAs could generate small RNA fragments through specific endonucleolytic cleavage events. The resulting tRNA-derived small RNAs (tsRNAs) were once dismissed as by-products of tRNA degradation.[35,36] Today, they are recognized as functionally active, highly regulated sncRNAs with diverse, non-canonical roles in gene expression, cellular homeostasis, and disease.[37]

tsRNAs are generated from either precursor tRNA (pre-tRNA) or mature tRNA and can be categorized as tRNA-derived fragments (tRFs) or tRNA-derived stress induced RNA (tiRNA) depending on their biogenesis and relative length (**Figure 1.2**). tRFs are approximately 14-45 nt long and are grouped into five major classes: tRF-1, tRF-2, tRF-3, tRF-5, and i-tRF.[36,38] tRNA genes are first transcribed as pre-tRNA which contain extra bases at the 5' end (leader sequence) and 3' end (trailer sequence). tRF-1 is produced by the cleavage of the 3' trailer sequence by RNase Z during tRNA maturation.[39] Along with tRF-1, two other tRF classes (tRF-3 and tRF-5) map to a terminal end of tRNA. These three classes have both a 5' phosphate and a 3' hydroxyl group which, in addition to their size, makes them notably alike to microRNA. The tRF-5 class originates from the 5' end of mature tRNA and relies on Dicer cleavage.[40] The tRF-5s are further categorized

into subclasses based on size: tRF-5a (14-16 nt), tRF-5b (22-24 nt), and tRF-5c (28-30 nt).[41] Conversely, the tRF-3 class originates from the 3' end of mature tRNA as the result of cleavage by Dicer or angiogenin (ANG) in the T loop. Most tRF-3s are either 18 nt (tRF-3a) or 22 nt (tRF-3b) in length and are grouped into subclasses as such.[41] The formation of tRF-2s, which contain the anticodon stem and loop, is induced by hypoxic conditions. This tRF class was initially characterized as YBX1-binding tumor suppressors in cancer, where hypoxic conditions are more prevalent.[42] Internal tRFs (i-tRFs) originate from anywhere in the body of a mature tRNA and are named by the origin of the 5' fragment end. Both tRF-2 and i-tRF may lack the 5' phosphate and 3' hydroxyl present in the other three tRF subclasses.[36]

On the other hand, tiRNAs, or tRNA halves, are 31-40 nt long and are formed by endonucleolytic cleavage in the anticodon loop of a mature tRNA.[36] Generation of tiRNAs is induced by cellular stress conditions such as heat shock, hypoxia, oxidative stress, amino acid deficiency, or viral infection.[43] However, tiRNAs can also be found in unstressed cells, and not all stress conditions trigger tRNA cleavage.[44,45] Although ANG is the primary endonuclease responsible for tiRNA formation, Su et al. (2019) demonstrated that other unidentified RNases also contribute to stress-induced tRNA cleavage.[46] The resulting tRNA halves contain a 5' hydroxyl rather than a 5' phosphate at the cleavage site, unlike the tRFs generated by Dicer. tiRNAs are further classified into 5'-tiRNAs and 3'-tiRNAs by whether they contain the sequence 5' or 3' of the endonuclease cleavage site, respectively (**Figure 1.2**).

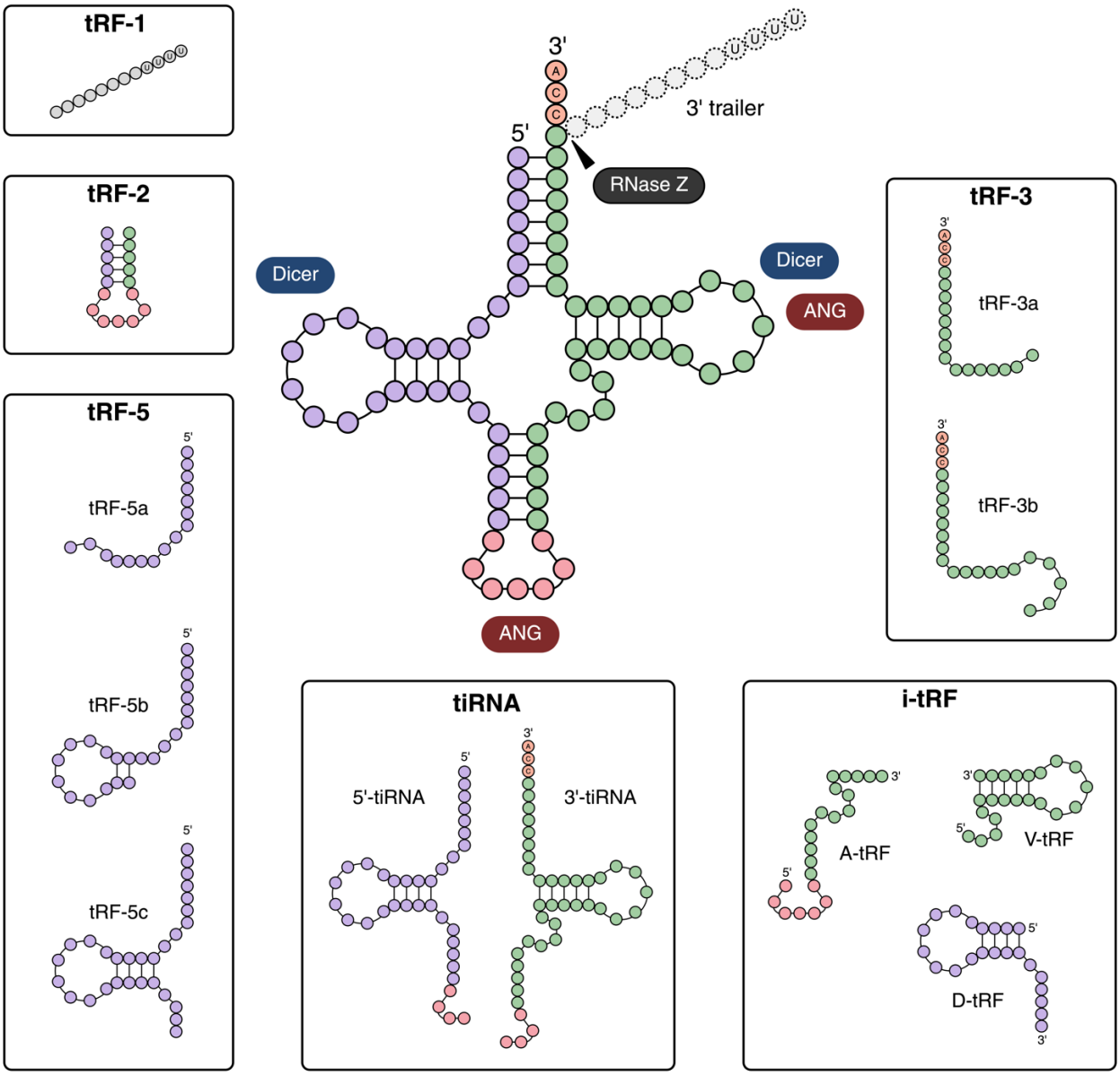

Figure 1.2: Classes of tsRNAs and key enzymes involved in their formation.

tRNA-derived small RNAs can be categorized based on the site(s) of endonucleolytic cleavage. tRF-1s are generated by cleavage of the 3' trailer by RNase Z; tRF-2s are the result of decomposition in hypoxic conditions; tRF-3s are produced primarily by Dicer or ANG cleavage in the T loop; tRF-5s are formed by Dicer cleavage; tiRNAs are largely generated by ANG cleavage in the anticodon loop; and the mechanisms of i-tRF formation are not well characterized. ANG: angiogenin, i-tRF: internal tRNA fragment, tiRNA: tRNA half, tRF: tRNA-derived fragment. Adapted from Kumar et al. (2016), Su et al. (2021), and Xie et al. (2020).[35,36,47]

Roles of tsRNAs in Eukaryotic Cell Physiology and Human Disease

Both tRFs and tiRNAs act as functional sncRNAs with diverse roles across cellular homeostasis, immunity, and disease. The role of tsRNAs as gene expression regulators has been well-established and is enacted through several pathways. For example, tRFs exhibit canonical miRNA-like activity and can suppress target gene expression by directly binding complementary sequences in the mRNA.[48,49] tRF-1s, tRF-3s, and tRF-5s also regulate mRNA expression through a non-canonical miRNA pathway by competitively binding to Argonaute (Ago) family proteins, a key component of RNA-induced silencing complexes, thereby affecting their silencing efficiency.[41,48] Of note, tRFs acting via one mechanism do not necessarily act via the other, pointing to the specificity of these interactions. For example, tRF-1^{Ser}TGA does not have a canonical miRNA-like gene silencing function but has been shown to bind Ago3 and Ago4.[50]

tiRNAs also act as gene expression regulators, particularly by suppressing translation in cellular stress conditions. Importantly, stress-induced production of tiRNAs does not significantly decrease steady-state levels of mature tRNAs.[46] Thus, tiRNA-mediated changes in translation are a direct result of their interactions with translational machinery, rather than of a diminished tRNA supply. Select 5'-tiRNAs from tRNA^{Ala} and tRNA^{Cys} contain conserved 5′-terminal oligoguanine (5′-TOG) motifs that promote the assembly of a RNA G-quadruplex (rG4) structure.[51] This bioactive rG4 structure competitively binds to eIF4G in the translation initiation complex, displacing it from the m^{7}GTP cap of mRNAs and inhibiting cap-dependent translation.[52] The translation of proteins mediated by internal ribosome entry sites, including those required for cell

survival and anti-apoptosis pathways, remains unaffected.[52,53] tiRNAs can also affect translation via direct interaction with the ribosome. For example, the mammalian 5'-tiRNA^{Pro} binds to the 18S rRNA of the 40S ribosomal subunit, causing ribosomal stalling and slowing translational elongation.[54] Beyond translational regulation, tiRNAs are involved in other stress response pathways. For example, the 5'-tiRNA rG4 structure binds YBX1 to promote the formation of stress granules, which are dynamic ribonucleoprotein complexes in the cytoplasm involved in stress response, in an eIF2α-independent manner.[55,56] Moreover, 3'-tiRNA and 5'-tiRNA species have been shown to associate with cytochrome C, inhibiting apoptosome formation and attenuating cell death signaling.[57,58]

Though they have important intracellular functions, tsRNAs are also involved in organism-wide immune regulation and are detectable in the bloodstream.[45] This is particularly true of 5'-tiRNAs, which form highly stable complexes in circulation. Blood levels of tsRNAs rapidly increase during the acute inflammatory stage, and baseline levels of 5'-tiRNAs are higher in hematopoietic and lymphoid systems than in other tissues.[59,60] Moreover, certain tsRNAs act as ligands for Toll-like receptors (TLRs), a family of pattern recognition receptors on the surface of some immune cells. For example, the 3'CCACCA sequence of tRNA^{Ala}UGC is recognized by TLR3[61] and the 5'-tiRNA^{His}GUG is recognized by TLR7[62]; both binding events promote innate immune responses. Moreover, a recent study found that T cell activation induced the selective release of tRFs in extracellular vesicles, suggesting a regulatory role of tRFs in adaptive immunity.[63]

Further, tsRNAs have been implicated in epigenetic inheritance. Published studies have shown that sperm acquire altered tsRNA profiles after a high-fat diet[64] or a low-protein diet[65] in mice, after fungicide exposure in rats,[66] or in obese humans.[67] The sperm tsRNAs are delivered to the zygote and can influence gene expression patterns in early embryos, contributing to the intergenerational transmission of environmental cues such as diet or metabolic stress.

Given their complex and extensive physiological roles, it is unsurprising that tsRNAs are increasingly implicated in a range of pathologies such as cancer, neurodegenerative diseases, viral infections, and metabolic disorders.[68,69] For example, tsRNA expression profiles are significantly altered in many cancers.[70] Some fragments promote tumorigenesis by modulating oncogene expression or by enhancing cell survival under hypoxic or oxidative stress.[71-74] Conversely, others act as tumor suppressors by inhibiting proliferation or inducing apoptosis.[75-77] In breast cancer, for instance, a subset of tRFs derived from $tRNA^{Glu}$, $tRNA^{Asp}$, $tRNA^{Gly}$, and $tRNA^{Tyr}$ disrupt oncogenic transcript stability by engaging in sequence-specific binding with YBX1, displacing the 3'UTRs of those transcripts.[42] These observations support the emerging view that tsRNAs influence disease progression in a context-dependent manner. Across disease areas, the stability, detectability, and clinical relevance of tsRNAs positions them as promising non-invasive biomarkers and potential therapeutic targets.[37,78,79] In fact, tRNA fragmentation profiles, in combination with abundance and modification information, have demonstrated utility as predictors of COVID-19 severity.[80]

1.3 tRNA Modifications

Overview of tRNA Modifications

For tRNAs and tsRNAs alike, posttranscriptional modifications are critical for structural and functional fidelity. Of the roughly 170 RNA modifications that have been described across all domains of life, about 80% were identified in tRNAs.[81] Indeed, eukaryotic tRNAs are the most extensively modified cellular RNA, with an average of 13 modifications per cytosolic tRNA and 5 modifications per mt-tRNA.[6] Known tRNA modifications have been reviewed extensively[6,82-84] and are cataloged in the MODOMICS database.[81] A selection of modifications identified since 2000 is found in **Table 1.1**.

In whole tRNAs, modifications present in the tRNA body (i.e., D arm, T arm, and variable loop) are required for proper folding, contribute to structural stability, and influence conformational rigidity.[85] A notable example is the m^1A58 (N^1-methyladenosine) modification, which is present in nearly all human tRNAs.[86,87] m^1A58 is required for the stability of initiator $tRNA^{Met}$ in yeast.[88] Several studies have found that the loss of a single tRNA body modification is sufficient to cause degradation of certain hypomodified tRNA species.[89-91] On the other hand, modifications at or near the anticodon are for translational fine-tuning. Wobble modifications can influence decoding by expanding or restricting wobble pairing with mRNA transcripts.[23] For example, mnm^5U34 (5-methylaminomethyluridine) or its 2-thiouridine derivative (mnm^5s^2U34) is required for decoding of synonymous codons AAA/G by $tRNA^{Lys}UUU$.[92] Wobble modifications are also the most diverse, with over 20 unique modifications identified in human tRNAs to date.[84] Position 37 is another modification hotspot in the anticodon loop, located 3'

adjacent to the anticodon. These modifications often ensure decoding accuracy and prevent frameshift mutations during translation.[93] Posttranscriptional modifications are also implicated in tsRNA biogenesis and bioactivity in a context-dependent manner. Some modifications – such as m^5C, queuosine, and 2'-O-methylation – confer resistance against ANG cleavage.[94] On the other hand, Ψ55 appears to facilitate tRF-5 formation for $tRNA^{Ala/Cys/Val}$,[95] whereas $m^2{}_2G26$ facilitates tRF formation for $tRNA^{Trp}$.[96]

tRNA Modification Dynamics

While some tRNA modifications are constitutive, many act as dynamic features that play key roles in stress response and development.[97] These changes are tightly regulated, demonstrated by the finding that different stressors result in agent-specific and dose-dependent shifts in tRNA modification profiles.[98] A prominent example is tRNA methylation, which is reversible through the enzymatic activity of "writers" (tRNA methylases) and "erasers" (tRNA demethylases). tRNA methylation fine-tunes translation and tsRNA biogenesis.[97] In humans, a tRNA has up to eight methylations,[81] and three erasers have been identified: ALKBH1,[99] ALKBH3,[58] and FTO.[100] Along with their unique functions, all three can demethylate m^1A58 in tRNAs. Crosstalk between modifications has also been reported. For example, m^5C38 on $tRNA^{Asp}$ is regulated by queuosine (Q), a wobble modification found on $tRNA^{Asn/Asp/His/Tyr}$. In *Schizosaccharomyces pombe*,[101] *Entamoeba histolytica*,[102] and human cells,[103] Q stimulated DNMT2-dependent m^5C38 methylation. The complex network of dynamic control and communication underscores the importance of tRNAs and their modifications in regulating cell physiology.

Modification	Relevant Enzyme(s)	Position(s)	Species	Function
acacp^{3}U	**AcpA** (N-acetyltransferase)	20B, 46, and 47	*V. cholerae*	tRNA structural stability[104]
ms^{2}C	damaged nucleoside of s^{2}C formed after methylating agent exposure; repaired by **AlkB**	32	tRNA^{Arg}CCG, tRNA^{Arg}ICG, tRNA^{Arg}UCU, and tRNA^{Ser}GCU of eubacteria	unknown[105]
τm^{5}U	**GTPBP3** (GTPbinding protein 3) complexes with **MTO1** (mitochondrial tRNA translation optimization 1)[106]	34	mt-tRNA in mammals	decoding accuracy of purine-ending codons; prevents misreading of pyrimidine-ending codons[107]
τm^{5}s^{2}U	**MTU1** (tRNA-specific 2-thiouridylase)[108]			
cnm^{5}U	unidentified	34	tRNA^{Ile} in haloarchaea and *M. maripaludis*	decoding accuracy[109]
mcmo^{5}Um	**TrmL** (2′-O-methyltransferase)	34	tRNA^{Ser1} in *Escherichia coli*	better UCG recognition than mcmo^{5}U[110]
cmnm^{5}ges^{2}U	**SelU** (2-selenouridine synthase)[111]	34	tRNA^{Gln}UUG in eubacteria	very hydrophobic; may impact frameshifting and codon bias[112]; low prevalence and are likely selenation intermediates.[111,113]
mnm^{5}ges^{2}U			tRNA^{Glu}UUC and tRNA^{Lys}UUU in eubacteria	
agm^{2}C	**TiaS** (tRNA^{Ile}-agm^{2}C synthetase)	34	tRNA^{Ile}AUA in archaea	promotes accurate decoding of AUA[114]
galQ	**QTGAL** (GT2 glycosyltransferase)	34	tRNA^{Tyr} in metazoans	translation optimization and proteostasis[115]
gluQ	**YadB** (a glutamyl-tRNA synthetase (GluRS) paralog)	34	tRNA^{Asp} in some eubacteria	unknown[116]
manQ	**QTMAN** (GT4 glycosyltransferase)	34	tRNA^{Asp} in metazoans	translation optimization and proteostasis[115]
ct^{6}A	**TcdA** (tRNA threonylcarbamoyladenosine dehydratase)	37	tRNA^{Lys} in fungi, planta, some bacteria, and some protists	facilitates decoding of the UAG stop codon[117]
ht^{6}A	unidentified	37	mt-tRNA^{Lys} of *M. nudus* (sea urchin)	prevents misreading of AAA codon, which encodes Asn in *M. nudus* mitochondria.[118]
ms^{2}ct^{6}A	**TcdA** and **MtaB** (methylthiotransferase)	37	*B. subtilis*, *T. brucei*, and plants	promotes decoding of adenosine-starting codons[119]
msms^{2}i^{6}A	**MiaB** (radical S-adenosylmethionine methylthiotransferase)	37	*E. coli*	hydrophobic; unknown function[120]
acp^{3}D	unidentified	47	tRNA^{Lys}UUU in *T. brucei*	unknown[121]
m^{1}s^{4}Ψ	involves **Pus10** (Igni_0342); **TrmY** (Igni_0291); **TtuA** (Igni_0707); **TtuB** (Igni_0506)	54	*I. hospitalis*	stability of tertiary fold in hyperthermic conditions[122]

Table 1.1: tRNA modifications and related enzymes discovered since 2000.

Table 1.1, continued.

This table includes tRNA modifications, related enzymes, and proposed biological functions (if known) that were identified in the twenty-first century.
acacp^{3}U: acetylated 3-(3-amino-3-carboxypropyl)uridine
ms^{2}C: 2-methylthiocytidine
τm^{5}U: 5-taurinomethyluridine
τm5s2U: 5-taurinomethyl-2-thiouridine
cnm5U: 5-cyanomethyluridine
mcmo5Um: 5-methoxycarbonylmethoxy-2′-O-methyluridine
cmnm^{5}ges^{2}U: 5-carboxymethylaminomethyl-2-geranylthiouridine
mnm^{5}ges^{2}U: 5-methylaminomethyl-2-geranylthiouridine
agm^{2}C: 2-agmatidinylcytidine
galQ: galactosyl-queuosine
gluQ: glutamyl-queuosine
manQ: mannosyl-queuosine
ht^{6}A: hydroxy-N^6-threonylcarbamoyladenosine
ct^{6}A: cyclic N^6-threonylcarbamoyladenosine
ms^{2}ct^{6}A: 2-methylthio cyclic N^6-threonylcarbamoyladenosine
msms^{2}i^{6}A: 2-methylthiomethylenethio-N^6-isopentenyladenosine
acp^{3}D: 3-(3-amino-3-carboxypropyl)-5,6-dihydrouridine
m^{1}s^{4}Ψ: 1-methyl-4-thiopseudouridine

1.4 The Queuosine Modification

Queuosine Structure and Bacterial Biogenesis

One of the most complex tRNA modifications is queuosine (Q), a guanosine analog with a 7-deazaguanine core bearing an amino-methyl side chain with a cyclopentanediol ring (**Figure 1.3A**).[123] The corresponding nucleobase is queuine (q). Q is a wobble modification found in tRNA families with a GUN anticodon (Asn/Asp/His/Tyr). Originally identified in *E. coli*,[124] has since been reported in many species of bacteria and eukaryotes but is absent from archaea, *Mycoplasma*, *S. cerevisiae*, and *Arabidopsis*.[125]

Though Q34 is highly conserved across kingdoms of life, its biogenesis varies between bacterial and eukaryotic systems. Bacteria synthesize Q-modification *de novo* through a series of eight enzymatic reactions occurring in two phases (**Figure 1.3B**).[8] The first phase converts guanosine triphosphate nucleoside (GTP) to the precursor base $preQ_1$ (7-aminomethyl-7-deazaguanine) via five enzymatic steps. GCH-I (GTP cyclohydrolase I) catalyzes the conversion of GTP to H_2NTP (7,8-dihydroneopterin triphosphate). QueD then converts H_2NTP into CPH_4 (6-carboxy-5,6,7,8-tetrahydropterin). Next, QueE synthesizes CDG (7-carboxy-7-deazaguanine) from CPH_4, releasing ammonia as the 7-deazaguanine core of Q is formed. The ATP-dependent QueC converts CDG into $preQ_0$ (7-cyano-7-deazaguanine) via an amide intermediate. Finally, QueF reduces the nitrile group, converting $preQ_0$ to $preQ_1$. In a base exchange reaction, bacterial tRNA guanine transglycosylase (TGT) removes guanine from position 34 of a substrate tRNA and inserts $preQ_1$ in its place, producing $preQ_1$-tRNA. In the second phase, the $preQ_1$ nucleotide is remodeled *in situ* via two final enzymatic steps.

First, QueA transfers the ribosyl group of S-adenosyl-L-methionine (SAM) to the amino group of $preQ_1$, producing oQ (epoxyqueuosine). As a final step, the cobalamin-dependent QueG reduces oQ to Q using an iron-sulfur cluster cofactor. In some bacteria, Q-$tRNA^{Asp}$ is further modified by the ATP-dependent YadB, which adds glutamate to the cyclopentanediol moiety of Q to form glutamyl-Q (gluQ) (**Figure 1.3A**).[116] Degradation of bacterial Q-tRNAs releases queuosine and its derivatives (i.e., queuine) as byproducts.

The last decade has seen several key advances in understanding bacterial Q biology. In 2017, Zallot et al. identified transmembrane protein YhhQ as a $preQ_0$/$preQ_1$ transporter, the first report of Q precursor salvage in bacteria.[126] That same year, *queH*, a family of genes encoding epoxyqueuosine reductase enzymes, was identified as the non-orthologous replacement for *queG*, which is absent in some bacterial genomes.[127] Like QueG, QueH catalyzes the reduction of oQ to Q but does not require cobalamin. In 2024, Adeleye and Yadavalli reported that the radical-SAM enzyme QueE moonlights as a cell division regulator in *E. coli* by interacting with FtsZ, a key cell division protein.[128] This interaction blocks division and causes filamentous growth. Recent work has also uncovered species-specific, alternative pathways for Q-tRNA biosynthesis. *Clostridium difficile*, a pathogenic bacterium of the gastrointestinal system, imports queuine and uses a queuine lyase CD1684, a member of the radical-SAM enzyme family, to convert it to $preQ_1$ *in vivo*.[129] *Chlamydia trachomatis*, an obligate intracellular bacterium, relies on YhhQ and TGT homologs with altered substrate specificities to salvage extracellular queuine that is directly inserted into substrate tRNAs.[129] Fascinatingly, this process mimics eukaryotic Q-tRNA biosynthesis, described below.

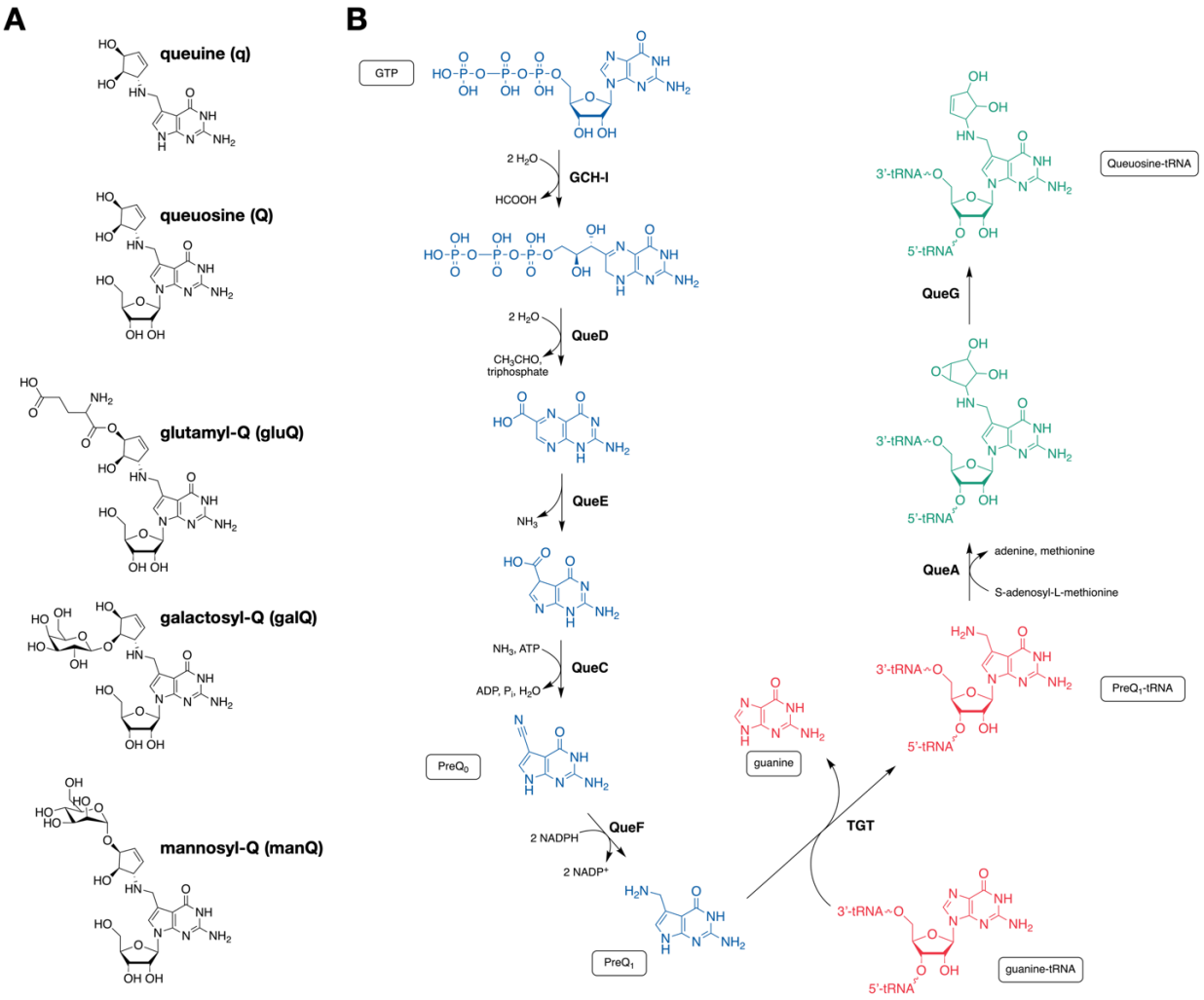

Figure 1.3: Chemical structures and bacterial biosynthesis of Q-tRNA.

(A) From top to bottom: chemical structures of queuine, queuosine, glutamyl-queuosine, galactosyl-queuosine, and mannosyl-queuosine.
(B) Bacterial biosynthesis pathway of Q-tRNA. First, GTP is modified through five enzymatic reactions to form preQ$_1$ (blue). TGT exchanges guanine for preQ$_1$ at position 34 of tRNAs for Asn, Asp, His, and Tyr (red). The resulting preQ$_1$-tRNA is modified in two final enzymatic steps to form Q-tRNA (green).

Eukaryotic Q-tRNA Biogenesis

Unlike bacteria, eukaryotes lack the cellular machinery to synthesize Q-tRNA *de novo*; instead, they rely on queuine acquired from the environment (i.e., gut microbiome or diet) to produce Q-tRNA (**Figure 1.4**).[8] Both queuine and queuosine are taken up through SLC35F2, the recently-identified selective q/Q importer. SLC35F2 is the sole transporter of Q (K_m = 174 nM) and believed to be one of two high-affinity transporters of q (K_m = 67 nM).[130] Intracellular queuine is exchanged for G34 of $tRNA^{Asn/Asp/His/Tyr}$ and mt-$tRNA^{Asn/Asp/His/Tyr}$ by the eukaryotic TGT homolog QTRT1/QTRT2 (queuine tRNA-ribosyltransferase 1 and 2) to produce Q-tRNA.[8] QTRT1/QTRT2 is a heterodimeric complex consisting of a catalytic subunit QTRT1 and a non-catalytic subunit QTRT2. QTRT1 recognizes the anticodon loop nucleotides $Y_{32}U_{33}G_{34}U_{35}$ (Y = C or U) and contains the active site for base exchange, while QTRT2 is required for tRNA binding.[131] Cytoplasmic QTRT1/QTRT2 localizes to the mitochondria via an unknown mechanism, and a portion is imported into mitochondria for modification of mt-$tRNA^{Asn/Asp/His/Tyr}$.[125]

A 2020 study by Zhang et al. revealed that QTRT1/QTRT2 does not modify each of the four tRNAs at the same rate; rather, there is a clear substrate hierarchy under experimental conditions such that $tRNA^{Asp}$ is modified most rapidly, followed by $tRNA^{His}$, then $tRNA^{Tyr}$, then $tRNA^{Asn}$.[132] This preference order (Asp > His > Tyr ≈ Asn) was observed under both high and limiting queuine conditions. Kinetic data indicate that $tRNA^{Asp}$ is queuosinylated ~10-fold faster than $tRNA^{Asn}$ under saturating queuine and ~4-fold faster than $tRNA^{Asn}$ at low queuine levels.[132] Nonetheless, QTRT1/QTRT2 exhibits stringent RNA substrate specificity for intact, properly folded $tRNA^{Asn/Asp/His/Tyr}$.[133] This is in contrast

to bacterial TGT which can act on minimal stem-loop RNA substrates.[131] However, QTRT1/QTRT2 has promiscuous nucleobase preference and can install a variety of exogenous 7-deazaguanine structures at position 34 of substrate tRNAs.[133]

After participating in translation, Q-tRNAs are eventually degraded, producing queuosine and queuosine-monophosphate (QMP) derivates (**Figure 1.4**). One of these nucleotide products, 5'-QMP, is the substrate for the queuine salvage enzyme QNG1.[134] QNG1 is a hydrolase which converts 5'-QMP to queuine, creating an intracellular supply of the nucleobase.[135]

In metazoans, Q34 in cytosolic $tRNA^{Tyr}$ and cytosolic $tRNA^{Asp}$ can be modified by recently-identified RNA glycosylases to form hypermodified residues. In $tRNA^{Tyr}$, Q34 is modified by QTGAL with galactose to form galactosyl-queuosine (galQ). In $tRNA^{Asp}$, Q34 is modified by QTMAN with mannose to form mannosyl-queuosine (manQ).[115] Kinetically, the glycosylation of Q-$tRNA^{Tyr}$ into galQ-$tRNA^{Tyr}$ proceeds at a rate comparable to Q insertion. On the other hand, the glycosylation of Q-$tRNA^{Asp}$ into manQ-$tRNA^{Asp}$ is relatively slow, which leads to an accumulation of unglycosylated Q-$tRNA^{Asp}$ intermediate in cells.[132]

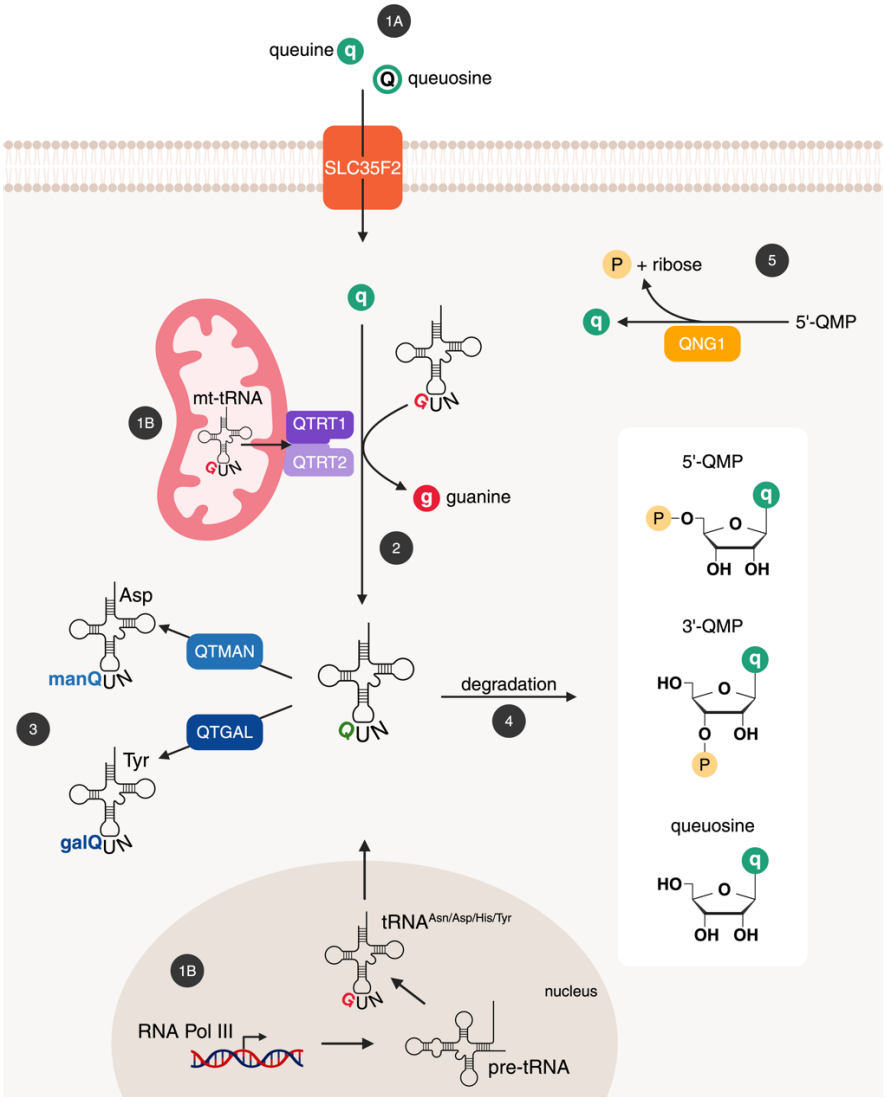

Figure 1.4: Eukaryotic Q-tRNA production and salvage.

Both queuine (q) and queuosine (Q) enter the cell via SLC35F2 (**1A**). $tRNA^{Asn/Asp/His/Tyr}$ and $mt\text{-}tRNA^{Asn/Asp/His/Tyr}$ are transcribed in the nucleus and mitochondria, respectively (**1B**). Queuine is exchanged for guanine at position 34 by the QTRT1/QTRT2 complex, producing Q-tRNA (**2**). In metazoans, the Q modifications of $Q\text{-}tRNA^{Asp}$ and $Q\text{-}tRNA^{Tyr}$ can be further glycosylated by QTMAN and QTGAL, respectively, to form manQ-tRNA and galQ-tRNA, respectively (**3**). Q-tRNAs are eventually degraded, producing a variety of queuosine derivatives (**4**). In a form of queuine salvage, QNG1 hydrolyzes 5'-QMP to produce free queuine intracellularly (**5**). gal: galactosyl, man: mannosyl, P: phosphate, Pol III: polymerase III, QMP: queuosine-monophosphate.

Diverse Roles of Eukaryotic Q-tRNA

Queuosine has been implicated in functions typical to that of a wobble modification: decoding accuracy, decoding speed (**Figure 1.5**), and tsRNA biogenesis.[136] Q34-modified tRNAs have expanded codon recognition compared to G34-tRNAs. Specifically, QUN codon recognition is expanded from NAC to NAC/U codons.[103] In $tRNA^{Asp}$ and $tRNA^{His}$, Q-modification decreases the decoding speed at cognate C-ending codons. Conversely, in $tRNA^{Asn}$ and $tRNA^{Tyr}$, Q-modification increases the decoding speed at cognate U-ending codons.[137] Importantly, the magnitude of the effect varies between species and even between cell types within a same species.[138] Queuosine glycosylation further impacts translational dynamics. The galactosylation of Q-$tRNA^{Tyr}$ was shown to slow stop codon read-through and slow decoding of the UAC codon but had little impact on UAU decoding. The mannosylation of Q-$tRNA^{Asp}$ slows decoding of both GAC/U codons. Of note, cells lacking Q-glycosylation exhibit increased protein aggregation, suggesting that Q-glycosylation is important for proteostasis by optimizing translational elongation speed.[125] Beyond translation, Q-modification has also been shown to protect $tRNA^{Asn}$ and $tRNA^{His}$ against ANG-mediated cleavage during oxidative stress.[139] Moreover, Q-modification is implicated in mitochondrial homeostasis, as knockout (KO) of QTRT1 or QTRT2 causes mitochondrial dysfunction, translational dysregulation, and mitochondrial metabolic pathway perturbations in HEK293T cells.[140]

At the organismal level, Q is not required for survival. Early work using germ-free mice on queuine-free diets did not report any obvious pathologies.[141,142] However, the nuanced physiological roles of queuosine have been elucidated through decades of

research. In a 2023 study, Cirzi et al. reported cognitive and memory aberrations in *Qtrt1* KO mice that were more pronounced in female mice.[143] This discovery was supplemented with ribosome profiling and proteomics data which revealed global perturbations to translation elongation speed and neuronal morphology, respectively, in the KO mice. Another study found that knockout of *qtgal* or *qtman* caused shortened body length in zebrafish, suggesting that Q-glycosylation is involved in post-embryonic growth in vertebrates.[115]

In humans, queuosine aberrations have been associated with neurodegenerative diseases,[144] cancer progression,[145] and inflammatory bowel disease (IBD).[146] In the case of IBD, downregulation of QTRT1 impairs cell junctions and intestinal barrier formation, causing intestinal inflammation. In colonoid cultures and an *in vivo* mouse model of IBD, queuine treatment reduced inflammation and protected against induced colitis. When considering the importance of the gut microbiome as a free queuine source, these data indicate an interconnectedness between host Q-modification, the intestinal microbiota, and host immune system.

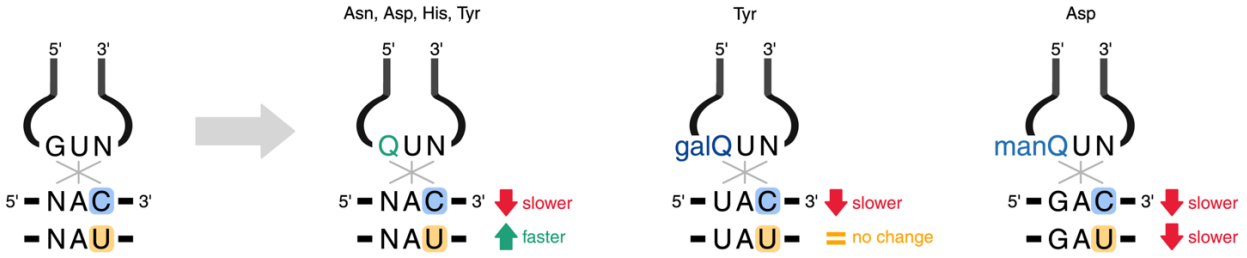

Figure 1.5: Q and its glycosylated derivates impact decoding speed.

Q modifications in $tRNA^{Asn/Asp/His/Tyr}$ generally reduce decoding speed of C-ending codons while enhancing decoding speed of U-ending codons relative to G34-tRNAs. In $tRNA^{Tyr}$, galQ slows UAC decoding but has minimal impact on UAU decoding. For $tRNA^{Asp}$, manQ slows decoding at both GAC and GAU codons. Adapted from Suzuki et al. (2025).[125]

1.5 Summary of Thesis Work: Mammalian Q and q

This dissertation aims to expand our understanding of queuine, queuosine, and related metabolites in the context of mammalian biology. To that end, three cell culture models were used: HEK293T cells, primary murine BMDCs; and HepG2 cells.

I first demonstrate that Q-modification is positively correlated with HEK293T and BMDC proliferation. Conversely, we find that $preQ_1$ treatment generally inhibits cell growth. Using propidium iodine staining, I show that $preQ_1$ slows proliferation via a cell-cycle-independent mechanism. Proliferation can be rescued by co-treatment with q, though sensitivity to both $preQ_1$ and q is cell-type-dependent. I follow up these results with MSR-seq analysis of the tRNAome in cells with low (0Q) and high (100Q) Q-modification and find an unexpected correlation between Q and $m^2{}_2G$ modifications. Additionally, using mRNA-seq, I identify cell-type-specific transcriptomic responses to q in HEK293T cells and BMDCs. I then conducted codon usage analysis of differentially expressed genes and find that C-ending codons are preferred over U-ending codons in 100Q cells, relative to 0Q cells, thereby driving translation of pro-proliferative transcripts.

Using flow cytometry, I find that MHC-II expression in BMDCs positively correlates with q but negatively correlates with $preQ_1$. These results, which identify novel relationships between Q-related metabolites and immune cell function, are in agreement with gene ontology results from our BMDC mRNA-seq data. Finally, I use crosslinking $preQ_1$ analog probes in HEK293T culture and report a binding interaction with histone mRNAs. Subsequent RT-qPCR of histone mRNAs in 0Q and 100Q cells revealed a Q-dependent effect on transcription in HepG2 cells but not HEK293T cells.

Chapter 2 – Mammalian queuosine tRNA modification influences fundamental cell physiology by altering codon usage bias

This chapter is derived from a manuscript published in the Journal of Molecular Biology on May 6th, 2025. The Authors are Olivia Zbihley, Kate Johnson, Luke Frietze, Wen Zhang, Marcus Foo, Hoang Anh Tran, Nicolas Chevrier, and Tao Pan. O.Z. and T.P. conceived the project and wrote the paper. O.Z. and K.J. performed BMDC cell and sequencing work under the guidance of N.C. O.Z. analyzed the sequencing data with assistance from L.F., W.Z., and M.F. H.T. performed HEK293T proliferation, mRNA-seq and biochemical characterization.

2.1 Introduction

Gene expression requires accurate decoding of mRNA, where each of the 61 codons is efficiently decoded by tRNAs in a context dependent manner. The flexibility of codon:anticodon interactions enables many tRNAs to decode more than one synonymous codon at varying efficiencies.[21] Post-transcriptional tRNA modifications play a critical role in fine-tuning translation dynamics, including through facilitation of codon usage.[83] tRNAs account for ~80% of known RNA modifications and are the most extensively modified cellular RNA, containing an average of ~13 modifications per molecule in eukaryotic cytosolic tRNAs and ~6 modifications in mitochondrial tRNAs (mt-tRNAs).[81,84] Various cells and tissues dynamically regulate tRNA abundance and modification status in response to stressors and environmental changes, affecting

translation speed, mRNA stability, and protein folding.[106,147,148] Modifications at or near the anticodon nucleotides are particularly impactful in decoding, ensuring translational efficiency and accuracy by stabilizing and modulating codon:anticodon interactions on the ribosome.[22,149]

One such tRNA modification is queuosine (Q), a hyper-modified guanosine analog consisting of a 7-deazaguanine core structure with an amino-methyl side chain and a cyclopentanediol moiety.[8] The corresponding nucleobase is termed queuine (q). Q is a wobble modification, occurring at position 34 (standard tRNA nomenclature) in four cytosolic and mitochondrial tRNA families of $tRNA^{Asn}$, $tRNA^{Asp}$, $tRNA^{His}$, and $tRNA^{Tyr}$. The Q-modified (Q-tRNAs) or their unmodified tRNAs (G-tRNAs) decode the synonymous NAU/NAC codons, where Q34/G34 pairs with C or U in the third codon position. Q plays a role in regulating mRNA decoding efficiency, promoting proper protein folding, protecting cognate tRNAs from ribonuclease cleavage, and affecting cellular tRF pools.[103,137,139,150] Q alters the codon reading preferences of endogenous tRNAs by increasing the decoding efficiency at certain codons, although the magnitude of this effect differs between organisms and among modified tRNAs within an organism.[151-153]

Though Q-modification is highly conserved across kingdoms, its biogenesis differs between bacteria and eukaryotes.[154] In bacteria, Q-tRNA is produced *de novo* through an eight-step biosynthetic pathway. First, several enzymatic reactions convert guanosine triphosphate (GTP) to $preQ_1$, a queuine precursor.[155,156] Bacterial tRNA guanine transglucosylase (TGT) facilitates the incorporation of $preQ_1$ into tRNA at position 34, where it is further modified to Q-tRNA.[127,156,157] Degradation of bacterial Q-

tRNAs releases queuine as a catabolic product. In eukaryotes, Q-tRNA is also produced via transglycosylation[131,158], but exclusively relies on the queuine sourced from diet or gut microbiome catabolism.[141,142,159] Queuine base is transported intracellularly by the recently-identified eukaryotic q/Q importer SLC35F2.[130] Additionally, queuine is made available through intracellular turnover of the Q nucleotide by the QNG1 enzyme.[134] Intracellular queuine is exchanged for guanine base in substrate tRNAs by the eukaryotic TGT homolog, QTRT1/QTRT2, producing Q34.[131,158] In vertebrates, Q-modified $tRNA^{Asp}$ and $tRNA^{Tyr}$ are further glycosylated with mannose and galactose, respectively, to form mannosyl-Q (manQ) and galactosyl-Q (galQ).[160,161] Glycosylated Q are involved in fine-tuning elongation speed, suppressing stop codon readthrough, and maintaining proteostasis.[115]

The physiological importance of Q has been described through decades of study. Initial research in germ-free mice on queuine-free diets showed that, under laboratory conditions, depletion of Q-modification does not result in obvious pathologies.[141,142] When fed a Tyr-deficient diet, however, these mice exhibited dramatic neurological abnormalities and died within three weeks. Remarkably, neurological function and viability were completely rescued simply by addition of queuine to the mouse diet.[162] Other work has implicated Q-modification in neuronal survival,[144] cognitive function,[143] virulence of resident gut microbes,[102] and cancer cell metabolism.[145] While it is not essential for life, it is becoming increasingly clear that Q-modification plays context-dependent roles across biological systems. Despite these exciting discoveries, the mechanisms through which Q elicits these effects remain incompletely elucidated. To

shed light on this question, we focused on a fundamental cellular process: growth and proliferation.

In this study, we investigated the role of Q-modification on cell proliferation in two mammalian cell systems: an immortalized human cell culture and primary, murine bone marrow dendritic cells (BMDCs). In both cases, elevated Q-tRNA modification levels enhanced cell proliferation. To understand the RNAome basis of this proliferation phenotype, we performed tRNA-seq and mRNA-seq, revealing a mechanistic underpinning at the RNA level. We found additional tRNA modification changes and mRNA codon preferences that are consistent with Q promoting proliferation through impacting translational dynamics.

2.2 Results

2.2.1 Q-tRNA levels elicit an effect on mammalian cell proliferation

To investigate the effect of Q-tRNA modification levels on cell proliferation, we generated cells that differed only in their Q-tRNA levels. The use of dialyzed fetal bovine serum (DFBS) in cell culture medium was shown to deplete Q-tRNA levels by limiting queuine availability.[163] Using this method, we generated human embryonic kidney 293T (HEK293T) cells of low Q-tRNA modification (termed 0Q cells hereafter) as described previously.[139] 0Q cells were plated in DFBS medium containing 0, 10, or 1000 nM queuine. We performed Northern blots after queuine reintroduction (**Figure 2.1A; Supplementary Figure S2.1A**) and confirmed Q-modification status at both 10 and 1000 nM queuine.[132]

We next examined the effects of Q-tRNA levels on cell proliferation using a CCK-8 assay (**Figure 2.1B**). 0Q HEK293T cells were grown in 0, 10, or 1000 nM queuine media. At Day 3, we observed an elevated cell count in queuine-supplemented cells when compared to 0Q cells. Although cell count was increased at both queuine concentrations tested here, the effect saturates at 10 nM queuine. This is in agreement with our Northern blot results, which show that Q-tRNA levels are also saturated at 10 nM queuine. Furthermore, upon QTRT1 knockdown, the proliferation rate of HEK293T cells is unchanged in response to queuine (**Supplementary Figure S2.1B**). This suggests that Q-tRNA levels, rather than just queuine itself, are involved in the pro-proliferative effect.

To investigate whether Q-tRNA could also affect proliferation of primary cells, rather than just immortalized cells such as HEK293T, we used murine bone marrow-derived dendritic cells (BMDCs). As above, 0Q BMDCs were generated by using DFBS in culture medium. 0Q cells were then grown in medium containing 0, 10, or 100 nM queuine for five days. Northern blot confirmed changes in Q-modification status (**Figure 2.1C; Supplementary Figure S2.1C**). In contrast with the HEK293T cells, in BMDCs we observe a mix of G- and Q-tRNA species at 10 nM queuine, and full Q-tRNA levels only at 100 nM queuine supplementation.

To evaluate cell proliferation, we cultured 0Q BMDCs in media supplemented with 0, 10, or 100 nM queuine, and measured live cell counts by flow cytometry every 24 hours for five days (**Figure 2.1D; Supplementary Figure S2.1D**). While there was no observed difference at 10 nM queuine supplementation, 100 nM queuine enhanced

proliferation compared to 0 nM queuine control. This is consistent with our Northern blot results where 10 nM queuine was insufficient for complete Q-modification in BMDCs.

Cells in later-stage apoptosis can sometimes be identified by morphological changes detectable by flow cytometry. Our analysis of BMDC morphology on Days 0 and 5 did not reveal any significant queuine-dependent changes (**Supplementary Figure S2.1D**). Nonetheless, reduction of apoptosis rate may also contribute to our reported pro-proliferative effect of Q-modification.

Taken together, these results show that Q-tRNA modification levels, through queuine supplementation, can have a positive effect on cell proliferation, albeit at a moderate magnitude. The culture medium queuine availability at which Q-tRNA levels saturate varies by cell type, with BMDCs requiring higher queuine concentrations to achieve full conversion to Q-tRNA. Likewise, the queuine supplementation required to achieve the proliferation effect differs among cell types.

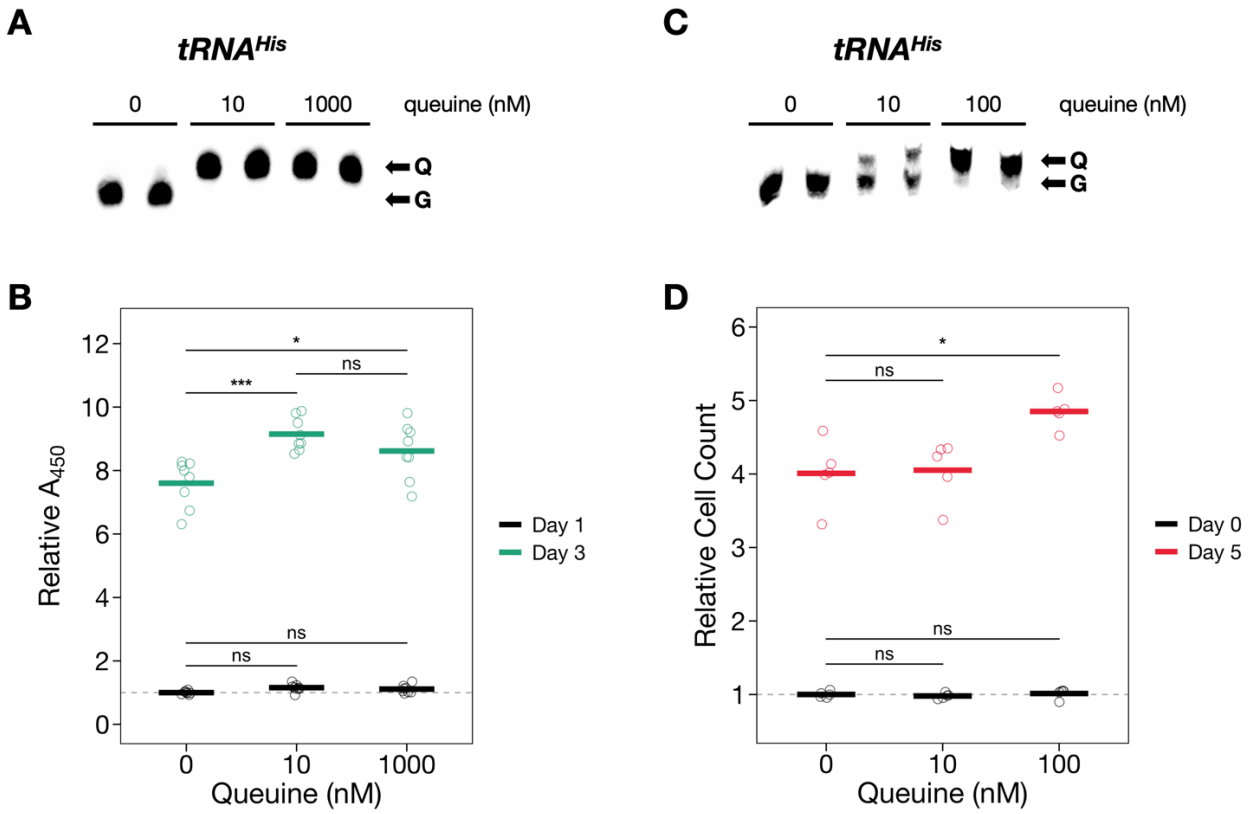

Figure 2.1: Proliferation rates of HEK293T and BMDC cultures are sensitive to Q-tRNA.

Adjusted *p*-values from Tukey's Honest Significant Difference (HSD) test are reported. ns: not significant, *: $p < 0.05$, **: $p < 0.01$, ***: $p < 0.001$.
(A) Northern blot of $tRNA^{His}$ in 0Q HEK293T cells grown in medium supplemented with 0, 10, or 1000 nM queuine, APB gel, biological duplicates. Total RNA was extracted from HEK293T cells 24 hours after queuine reintroduction. G: unmodified G34-tRNA, Q: Q-modified Q34-tRNA.
(B) HEK293T cell proliferation was assessed by CCK-8 assay, which reports absorbance at 450nm (A_{450}). Relative A_{450} for each well was calculated as the A_{450} divided by the mean A_{450} for 0 nM queuine at Day 1. Horizontal bars represent the group mean, while points correspond to individual wells. $n = 8$ biological replicates.
(C) Northern blot of $tRNA^{His}$ in 0Q BMDCs grown in medium supplemented with 0, 10, or 100 nM queuine, APB gel, biological duplicates. Total RNA was collected from BMDCs 5 days after retrieval from mouse and plating. G: unmodified G34-tRNA, Q: Q-modified Q34-tRNA.
(D) BMDC proliferation was measured by acquiring live cell count. Relative cell count for each well was calculated as the live cell count divided by the mean cell count for 0 nM queuine at Day 0. Bars represent the group mean, while points correspond to individual wells. $n = 5$ biological replicates.

2.2.2 Q-tRNA modification has additional effects on tRNA properties

To investigate the Q-tRNA modification effects on tRNA properties, we carried out multiplex small RNA sequencing (MSR-seq)[96] – which simultaneously reports tRNA abundance, modification, charging, and fragmentation – comparing HEK293T and BMDCs with and without queuine supplementation. Since comparative tRNA abundance, modification, charging, and fragmentation can be assessed at the same time, we describe their results for a comprehensive assessment on Q-modification effects.

We first confirmed Q-modification status by PAQS-seq,[164] which measures Q-modification of cytosolic and mitochondrial tRNAs through a change in the deletion signatures in sequencing reads (**Figure 2.2A,B; Supplementary Figure S2.2A,B**). As expected, both 100Q HEK293T cells and 100Q BMDCs show an increase in Q34 levels in all four Q-modified tRNA families. Given that the BMDCs were derived from mice with intact gut microbiomes and standard diets, it is expected that even the 0Q BMDCs will show residual levels of tRNA Q-modification, as we indeed observe (**Figure 2.2B; Supplementary Figure S2.2B**).

Q-tRNA modification did not significantly change the abundance of most full-length tRNA anticodon families (**Figure 2.2C,D**). In HEK293T cells, only $tRNA^{Asp}$ and $mt\text{-}tRNA^{Met}$ levels were elevated in 100Q cells (**Figure 2.2C**). In BMDCs, $tRNA^{Gln}$ levels were elevated in 100Q cells (**Figure 2.2D**). We also evaluated tRNA charging in 0Q and 100Q cells (**Figure 2.2E,F**). In HEK293T cells, tRNA charging levels are globally decreased in cytosolic tRNAs, but not mitochondrial tRNAs (**Figure 2.2E**). However, the observed

change in charging is quite small, with the difference in means being less than 1%. In BMDCs, neither cytosolic nor mitochondrial tRNA charging level was significantly altered overall when comparing 100Q and 0Q cells (**Figure 2.2F**). Interestingly, charging level changes in BMDC tRNA show a greater variability in mitochondrial tRNA species than cytosolic tRNA species (**Figure 2.2G**).

tRNA-derived fragments (tRFs) are a family of tRNA-derived small RNAs that regulate many aspects of gene expression.[28,69] We evaluated changes in tRF levels between 0Q and 100Q cells from the MSR-seq data (**Figure 2.2H,I; Table 2.1 and Table 2.2**). In our analysis, tRFs are stratified by whether their 3' ends are approximately in the anticodon stem-loop (30-40), variable loop and adjacent region (40-50), or the T loop (50-60).[165] In HEK293T cells, the Q-modifiable cyt-His-GTG-30-39 fragment is present in lower levels in 100Q cells versus 0Q cells (**Figure 2.2H; Table 2.1**), consistent with our previous reports.[139] Conversely, fragments levels from several tRNAs that do not contain Q-modification (GlnCUG, mt-TrpUCA, mt-CysGCA) are elevated in 100Q cells compared to 0Q cells. In BMDCs, we did not observe a decrease in cyt-His-GTG-30-39 fragment levels when comparing 100Q to 0Q cells (**Figure 2.2I; Table 2.2**). On the other hand, tRF levels were significantly elevated for several tRNA families including tRNAs of GluUUC, GlnCUG, GlnUUG, GlyUCC, eMet, ValCAC with the 3' ends near the variable loop (40-50) and tRNAs of ArgUCU, GlnCUG, GlyUCC, His, IleUAU, LeuAAG, eMet, and ValAAC with the 3' end near the T loop (50-60). For some tRNAs, their tRF abundance increase in 100Q cells may be related to their changes in other tRNA modifications (see below).

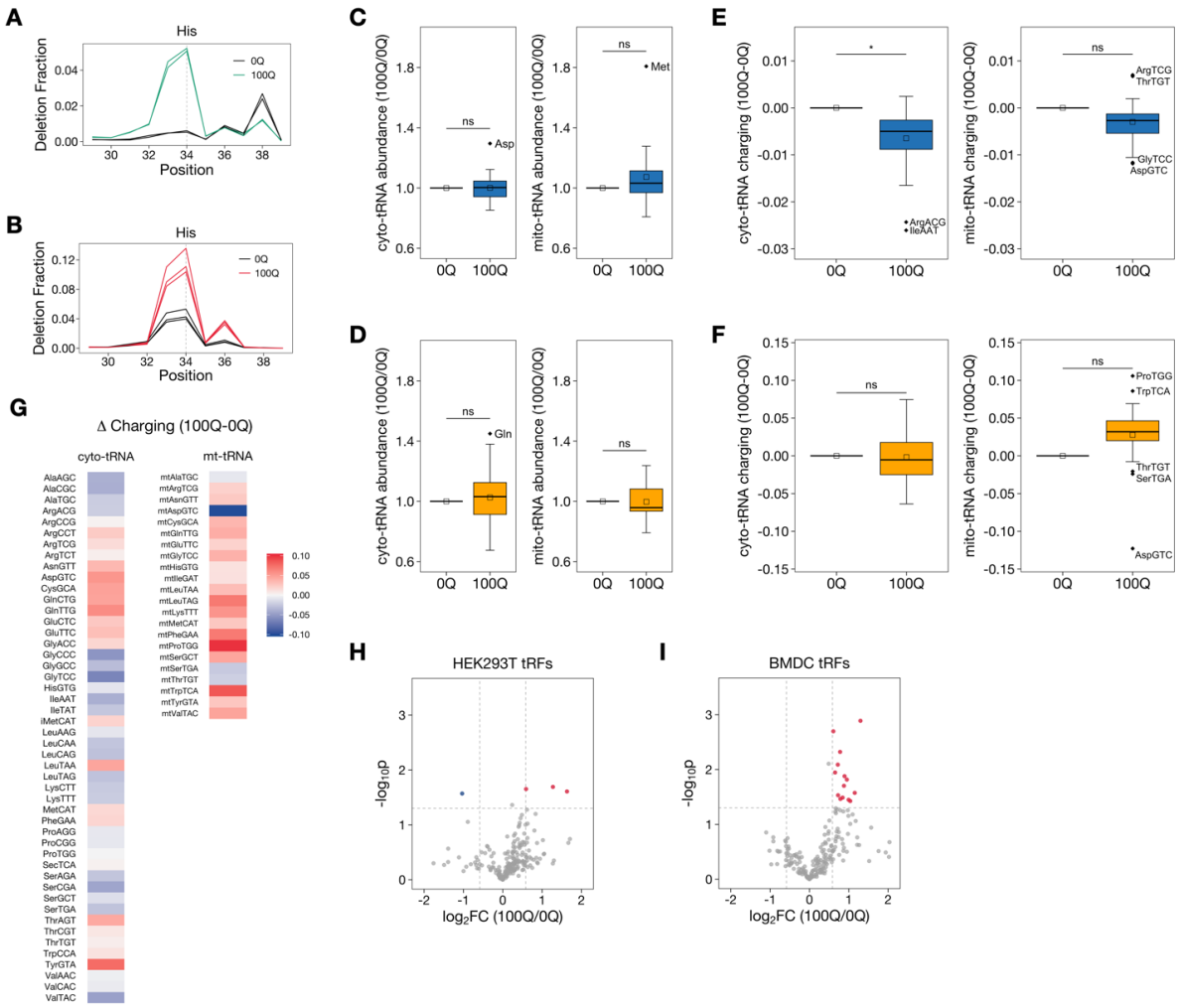

Figure 2.2: Q-modification levels impact global tRNA properties.

Welch's *t*-test was used to determine significance. ns: not significant, *: $p < 0.05$. For HEK293T, $n = 2$ replicates per condition. For BMDC, $n = 3$ replicates per condition.

(A-B) Deletion signature of $tRNA^{His}$ in (**A**) HEK293T cells and (**B**) BMDCs in the MSR-seq data. Regions shown are ±5 nucleotides (nt) to the Q34 residue (dashed line). Biological replicates are overlaid. Only the most abundant isodecoder of the $tRNA^{His}$ anticodon family is shown.

(C-D) Changes in abundance of cytosolic (left) and mitochondrial (right) tRNA species in (**C**) HEK293T cells and (**D**) BMDCs. Data are expressed as the relative change of anticodon family abundance compared to 0Q cells, using the mean of *n* replicates.

(E-F) Changes in charging levels of cytosolic (left) and mitochondrial (right) tRNA species in (**E**) HEK293T cells and (**F**) BMDCs. Data are expressed as the difference in charging levels compared to 0Q cells, using the mean of *n* replicates.

(G) Heatmap of changes in mouse BMDC tRNA charging levels. Data is expressed as the difference between the mean charging levels of *n* replicates for 100Q and 0Q samples. For cytosolic tRNA species (left), only the most abundant isodecoder of each tRNA anticodon family is shown.

(H-I) Volcano plot of tRNA fragment levels in 100Q vs. 0Q (**H**) HEK293T cells and (**I**) BMDCs. Detailed results are presented in **Supplementary Table S1** and **Supplementary Table S2**, respectively. The decrease in cyt-His-GTG-30-39 fragment in 100Q HEK293T cells is consistent with previous reports that Q-modification can be protective against tRNA cleavage at the anticodon loop. The previously reported change in tRF^{Asn} was not observed in MSR-seq because it is a 3' tRF.[139]

tRNA fragment	$\log_2$(FC)	-$\log_{10}$(*p*-value)
mt-Cys-GCA-50-59	1.633	1.608
mt-Trp-TCA-50-59	0.593	1.653
cyt-Gln-CTG-40-49	1.275	1.692
cyt-His-GTG-30-39	-1.033	1.571

Table 2.1: HEK293T tRNA fragmentation analysis results.

Fragment species with fold change (FC) > 1.5 and *p*-value < 0.05, corresponding to red and blue points in **Figure 2.2H**. cyt: cytosolic tRNA, mt: mitochondrial tRNA.

tRNA fragment	$\log_2$(FC)	-$\log_{10}$(*p*-value)
cyt-Met-CAT-50-59	1.037	1.426
cyt-His-GTG-50-59	0.995	1.448
cyt-Ile-TAT-50-59	0.787	1.464
cyt-Arg-TCT-50-59	0.844	1.488
cyt-Glu-TTC-40-49	0.728	1.531
cyt-Gln-CTG-50-59	1.151	1.575
cyt-Val-AAC-50-59	0.877	1.704
cyt-Gln-TTG-40-49	0.951	1.817
cyt-Gly-TCC-40-49	0.892	1.879
cyt-Leu-AAG-50-59	0.652	1.946
cyt-Val-CAC-40-49	0.721	2.090
cyt-Gly-TCC-50-59	0.779	2.322
cyt-Gln-CTG-40-49	0.607	2.698
cyt-Met-CAT-40-49	1.297	2.890

Table 2.2: BMDC tRNA fragmentation analysis results.

Fragment species with fold change (FC) > 1.5 and *p*-value < 0.05, corresponding to red points in **Figure 2.2I**. cyt: cytosolic tRNA, mt: mitochondrial tRNA.

2.2.3 m^2_2G modification is correlated with Q-modification

Unexpectedly, we observed a correlative effect between Q34 modification and m^2_2G (N^2,N^2-methylguanosine) modification (**Figure 2.3**). In eukaryotes, the m^2_2G modification is deposited by TRMT1 (tRNA methyltransferase 1) at position 26 in the structural hinge region between the D stem and anticodon stem.[166] TRMT1 methylates any tRNA bearing a G26 residue, meaning that over half of all tRNAs are modifiable by TRMT1.[167] Additionally, vertebrate genomes encode a TRMT1 paralog, TRMT1L (tRNA methyltransferase 1 like), which is known to install m^2_2G at position 27 of $tRNA^{Tyr}$.[168] Among the four Q-modified tRNAs, only $tRNA^{Asn}$ and $tRNA^{Tyr}$ contain m^2_2G.[86] The m^2_2G modification increases the structural rigidity and thermal stability of tRNA and is involved in accommodating the ribosome's conformational changes during translational elongation to promote translational efficiency.[6] At the cellular level, dynamic regulation of m^2_2G is required for redox homeostasis, and cells deficient in either writer enzyme become hypersensitize to oxidative stress.[98,168,169]

In HEK293T $tRNA^{Asn}$, m^2_2G is increased in 100Q cells for four of the five most abundant $tRNA^{Asn}$ isodecoders (**Figure 2.3A,B**). Changes in m^2_2G modification levels between 0Q and 100Q BMDCs are much more extensive, with widespread increases of m^2_2G in many tRNA isodecoders in 100Q cells (**Figure 2.3C,D**). tRNAs with m^2_2G increases include Q-modifiable $tRNA^{Tyr}$, but also non-Q-containing tRNAs of ArgACG, ArgUCG, eMet, Phe, ThrAGU, and Trp. In fact, the majority of m^2_2G-modifiable tRNA species are impacted by Q-modification levels (**Supplementary Figure S2.3A**). The

m^2_2G modification has been shown to enhance tRF biogenesis,[96] which may explain the elevated tRF levels in 100Q BMDCs described above (**Figure 2.2I**).

Despite the apparent correlation between Q and m^2_2G modifications in tRNA, mRNA levels for m^2_2G writers TRMT1 and TRMT1L were not sensitive to Q levels in either cell type from our mRNA-seq data (**Supplementary Figure S2.3B,C**). This suggests that Q and m^2_2G modifications are linked via other cellular mechanisms, rather than through direct modulation of *TRMT1* or *TRMT1L* expression. One possibility is that queuine itself acts as a signaling molecule for pathways regulating TRMT1 or TRMT1L activity, a paradigm which has been previously explored.[170]

Taken together, our results reveal that Q-modification impacts the tRNAome in context-dependent ways. While Q-modification did not significantly alter tRNA abundance or charging levels in either cell type, we identify a positive correlation between Q and m^2_2G modifications. The interplay between Q34 and other tRNA modifications may have functional implications for translational efficiency, particularly in the dynamic cellular environments such as those encountered by immune cells.

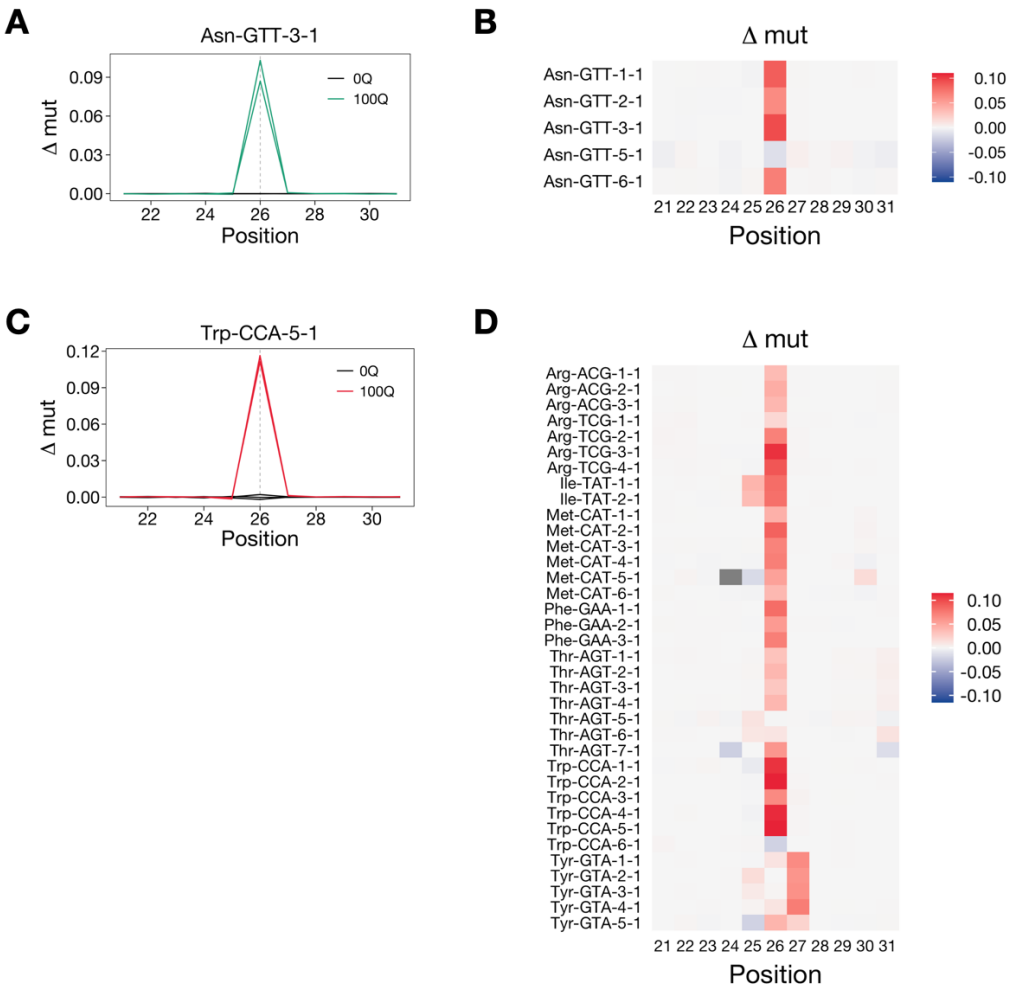

Figure 2.3: Q-modification levels impact other tRNA modifications.

$\Delta\, mut$ is calculated as the difference between the mutation rate of a sample in the MSR-seq data and the mean mutation rate of 0Q samples, where mutation rate is the frequency of mutations in sequence reads relative to the reference sequence at a given position. Regions shown are ±5 nucleotides (nt) to the G26 residue.

(A) $\Delta\, mut$ in Asn-GTT-3-1 corresponding to $m^2{}_2G26$ modification in HEK293T cells. The G26 residue is marked with a dashed line. Biological replicates (n = 2) are overlaid.

(B) Heatmap of $\Delta\, mut$ in 100Q HEK293T cells near position 26 of the five most abundant cytosolic Asn-GTT isodecoders, corresponding to the $m^2{}_2G26$ modification. Data shown is the mean $\Delta\, mut$ (100Q-0Q) of n = 2 replicates per condition.

(C) $\Delta\, mut$ in Trp-CCA-5-1 corresponding to $m^2{}_2G26$ modification in murine BMDCs. The G26 residue is marked with a dashed line. Biological replicates (n = 3) are overlaid.

(D) Heatmap of $\Delta\, mut$ in 100Q BMDCs near position 26 of select cytosolic tRNA isodecoders, corresponding to the $m^2{}_2G26$ modification. Data shown is the mean $\Delta\, mut$ (100Q-0Q) of n = 3 replicates per condition.

2.2.4 Q-modification modulates gene expression in a codon-dependent manner

We next carried out mRNA-seq to evaluate transcriptomic changes in 100Q versus 0Q cells (**Figure 2.4; Supplementary Figure S2.4A**). In HEK293T cells, we identified 97 gene transcripts that are upregulated and 76 gene transcripts that are downregulated (**Figure 2.4A**). Gene ontology (GO) analysis revealed that genes upregulated in 100Q cells were associated with amine catabolic processes and ion transport and signaling (**Figure 2.4B**). Codon usage analysis of the differentially expressed genes shows that high Q-modification was associated with a preference for C-ending codons in general, including those of the four amino acids decoded by the Q-modified tRNAs (Asn/Asp/His/Tyr, **Figure 2.4C**).

In BMDCs, we identified 130 gene transcripts that are upregulated and 71 gene transcripts that are downregulated (**Figure 2.4D**). GO analysis of upregulated genes revealed significant enrichment in immune-related biological processes (**Figure 2.4E**). Notably, upregulated genes were involved in leukocyte proliferation, supporting our observation that 100Q BMDCs proliferate more rapidly than 0Q BMDCs. Several genes relating to “production of molecular mediator of immune response” were upregulated. Processes related to immunoglobulins and immune receptor diversification were also enriched, indicating potential impacts on immune response and adaptation. Codon usage analysis of the differentially expressed genes again reveals a general preference for C-ending codons in 100Q BMDCs, including those for Q-tRNA decoded codons of Asp, Tyr, and His (**Figure 2.4F**). Taken together, our results indicate that Q-modification

likely plays a role in murine DC immune response functions at the translational level through decoding codon bias.

We took a closer look at changes in mRNA levels (in counts per million, CPM) of several genes important for Q-tRNA modification: *SLC35F2* (q/Q importer), *QNG1* (queuine salvage protein), *QTRT1* and *QTRT2* (catalytic and non-catalytic subunits, respectively, of the Q writer complex). No queuine-dependent change in expression is observed for these genes in either cell type (**Supplementary Figure S2.4B,C**). For BMDCs, *SLC35F2* mRNA expression was below the detectable level. We evaluated expression changes for the three most highly-expressed *SLC35* family genes – *SLC35A1*, *SLC35B1*, and *SLC35F6* – and found no queuine-dependent response (**Supplementary Figure S2.4C**). We do find that *QNG1, QTRT1*, and *QTRT2* CPM values are approximately 5-fold lower in BMDCs than in HEK293T cells. This result is consistent with BMDCs having lower tRNA Q-modification levels at 10 nM queuine (**Figure 2.1A,C**) and requiring higher queuine supplementation to obtain the same effect on cell proliferation (**Figure 2.1B,D**) when compared to HEK293T cells.

It is well established that Q-modification equalizes the decoding of U- with C-ending codons, whereas unmodified G-tRNAs prefer C- over U-ending codons.[103,136,143,150] We were therefore surprised to find that in both HEK923T cells and BMDCs, 100Q cells exhibit bias towards C-ending codons in the up- over down-regulated mRNA transcripts. Cell proliferation requires high levels of translation of house-keeping genes such as those encoding ribosomal proteins. In both human and mouse transcriptomes, these mRNAs are highly enriched in C-ending over U-ending codons

(**Figure 2.4G,H**), including the codons for all 4 amino acids decoded by Q-modified tRNAs. To reconcile these results, a plausible explanation is that Q-modified tRNA may remain more efficient in decoding C-ending codons than their corresponding unmodified tRNAs, while still equalizing the decoding of U- and C-ending codons. This idea is reminiscent of galQ and manQ modifications further balancing the decoding of C-ending codons to optimize translation,[115] and of a previously proposed role of Q-modification in Drosophilidae genome reprogramming.[171] Increased proliferation of 100Q cells is then associated with their increased efficiency in translating the highly biased C-ending codons in ribosomal protein genes.

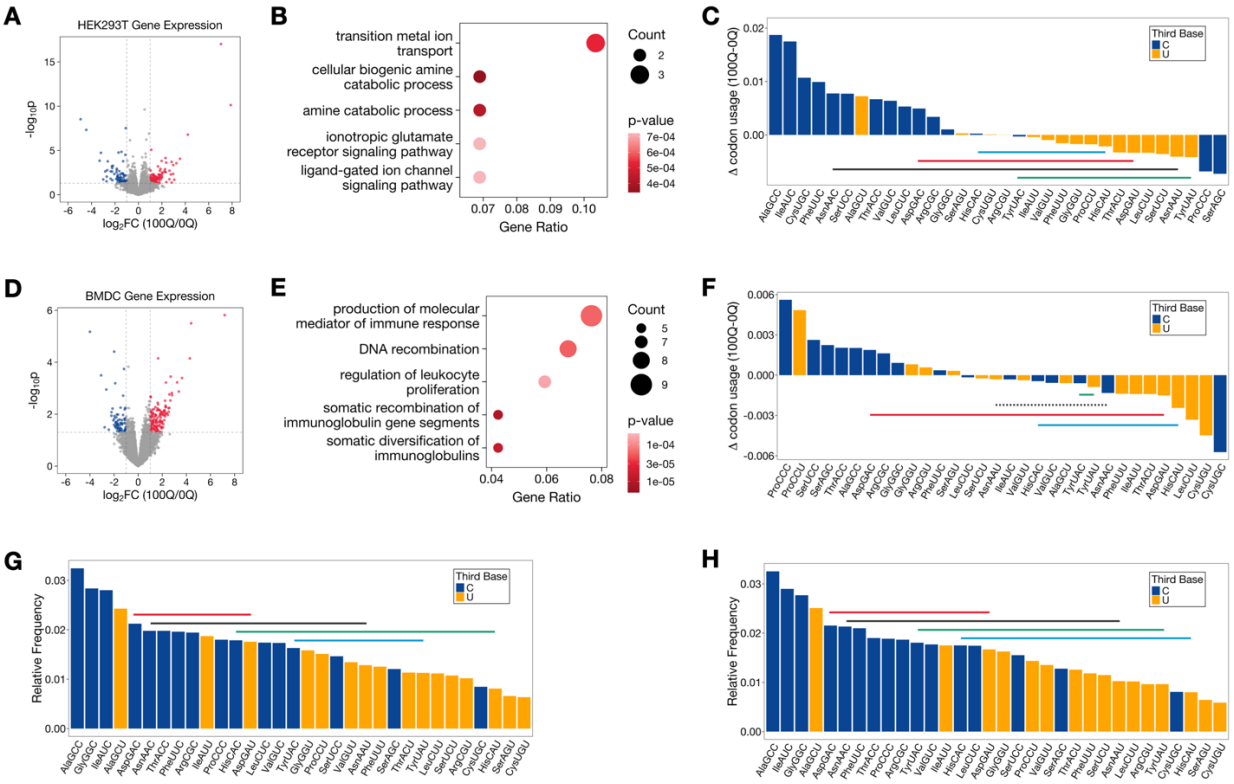

Figure 2.4: Q-modification levels impact human and mouse transcriptomes.

For Fig. 4C,F-H; horizontal lines connect synonymous codons read by Q-modified tRNAs (grey – AsnAAC/U; red – AspGAC/U; blue – HisCAC/U; green - TyrUAC/U).
(A) Volcano plot of differential expression (DE) analysis in 100Q vs. 0Q HEK293T cells. Upregulated genes (*n* = 97) are shown in red; downregulated genes (*n* = 76) are in blue.
(B) Gene ontology (GO) analysis of transcripts upregulated in 100Q vs. 0Q HEK293T cells. The top 5 GO terms are displayed.
(C) Changes in codon usage in DE genes in 100Q vs. 0Q HEK293T cells.
(D) Volcano plot of DE analysis in 100Q vs. 0Q mouse BMDCs. Upregulated genes (*n* = 130) are shown in red; downregulated genes (*n* = 71) are in blue.
(E) GO analysis of transcripts upregulated in 100Q vs. 0Q mouse BMDCs. The top 5 GO terms are displayed.
(F) Changes in codon usage in DE genes in 100Q vs. 0Q mouse BMDCs. Dashed line represents a cognate codon pair that does not follow the observed codon preference trend.
(G-H) Relative codon usage of transcripts encoding ribosomal proteins in (**G**) human and (**H**) mouse transcriptomes.

2.3 Discussion

In this work, we provide insights into the role of Q-tRNA modification in mammalian cell physiology. We show that Q34 exhibits a pro-proliferative effect in both HEK293T cells and murine BMDCs and, using a multi-transcriptomics approach, propose a mechanistic hypothesis by which this tRNA modification can enhance the production of ribosomal proteins in a codon-dependent manner.

In both our proliferation studies and Northern blots, it is apparent that HEK293T cells and BMDCs differ in their sensitivity to queuine. For example, 10 nM queuine supplementation is sufficient to saturate Q-tRNA levels in HEK293T cells, but not in BMDCs. This may be explained, in part, by the fact that *QNG1*, *QTRT1*, and *QTRT2* mRNA levels (in CPM) were substantially lower in BMDCs than in HEK293T cells. Consequently, the efficiencies of pathways required for Q salvage and Q-tRNA formation likely vary between these two cell types.

We also identify a positive correlation between Q34 and $m^2{}_2G$ modifications for many tRNA isodecoders, including those that are not Q-modifiable. mRNA expression for both $m^2{}_2G$ writers is unchanged, however, when comparing 0Q and 100Q cells, suggesting an alternative mechanism through which these two modifications are linked. Queuine has been previously shown to promote antioxidant defense systems in cancer via modulation of enzymatic activity.[170] Likewise, it is established that dynamic modulation of $m^2{}_2G$ levels is important for regulation of oxidative stress in cells.[98,168,169] Perhaps, then, it is through cellular redox homeostasis pathways that these two tRNA modifications are connected.

Our mRNA-seq data identifies global gene expression changes in response to Q-modification levels, albeit in a cell-dependent manner. While 100Q HEK293T cells upregulate genes involved in ion transport and ion receptor signaling pathways, 100Q BMDCs upregulate genes involved in immune response mediators and proliferation. To better understand the differing transcriptomic responses, we conducted a codon usage analysis in up- and down-regulated genes. Our analyses reveal that, in both cell types, changes in the transcriptome may be driven by Q-induced biases in codon preference. For both HEK293T cells and BMDCs, high Q-modification levels result in a preference for C-ending codons, presenting a plausible mechanism underpinning the observed gene expression changes. A similar effect has been reported in *Schizosaccharomyces pombe*, where Q-modifications enhanced decoding speed for NAC codons more so than NAU codons.[137]

Our results illuminate a surprising relationship between Q and $m^2{}_2G$ tRNA modifications and provide a codon-based mechanism for observed proliferative changes. Importantly, this work underscores the context-dependence of Q-tRNA's impact on a biological system, highlighting the value in continued study of this fascinating modification.

2.4 Materials and Methods

HEK293T Cell Culture and RNA Extraction

Both 0Q and 100Q human embryonic kidney HEK293T cells were obtained as previously reported.[139,163] Briefly, HEK293T cells (ATCC, CRL-11268) were cultured at

37°C in Dulbecco's modified Eagle's medium (DMEM) (Cytiva; SH30022.01) supplemented with 10% volume/volume (v/v) dialyzed fetal bovine serum (Gibco; 26400044) and 1% v/v Penicillin-Streptomycin (Thermo Fisher; 15070063) to 80% confluency. 100Q cells were obtained by culturing 0Q cells with 1 μM queuine (Toronto Research Chemicals) for 24 hours. TRIzol™ reagent (Thermo Fisher; 15596026) was used to extract total RNA according to the manufacturer's manual.

HEK293T Proliferation Assay

0Q HEK293T cells were plated at 5×10^3 cells/well in a tissue culture treated 96-well plate (Dot Scientific; 667195) in 100 μL of DMEM as described above. Appropriate volumes of queuine were added to achieve the 4 treatment conditions (0, 1, 10, and 1000 nM queuine) with 8 replicates each. Four 96-well plates were prepared – one per measurement time point (0, 1, 2, and 3 days).

HEK293T cell proliferation was measured using the Cell Counting Kit-8 (CCK-8) (Dojindo; CK04-13) according to manufacturer protocol. Briefly, immediately after plating, 10 μL of WST-8 solution was added to each well of the Day 0 plate. The plate was wrapped in aluminum foil and incubated at 37°C for 2 hours. Following incubation, absorbance at 450 nm was measured using a microplate reader to assess cell viability. WST-8 addition, incubation, and absorbance measurement steps were repeated every 24 hours using the corresponding plate.

The data were visualized using R. One-way analysis of variance (ANOVA) was performed to assess differences in treatment conditions. Tukey's Honest Significant Difference (HSD) post-hoc test was applied to assess pairwise comparisons between

treatments when ANOVA indicated statistical significance ($p < 0.05$). Adjusted *p*-values from the Tukey test are reported, and significance levels were annotated on the plots as follows: $p < 0.05$ (*), $p < 0.01$ (**), and $p < 0.001$ (***).

HEK293T QTRT1 Stable Knockdown Cell Line

QTRT1 and Control shRNA (shCtrl) lentiviral particles were obtained from Santa Cruz Biotechnology and used to generate a QTRT1 stable knockdown (QTRT1 KD) cell line per manufacturer protocol. Briefly, 1×10^5 HEK293T 0Q cells were plated into a 12-well plate. After 24 hours of incubation, the medium was replaced with complete medium containing 8 µg/mL polybrene (Santa Cruz; CAS 28728-55-4). Lentiviral particles were thawed at room temperature and used promptly. QTRT1 or shCtrl lentiviral particles were added to each well to infect the cells at Multiplicity of Infection (MOI) = 1, 5, and 10. The infected cells were incubated for 48-72 hours. Then, the culture medium was replaced with complete DMEM containing 5 µg/mL puromycin (Santa Cruz; CAS 58-58-2) to select stable clones expressing the shRNAs. For several days, the transduced cells were continuously incubated with medium containing puromycin. Cells were split 1:3–1:5 as necessary until cells without virus transduction were completely absent. Stable knockdown cells were harvested and stocked after sufficient expansion.

Proliferation assays were performed as described above using 0Q QTRT1 KD and 0Q shCtrl cells under 0 nM and 10 nM queuine supplementation conditions.

Western Blot

Cell lysates were collected from shCtrl and QTRT1 KD HEK293T cells using CelLytic™ M buffer (Millipore Sigma; C2978) with protease inhibitor. Samples were

prepared by incubating 50 µg lysate with loading buffer (Thermo Fisher; NP0007) and 50 mM DTT at 95°C for 10 minutes. Samples were separated on 4–12% polyacrylamide Bis-Tris protein gels (Invitrogen; NP0322BOX) along with protein ladder (Bio-Rad, 161-0376) and transferred to polyvinylidene fluoride membranes (Millipore Sigma; IPVH00010). The membranes were blocked in 5% w/v milk (Bio-Rad; 1706404) in PBST (1× PBS with 0.05% Tween-20) before probing with 1/200 v/v QTRT1 antibody (Santa Cruz; sc-398918) or 1/200 v/v GAPDH antibody (Santa Cruz; sc-47724). The blots were visualized with ECL Prime Western Blotting Detection Reagents (Amersham; RPN2232) using a Bio-Rad Chemi-Doc MP.

Mice

Female C57BL/6J mice were obtained from Jackson Laboratories. Mice were housed under specific pathogen-free and BSL2 conditions at the University of Chicago. All experiments were conducted following the guidelines set by the US National Institutes of Health Guide for the Care and Use of Laboratory Animals and were approved by the Institutional Animal Care and Use Committee at the University of Chicago.

BMDC Cell Culture

Murine BMDCs were generated from 6-8 week-old C57BL/6J female mice. Bone marrow cells were collected from femora and tibiae and cultured at 37°C in RPMI-1640 (Gibco; AM9260G) supplemented with 10% v/v dialyzed fetal bovine serum (Gibco; 26400044), 1% v/v L-glutamine (Gibco; 25030081), 1% v/v penicillin-streptomycin (Gibco; 15140122), 1% v/v MEM non-essential amino acids (Corning; MT25025CI), 1% v/v HEPES (Gibco; 15630080), 1% v/v sodium pyruvate (Corning; MT25000CI), and

0.1% v/v β-mercaptoethanol (Gibco; 21985023). Recombinant murine granulocyte-macrophage colony-stimulating factor (GM-CSF; Peprotech 315–03-100µg) at 15 ng/mL was added to the complete RPMI medium. Cells were fed at Days 2 and 4 with complete RPMI medium containing GM-CSF.

BMDC Proliferation Assay

For proliferation measurements, bone marrow cells were plated at 1×10^5 cells/well in a flat-bottom, non-tissue culture treated 96-well plate (GenClone; 25-104) in 150 µL of complete RPMI-1640, described above. Cells were plated in quintuplicate with either media alone or supplemented with a screen of queuine concentrations. Cells were fed at Days 2 and 4 with 50 µL of complete RPMI medium containing GM-CSF ± queuine to maintain concentration. Six 96-well plates were prepared – one per measurement time point (0, 1, 2, 3, 4, and 5 days). Live cell count was recorded every 24 hours with the following protocol.

At time of measurement, BMDCs were resuspended and transferred to a 96-well V-bottom acquisition plate (Sarstedt; NC0068972). To loosen adherent cells, 100 µL of 10 mM EDTA (Invitrogen; AM9260G) in 1× DPBS (Gibco; 14190094) was added to the flat-bottom seeding plate, which was then incubated at 37°C for 10 minutes. After incubation, the cells were again resuspended and transferred to the corresponding well of the acquisition plate. The seeding plate was washed once more with 50 µL 1× DPBS to transfer remaining cells to the acquisition plate. The acquisition plate was centrifuged at 1500 rpm for 5 minutes at 4°C. The supernatant was removed, and cell pellets were

resuspended in 130 µL cold FACS buffer (DPBS containing 0.05% v/v dialyzed FBS and 2 mM EDTA) with 0.1 µg/mL DAPI (Biotium; 40043) for counting.

Data were acquired using the NovoCyte Penteon. FlowJo software was used to obtain live cell counts for each well, which were analyzed further using R. One-way analysis of variance (ANOVA) was performed to assess differences in treatment conditions. Tukey's Honest Significant Difference (HSD) post-hoc test was applied to assess pairwise comparisons between treatments when ANOVA indicated statistical significance ($p < 0.05$). Adjusted *p*-values from the Tukey test are reported, and significance levels were annotated on the plots as follows: $p < 0.05$ (*), $p < 0.01$ (**), and $p < 0.001$ (***).

Flow cytometry was performed at the Cytometry and Antibody Technology Facility at University of Chicago, which receives financial support from the Cancer Center Support Grant (P30CA014599). RRID: SCR_017760.

BMDC RNA Extraction

For mRNA-seq and tRNA-seq experiments, bone marrow cells were plated at 2×10^6 cells in non-tissue culture treated 100mm dishes (Corning 351029) in 10 mL of complete RPMI medium, described above. Cells were plated in triplicate with either media alone or supplemented with 100 nM queuine. Cells were fed at Days 2 and 4 with 3 mL of complete RPMI medium containing GM-CSF ± queuine to maintain treatment concentration.

On Day 5, plates were scraped gently to lift adherent cells. Media was transferred to conical tubes and centrifuged at 3000 rpm for 3 minutes at 4°C. Pellets were washed

with cold Dulbecco's phosphate-buffered saline (DPBS) (Gibco; 14190094) and centrifuged once again at 3000 rpm for 3 minutes at 4°C. TRIzol™ reagent (Thermo Fisher; 15596026) was used to extract total RNA from the pellets according to the manufacturer's manual.

Northern Blots

Northern blots for queuosine level quantification were performed as previously described[132] using 1-3 µg of total RNA. In $tRNA^{Asp}$ and $tRNA^{Tyr}$, Q34 is glycosylated to form manQ and galQ, respectively. These hypermodified tRNAs require an acid denaturing gel to be distinguishable from unmodified, G34-tRNAs. APB gels were used for $tRNA^{Asn}$ and $tRNA^{His}$ to distinguish between G34-tRNAs and Q34-tRNAs. All blots were visualized with Clarity Western ECL Substrate (Bio-Rad; 1705061) using a Bio-Rad Chemi-Doc MP. The blots were then stripped by two rounds of incubation with boiling 1% SDS (aq.) for 30 seconds, followed by incubation at room temperature for 15 minutes. The stripped blots were then incubated with probes of other tRNA.

The oligonucleotide probe sequences used here are:

$tRNA^{Asn}$:

5′-biotin-

CGTCCCTGGGTGGGCTCGAACCACCAACCTTTCGGTTAACAGCCGAACGCGC

TAACCGATTGCGCCACAGAGAC

tRNA^{Asp}:

5′-biotin-

CTCCCCGTCGGGGAATCGAACCCCGGTCTCCCGCGTGACAGGCGGGGATAC

TCACCACTATACTAACGAGGA

tRNA^{His}:

5′-biotin-

TGCCGTGACTCGGATTCGAACCGAGGTTGCTGCGGCCACAACGCAGAGTACT

AACCACTATACGATCACGGC

tRNA^{Tyr}:

5′-biotin-

TCCTTCGAGCCGGA**S**TCGAACCAGCGACCTAAGGATCTACAGTCCTCCGCTC

TACCA**R**CTGAGCTATCGAAGG; **S** = G/C; **R** = A/G

Sequencing Library Preparation

MSR-seq and HEK293T mRNA-seq

HEK293T and murine BMDC total RNA MSR-seq libraries and HEK293T mRNA-seq libraries were prepared as described by Watkins et al.[96]

BMDC mRNA-seq

Multiplexed mRNA-seq libraries were prepared using the following overall workflow[172-174]: (1) oligo(dT)-primed RT reaction with sample barcoding; (2) cDNA pooling; (2) single-primer PCR amplification; (3) full-length cDNA tagmentation; (4) PCR amplification; and (5) gel extraction.

For each sample, 100 ng RNA was used as the starting input material. First, custom RT primer, which is biotinylated in 5′ and containing sequences from 5′ to 3′ for the Illumina read 1 primer, a 6-bp barcode, a 10-bp unique molecular identifier (UMI) and an anchored oligo$(dT)_{30}$ for priming, were added to RNA. RT reaction by Maxima H Minus Reverse Transcriptase (Thermo Fisher; EP0753) was used to generate cDNA. Double-stranded cDNA was pooled using DNA Clean & Concentrator-5 columns (Zymo Research; D4013). Excess RT primers were digested using exonuclease I (New England Biolabs; M0293). Full-length cDNAs were amplified by single-primer PCR, cleaned up with magnetic beads, and quantified with the Qubit dsDNA High Sensitivity Assay Kit (Thermo Fisher; 32851). 50 ng of cDNA per sample pool was tagmented using the Tagment DNA Enzyme I (Illumina; 20034197) and amplified using the NEBNext Ultra II Q5 Master Mix (New England BioLabs, M0544L). Libraries were gel purified using 2% E-Gel EX Agarose Gels (Thermo Fisher; G402002), quantified with the Qubit dsDNA High Sensitivity Assay Kit (Thermo Fisher; 32851) and a Tapestation 4200 (Agilent Technologies), and sequenced on the Illumina NextSeq 2000 platform.

Sequencing Data Analysis

MSR-seq Data

Data processing followed the MSR-seq analysis pipeline as previously reported.[96] The analysis pipeline is available at GitHub (https://github.com/ckatanski/CHRIS-seq). Paired-end reads were demultiplexed by barcode sequence using Je demultiplex.[175] Barcode sequences are as previously described.[96] The following parameters were used, optimized for samples where the barcode is located in read 2: BPOS = BOTH BM =

READ_2 LEN = 6:4 FORCE = true C = false. Following demultiplexing, data were aligned using bowtie2[176] (version 2.3.3.1) with the following parameters: -q -p 10 --local --no-unal. For HEK293T samples, reads were mapped to the GtRNAdb hg38 reference genome. For BMDC samples, reads were mapped to the GtRNAdb mm39 reference genome.[13]

Bowtie2 output sam files were converted to bam files, then sorted using samtools.[177] IGVtools count was used to collapse reads into a 1nt window using the following parameters: -z 5 -w 1 -e 250 —bases. The resulting IGV output.wig files were reformatted using custom Python scripts to obtain mutation rate, read coverage, and fragmentation information[165] compatible with R for data visualization and analysis. To obtain more accurate mutation rate positions, alignment was done from the 3′ CCA end. Where shown, Welch's unequal variances *t*-test was used to determine significance. Significance levels were annotated on the plots as follows: $p < 0.05$ (*), $p < 0.01$ (**), and $p < 0.001$ (***).

mRNA-seq Data

Raw sequencing reads were first demultiplexed by barcode sequence using Je demultiplex.[175] Read quality was assessed using FastQC.[178] Reads were trimmed using FastP.[179] Post-trimming, quality control was repeated with FastQC to confirm the removal of low-quality bases and adapter sequences.

Trimmed reads were aligned to the reference genome using STAR.[180] For HEK293T samples, reads were aligned to hg38 (GRCh38.p14). For BMDC samples, reads were aligned to mm39 (GRCm39). Once mapped, reads were counted with the

RSEM software.[181] Subsequent differential expression (DE) analysis was completed using custom scripts in R. Raw count matrices were normalized across samples using the calcNormFactor function in edgeR.[182] DE genes were further analyzed for functional enrichment using the clusterProfiler package in R.[183] The analysis was conducted for the Biological Process (BP) gene ontology (GO). The hypergeometric test was used to evaluate the overrepresentation of GO terms and multiple testing correction was applied using the Benjamini-Hochberg (BH) method.

Codon usage analysis was conducted for DE genes. DE genes were subset into upregulated ($\log_2$FC > 0) and downregulated genes ($\log_2$FC < 0). For each codon i, the change in codon usage Δ_i was calculated as follows:

$$\Delta_i = \frac{C_i^{up}}{T^{up}} - \frac{C_i^{down}}{T^{down}}$$

where C_i^{up} is the count of codon i across all upregulated genes, C_i^{down} is the count of codon i across all downregulated genes, T^{up} is the summed count of all codons across upregulated genes, and T^{down} is the summed count of all codons across downregulated genes. The Δ_i is a value $-1 < \Delta_i < 1$ with $\Delta_i < 0$ indicating a lower observed usage than expected, and vice versa.

Data Deposition

HEK293T MSR-seq data are from GSE196016.[164] BMDC MSR-seq and HEK293T and BMDC mRNA-seq data are deposited to NCBI GEO with the accession numbers of GSE284148, GSE284149, and GSE284168.

Chapter 3 – A microbe-derived metabolic precursor of queuosine-tRNA perturbs gene expression to halt proliferation

Part of this chapter is derived from a manuscript accepted for publication at Nature Cell Biology as of June 2025. The Authors are Wen Zhang, Kuldeep Lahry, Denis Cipurko, Sihao Huang, Olivia Zbihley, Dominika Rudzka, Luke R. Frietze, Mahdi Assari, Christopher D. Katanski, Marisha Singh, Aurore Attina, Hélène Guillorit, Christopher P. Watkins, Delphine Gourlain, Didier Varlet, Jennifer Falconi, Alexandre Djiane, Christophe Hirtz, Hankui Chen, Françoise Macari, Kate Johnson, Nicolas Chevrier, Alexandre David, and Tao Pan. W.Z., N.C., A.D., T.P. conceived the project and wrote the paper. W.Z. performed cell culture preQ$_1$ experiments and polysome profiling. W.Z. and D.R. performed IRE1 and tRNA cleavage characterizations. K.L., H.G., A.A., F.M. developed LC/MS/MS methods for queuosine and preQ$_1$sine measurements, performed extraction and MS measurements and analysis of the cells and mouse tissues. D.G., D.V. synthesized the queuosine and preQ$_1$sine nucleosides. D.C., N.C. designed and performed all mouse preQ$_1$ and tumor experiments. O.Z., K.J. performed BMDC experiments, C.D.K., C.P.W. H.C performed MSR-seq and PAQS-seq experiments. S.H, L.F., C.D.K. performed RNA-seq data analysis. W.Z., A.D., T.P wrote the paper.

3.1 Introduction

The guanine analog preQ$_1$ (pre-queuosine 1, 7-aminomethyl-7-deazaguanine) is an important metabolite in bacteria. It is recognized and bound by a class of

riboswitches, a type of non-coding RNA in the 5' UTR of some bacterial mRNAs, to regulate gene expression.[184] Moreover, $preQ_1$ is a metabolic precursor to Q-tRNA in the bacterial biosynthetic pathway. In bacteria, $preQ_1$ is the substrate for the enzyme TGT, which exchanges $preQ_1$ for guanine at position 34 of $tRNA^{Asn/Asp/His/Tyr}$. The $preQ_1$-modified tRNA is then further modified by QueA and QueG to form Q-tRNA. It has been demonstrated that the human TGT homolog, QTRT1/QTRT2, can also incorporate $preQ_1$ into cognate tRNAs *in vitro*.[133,185] Because $preQ_1$ is perpetually present in bacteria, microbial turnover in the gut could expose host cells to the metabolite.[186-189]

Here, we explored the effect of $preQ_1$ on mammalian cell proliferation using both HEK293T cells and murine BMDCs. We find that $preQ_1$ significantly slows proliferation in both cell types, an effect which can be rescued by co-treatment with queuine. Furthermore, we conducted mRNA-seq of $preQ_1$-treated BMDCs and find sweeping transcriptional changes. Addition of queuine reverses the transcriptome response. Our results reveal that $preQ_1$ and queuine act in opposite ways on mammalian cell physiology, despite their structural similarities (**Figure 1.3A**).

3.2 Results

3.2.1 $preQ_1$ attenuates proliferation of immortalized and primary cells

Our previous results demonstrated that queuine supplementation has a pro-proliferative effect in both HEK293T cells and BMDCs. We wondered, then, whether $preQ_1$ also elicits an effect on cell growth. To investigate, we measured the proliferation of $preQ_1$-treated cells using a CCK-8 assay (**Figure 3.1A**). 0Q HEK293T cells were grown

in media containing 0, 0.1, 1, or 10 μM $preQ_1$ for five days. Unlike queuine, $preQ_1$ does not enhance proliferation. Instead, we observe a stark decrease in proliferation at 1 μM $preQ_1$. Cell viability was unchanged in response to $preQ_1$ treatment at any concentration. Fascinatingly, the observed effect exists on a bell curve such that proliferation is restored to baseline levels at 10 μM $preQ_1$. Since $preQ_1$ and queuine treatment alone produce opposing proliferation phenotypes in HEK293T cells, we were next interested in evaluating the phenotype resulting from co-treatment with both nucleobases. To that end, 0Q HEK293T cells were grown in media containing 1 μM $preQ_1$ with 0, 1, 2, 4, 8, 16, or 32 nM queuine for 5 days (**Figure 3.1B**). As described previously, 1 μM $preQ_1$ alone resulted in a significant attenuation of cell proliferation. Co-treatment with queuine, however, rescues cell proliferation in a concentration-dependent manner. This effect is observed with as little as 1 nM queuine, though approximately 4-8 nM queuine is required to restore cell proliferation to control (0Q) levels. Notably, the concentration of queuine sufficient for proliferation rescue is significantly less than the concentration of $preQ_1$ present in culture medium. Indeed, at 1 μM $preQ_1$ and 4 nM queuine, $preQ_1$ availability is 250-fold that of queuine. Our previous results using QTRT1 KD HEK293T suggest that Q-tRNA formation, rather than queuine itself, is responsible for the pro-proliferative effect observed in queuine-supplemented cells (**Figure S2.1B**). The potency of queuine in competition with $preQ_1$, then, can likely be attributed to its higher binding affinity to the QTRT1/QTRT2 complex.[190] Taken together, our results demonstrate that queuine and $preQ_1$ act competitively to enhance or attenuate cell proliferation, respectively, with queuine acting more efficaciously in HEK293T cells.

There are many molecules that reduce cell proliferation by inducing cell cycle arrest at a particular phase of the cell cycle. We wondered whether $preQ_1$, too, slowed cell growth by perturbing cell cycle progression. **Figure 3.1C** illustrates a simplified schematic of the eukaryotic cell cycle, highlighting the key regulatory phases: G_0, G_1, S, G_2, and M.[191] In this model, cells in the G_0 phase are in a quiescent, non-proliferative state and can re-enter the cycle in G_1 upon receiving appropriate signals. During G_1, cells grow and prepare for DNA replication, followed by S phase where DNA synthesis occurs. The cycle then proceeds to G_2, a second growth phase that prepares the cell for mitosis (M phase). This model serves as a reference for interpreting the distribution of HEK293T cells across these phases, described below.

To assess cell cycle progression, we performed propidium iodide (PI) staining and flow cytometry analysis to quantify DNA content in HEK293T cells (**Figure 3.1D**). PI intercalates into DNA, allowing distinction between G_0/G_1-phase cells (with 2N DNA content), S-phase cells (with intermediate DNA content due to ongoing replication), and G_2-phase cells (with 4N DNA content). 0Q HEK293T cells were treated with 1 μM $preQ_1$ ("$preQ_1$"), 10 nM queuine ("q"), or both ("Both") for 24 hours prior to PI staining. Across all conditions tested, cell distribution across the cycle phases was unchanged. Approximately 45% of cells were in G_0/G_1, 20% were in S, and 20% were in G_2. These results suggest that $preQ_1$ significantly reduces HEK293T proliferation, but not via inhibition of cell cycle progression.

In Chapter 2, we describe the cell-type-dependent sensitivity to queuine, both in the context of proliferation changes and of Q-tRNA formation, where murine BMDCs

were less sensitive to queuine than HEK293T cells (**Figure 2.1**). We were interested in evaluating this phenomenon in $preQ_1$-treated cells as well. To that end, 0Q BMDCs were grown in control medium ("0Q"), with 0.1 μM $preQ_1$ alone, or co-treated with 10 or 100 nM queuine for five days (**Figure 3.1E**). In the presence of $preQ_1$, BMDC proliferation is also significantly attenuated with no change in overall cell viability. Fascinatingly, although they are less sensitive to queuine than HEK293T cells, BMDCs appear to be more sensitive to $preQ_1$ and exhibit a significant reduction in growth at just 0.1 μM $preQ_1$. The relative concentration of queuine required to rescue proliferation levels in BMDCs is also significantly higher in BMDCs than in HEK293T cells. Whereas a 1:100 ratio of q:$preQ_1$ returned proliferation to baseline levels in HEK293T cells, a 1:1 ratio was required for the same effect in BMDCs. These results reveal a significant cellular response to a microbe-derived metabolite and underscore the context-dependence of queuosine biology.

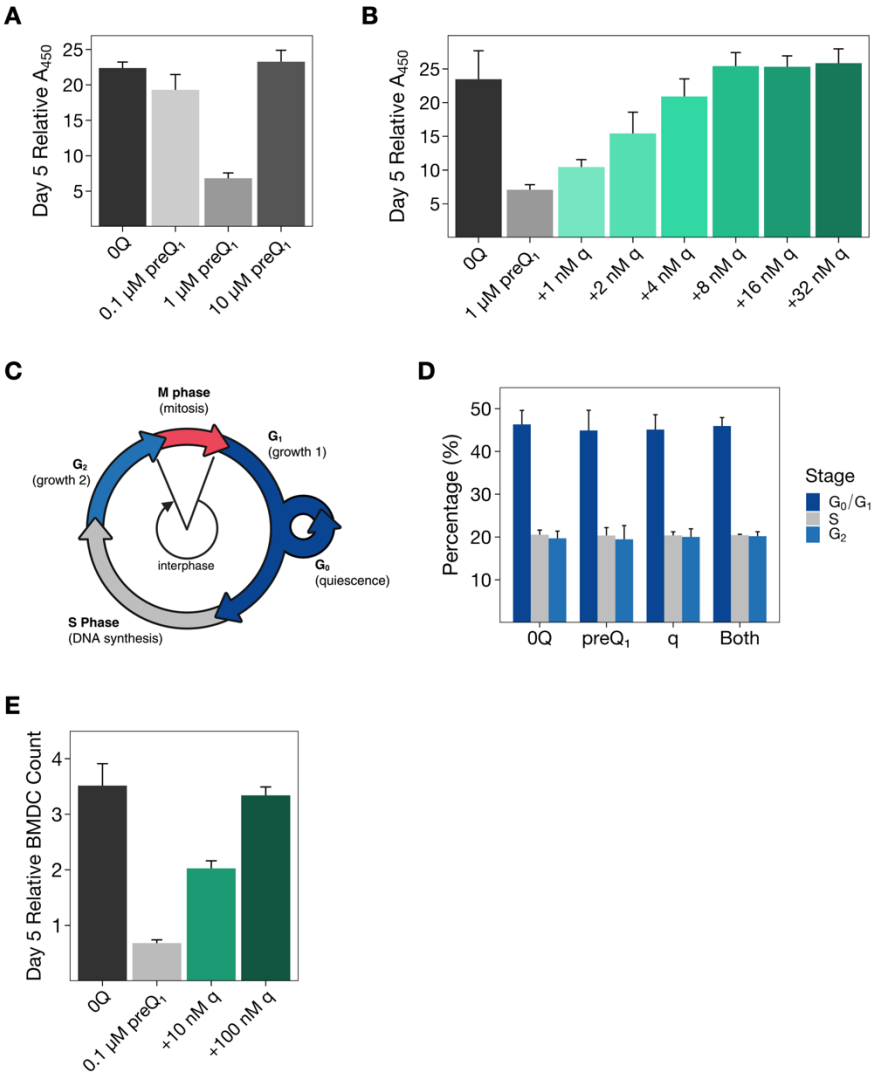

Figure 3.1: preQ$_1$ attenuates cell proliferation but not via cell cycle arrestation.

(A-B) HEK293T cell proliferation, measured by CCK-8 assay, in response to (**A**) preQ$_1$ alone and (**B**) cotreatment with a screen of queuine concentrations. Relative A_{450} was calculated as the sample A_{450} divided by the mean A_{450} for 0 nM queuine at Day 0. Bars represent the mean of n = 8 replicates, and error bars represent one standard deviation.
(C) Schematic of the cell cycle.
(D) Percentage of 0Q HEK293T cells in each cell cycle stage, as measured by propidium iodide staining, with no treatment ("0Q"), 1 μM preQ$_1$ ("preQ$_1$"), 10 nM queuine ("q"), or co-treatment with 1 μM preQ$_1$ + 10 nM queuine ("Both"). Bars represent the mean of n = 3 replicates, and error bars represent one standard deviation.
(E) BMDC proliferation in response to preQ$_1$ ± queuine. Relative cell count for each well was calculated as the live cell count divided by the mean cell count for 0Q at Day 0. Bars represent the mean of n = 5 replicates, and error bars represent one standard deviation.

3.2.2 $preQ_1$ and queuine act in opposition on the dendritic cell transcriptome

Intrigued by the antiproliferative effects of $preQ_1$ reported above, we next carried out mRNA-seq to evaluate transcriptional changes in $preQ_1$-treated BMDC cells (**Figure 3.2**). BMDCs were grown in media alone ("0Q"), supplemented with 0.1 μM $preQ_1$ ("$preQ_1$"), or supplemented with 0.1 μM $preQ_1$ + 0.1 μM queuine ("Both") prior to RNA extraction. We conducted two analyses: one comparing $preQ_1$-treated cells to 0Q cells (**Figure 3.2A-C**) and one comparing co-treated cells to $preQ_1$-treated cells (**Figure 3.2D-F**). Relative to 0Q cells, $preQ_1$-treated BMDCs exhibit sweeping transcriptional changes, with 259 upregulated genes and 555 downregulated genes (**Figure 3.2A**). We next conducted GO analysis of differentially expressed genes. For genes upregulated in $preQ_1$-treated BMDCs, four of the top five GO terms were associated with cellular movement: "myeloid leukocyte migration", "leukocyte chemotaxis", "granulocyte chemotaxis", and "granulocyte migration" (**Figure 3.2B**). On that other hand, the top five GO terms for downregulated transcripts are all associated with processes required for cellular division (**Figure 3.2C**). This is consistent with our results that $preQ_1$ significantly slows cell proliferation. These data suggest that dendritic cells respond to $preQ_1$ by increasing cellular movement but attenuating cell division.

Because queuine co-treatment rescued $preQ_1$-induced proliferation changes, we conducted a second mRNA-seq comparison between co-treated ("Both") cells and $preQ_1$-treated cells (**Figure 3.2D-F**). Addition of 0.1 μM queuine resulted in many changes in the transcriptome, with 615 upregulated genes and 262 downregulated genes (**Figure 3.2D**). GO analysis of upregulated genes revealed strong associations

with processes involved in cellular growth and division (**Figure 3.2E**). Again, this is consistent with our findings that queuine co-treatment rescues the antiproliferative effects of $preQ_1$. Downregulated genes in co-treated cells were associated with cellular movement processes and negative regulation of immune response (**Figure 3.2F**), meaning that queuine increases the immune activity of BMDCs. This is consistent with our finding that 100Q BMDCs upregulate genes involved in immune response mediation and immunoglobulin diversification compared to 0Q BMDCs (**Figure 2.4E**). Of note, the GO terms presented in **Figure 3.2E** and **Figure 3.2F** are nearly the same as those in **Figure 3.2B** and **Figure 3.2C**, but with reversed expression directionality. Taken together, our results indicate that $preQ_1$ induces sweeping changes in the BMDC transcriptome to reduce cell growth, but queuine competes with $preQ_1$ at a 1:1 ratio to reduce these effects.

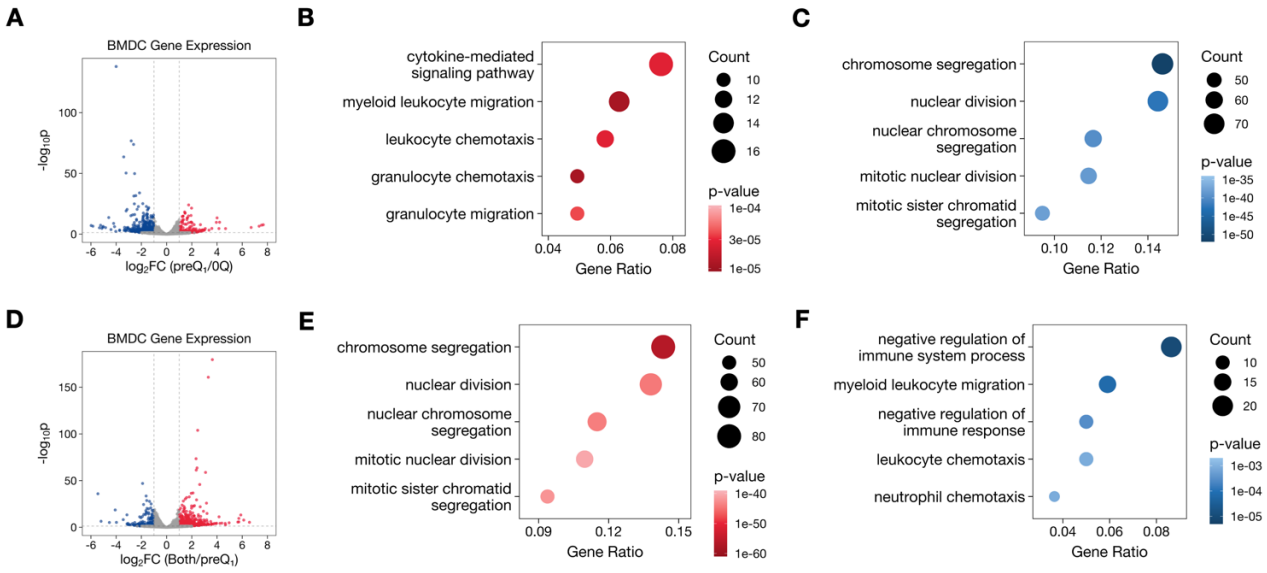

Figure 3.2: preQ$_1$ and queuine affect the BMDC transcriptome in opposing ways.

(A) Volcano plot of DE analysis in preQ$_1$-treated (0.1 μM) vs. 0Q BMDCs. Upregulated genes (*n* = 259) are shown in red; downregulated genes (*n* = 555) are in blue.
(B) Gene ontology (GO) analysis of transcripts upregulated in preQ$_1$-treated vs. 0Q BMDCs. The top 5 GO terms are displayed.
(C) GO analysis of transcripts downregulated in preQ$_1$-treated vs. 0Q BMDCs. The top 5 GO terms are displayed.
(D) Volcano plot of DE analysis in "Both" (0.1 μM preQ$_1$ + 0.1 μM q) vs. preQ$_1$-treated BMDCs. Upregulated genes (*n* = 615) are shown in red; downregulated genes (*n* = 262) are in blue.
(E) GO analysis of transcripts upregulated in "Both" vs. preQ$_1$-treated BMDCs. The top 5 GO terms are displayed.
(F) GO analysis of transcripts downregulated in "Both" vs. preQ$_1$-treated BMDCs. The top 5 GO terms are displayed.

3.3 Discussion

In this study, we investigated how two structurally similar metabolites act on mammalian cell physiology in opposite ways. We show that $preQ_1$ has a strong antiproliferative effect in both HEK293T cells and BMDCs, and this effect can be rescued by addition of queuine. Additionally, neither metabolite affects cell cycle progression. We also present mRNA-seq data that corroborates the observed proliferation phenotype in BMDCs.

In both of our cell culture models, $preQ_1$ elicits a strong antiproliferative effect. Moreover, queuine co-treatment restores proliferation in a concentration-dependent manner. Though we hypothesized that $preQ_1$ may be causing cell cycle arrest, our PI staining experiment suggests that $preQ_1$-treated cells are progressing through the cell cycle, albeit at a much-inhibited rate. Given that queuine enhances proliferation via translation of ribosomal genes (Chapter 2), the $preQ_1$-driven attenuation of cell growth is likely due to a global slowing of translation. Since $preQ_1$ can act as a substrate for mammalian QTRT1/QTRT2,[133] a plausible explanation for this is that $preQ_1$-modified tRNAs are marked for degradation, reducing the levels for the cognate $tRNA^{Asn/Asp/His/Tyr}$. As queuine concentration is increased, QTRT1/QTRT2 preferentially uses it as a substrate for tRNA modification, returning levels of $tRNA^{Asn/Asp/His/Tyr}$ to baseline and restoring translational efficiency. Of note, the antiproliferative effect disappears at 10 μM $preQ_1$, such that HEK293T proliferation returned to control levels. We hypothesize that, at $preQ_1$ concentration increases, $preQ_1$-tRNA levels eventually become saturated. Comparatively, at lower $preQ_1$ concentrations, a mixture of $preQ_1$-tRNAs and unmodified

G-tRNAs exist. Once $preQ_1$-tRNA levels reach saturation, $preQ_1$-induced irregularities in translation become equilibrated, causing cellular phenotypes to return towards normal.

From our proliferation experiments, it is apparent that HEK293T cells and BMDCs differ in their sensitivities to $preQ_1$. Interestingly, in the context of proliferation, BMDCs are less sensitive to queuine but more sensitive to $preQ_1$ than HEK293T cells. As a result, a 1:1 ratio of queuine:$preQ_1$ was required to rescue BMDC proliferation levels, whereas a 1:250 ratio was sufficient in HEK293T cells. Given that $preQ_1$ is a naturally-occurring microbial metabolite, it is interesting to consider whether DCs are more responsive to $preQ_1$ treatment due to their immunological function. Indeed, we found that $preQ_1$-treated BMDCs upregulated gene transcripts associated with cell migration and chemotaxis. These processes are triggered by chemokine signaling, regulated by several intracellular mechanisms, and critical for DC function.[192,193] Though the effect of $preQ_1$ on DC function has not been explicitly investigated, DCs have been shown to respond to both endogenous and exogenous metabolites.[194,195] Moreover, it is well understood that there is interplay between the gut microbiome and mammalian immune systems through many mechanisms.[196-198]

Our results highlight that two microbe-derived metabolites belonging to the same biosynthetic pathway act on mammalian cell physiology in opposing ways and shed light on a plausible molecular mediator of crosstalk between the gut microbiome and the host immune system.

3.4 Materials and Methods

HEK293T Cell Culture

0Q HEK293T cells were obtained as previously reported.[139,163] Briefly, HEK293T cells (ATCC, CRL-11268) were cultured at 37°C in DMEM (Cytiva; SH30022.01) supplemented with 10% volume/volume (v/v) DFBS (Gibco; 26400044) and 1% v/v Penicillin-Streptomycin (Thermo Fisher; 15070063) to 80% confluency.

HEK293T Proliferation Assays

0Q HEK293T cells were plated at 5×10^3 cells/well in a tissue culture treated 96-well plate (Dot Scientific; 667195) in 100 µL of DMEM as described above. For the $preQ_1$ study, appropriate volumes of $preQ_1$ (Cayman Chemical) were added to achieve the three treatment conditions (0.1, 1, and 10 µM $preQ_1$), with 0Q cells serving as the untreated control. All conditions were plated with n = 8 replicates. For the queuine proliferation rescue study, $preQ_1$ (Cayman Chemical) was added to cells to achieve a final concentration of 1 µM. Queuine (Toronto Research Chemicals) was also added to achieve treatment concentrations of 0, 1, 2, 4, 8, 16, and 32 nM queuine. 0Q cells were used as the untreated control, and all conditions were plated with n = 8 replicates. For both experiments, six 96-well plates were prepared – one per measurement time point (0, 1, 2, 3, 4, and 5 days).

HEK293T cell proliferation was measured using the Cell Counting Kit-8 (CCK-8) (Dojindo; CK04-13) according to manufacturer protocol. Briefly, immediately after plating, 10 µL of WST-8 solution was added to each well of the Day 0 plate. The plate was wrapped in aluminum foil and incubated at 37°C for 2 hours. Following incubation,

absorbance at 450 nm was measured using a microplate reader to assess cell viability. WST-8 addition, incubation, and absorbance measurement steps were repeated every 24 hours using the corresponding plate.

The data were visualized using R. Day 5 Relative A_{450} for each well was calculated as the A_{450} on Day 5 divided by the mean A_{450} for 0 nM queuine at Day 0. Bar heights represent the mean of samples, and error bars represent one standard deviation.

HEK293T Cell Cycle Analysis

To assess cell cycle status in response to $preQ_1$ or queuine supplementation, 0Q HEK293T cells were grown in 6-well plates (Corning; 353046) in queuine-depleted DMEM and grown to ~50% confluency. Once ~50% confluence was reached, culture medium was swapped for control medium ("0Q"), medium with 1 μM $preQ_1$ ("$preQ_1$"), or medium with 10 nM queuine ("q") and returned to the incubator for 24 hours. All conditions were plated in triplicate. The next day, cells were lifted with 0.25% Trypsin-EDTA (Thermo Fisher; 25200056) and pelleted in a 15 mL conical tube by centrifugation. The supernatant was aspirated and 1 mL of ice cold 70% ethanol in 1× DPBS (Gibco; 14190094) was added dropwise to each sample while vortexing. Samples were incubated at 4°C overnight.

The following day, cells were washed three times with cold 5 mM EDTA (Invitrogen; AM9260G) in 1× DPBS (Gibco; 14190094). After the third wash, cells were resuspended in 1 mL staining solution (25 μg/mL propidium iodide (BioLegend; 421301), 30 μg/mL RNase A (Millipore Sigma; 10109142001), and 2 mM sodium citrate in 1× DPBS (Gibco; 14190094)). Conical tubes were shielded from light with aluminum foil and

incubated at 4°C overnight. Samples were transferred to round-bottom 12x75 mm tubes for data acquisition by NovoCyte Penteon. Flow cytometry was performed at the Cytometry and Antibody Technology Facility at University of Chicago. FlowJo software was used to obtain population sizes for each cell cycle stage. The data were visualized using R, where bar heights represent the mean of samples and error bars represent one standard deviation.

Mice

Female C57BL/6J mice were obtained from Jackson Laboratories. Mice were housed under specific pathogen-free and BSL2 conditions at the University of Chicago. All experiments were conducted following the guidelines set by the US National Institutes of Health Guide for the Care and Use of Laboratory Animals and were approved by the Institutional Animal Care and Use Committee at the University of Chicago.

BMDC Cell Culture

Murine BMDCs were generated from 6-8 week-old C57BL/6J female mice. Bone marrow cells were collected from femora and tibiae and cultured at 37°C in RPMI-1640 (Gibco; AM9260G) supplemented with 10% v/v dialyzed fetal bovine serum (Gibco; 26400044), 1% v/v L-glutamine (Gibco; 25030081), 1% v/v penicillin-streptomycin (Gibco; 15140122), 1% v/v MEM non-essential amino acids (Corning; MT25025CI), 1% v/v HEPES (Gibco; 15630080), 1% v/v sodium pyruvate (Corning; MT25000CI), and 0.1% v/v β-mercaptoethanol (Gibco; 21985023). Recombinant murine granulocyte-macrophage colony-stimulating factor (GM-CSF; Peprotech 315–03-100µg) at 15 ng/mL

was added to the complete RPMI medium. Cells were fed at Days 2 and 4 with complete RPMI medium containing GM-CSF.

BMDC Proliferation Assay

For the proliferation rescue study, bone marrow cells were plated at 1×10^5 cells/well in a flat-bottom, non-tissue culture treated 96-well plate (GenClone; 25-104) in 150 µL of complete RPMI-1640, described above. Cells were plated with media alone ("0Q") or treated with 0.1 µM $preQ_1$ (Cayman Chemical). Queuine (Toronto Research Chemicals) was also added to achieve final co-treatment concentrations of 10 and 100 nM queuine. All conditions were plated with $n = 5$ replicates. Six 96-well plates were prepared – one per measurement time point (0, 1, 2, 3, 4, and 5 days). Cells were fed at Days 2 and 4 with 50 µL of complete RPMI medium containing GM-CSF ± $preQ_1$ ± queuine to maintain concentration. Live cell count was recorded every 24 hours with the following protocol.

At time of measurement, BMDCs were resuspended and transferred to a 96-well V-bottom acquisition plate (Sarstedt; NC0068972). To loosen adherent cells, 100 µL of 10 mM EDTA (Invitrogen; AM9260G) in 1× DPBS (Gibco; 14190094) was added to the flat-bottom seeding plate, which was then incubated at 37°C for 10 minutes. After incubation, the cells were again resuspended and transferred to the corresponding well of the acquisition plate. The seeding plate was washed once more with 50 µL 1× DPBS to transfer remaining cells to the acquisition plate. The acquisition plate was centrifuged at 1500 rpm for 5 minutes at 4°C. The supernatant was removed, and cell pellets were

resuspended in 130 µL cold FACS buffer (DPBS containing 0.05% v/v dialyzed FBS and 2 mM EDTA) with 0.1 µg/mL DAPI (Biotium; 40043) for counting.

Data were acquired using the NovoCyte Penteon. FlowJo software was used to obtain live cell counts for each well. The data were then visualized using R, where bar heights represent the mean of samples and error bars represent one standard deviation. Flow cytometry was performed at the Cytometry and Antibody Technology Facility at University of Chicago.

BMDC RNA Extraction

For mRNA-seq experiments, BMDCs were plated at 2×10^6 cells in 10-cm non-tissue culture treated 100mm dishes (Corning 351029) in 10 mL of complete RPMI medium, described above. Cells were plated in triplicate with media alone ("0Q"), supplemented with 0.1 µM $preQ_1$ ("$preQ_1$"), or supplemented with 0.1 µM $preQ_1$ + 0.1 µM queuine ("Both"). Cells were fed at Days 2 and 4 with 3 mL of complete RPMI medium containing GM-CSF ± $preQ_1$ ± queuine to maintain treatment concentration.

On Day 5, plates were scraped gently to lift adherent cells. Media was transferred to conical tubes and centrifuged at 3000 rpm for 3 minutes at 4°C. Pellets were washed with cold DPBS (Gibco; 14190094) and centrifuged once again at 3000 rpm for 3 minutes at 4°C. TRIzol™ reagent (Thermo Fisher; 15596026) was used to extract total RNA from the pellets according to the manufacturer's manual.

mRNA-seq Library Preparation

Multiplexed mRNA-seq libraries were prepared using the following overall workflow[172-174]: (1) oligo(dT)-primed RT reaction with sample barcoding; (2) cDNA

pooling; (2) single-primer PCR amplification; (3) full-length cDNA tagmentation; (4) PCR amplification; and (5) gel extraction.

For each sample, 100 ng RNA was used as the starting input material. First, custom RT primer, which is biotinylated in 5′ and containing sequences from 5′ to 3′ for the Illumina read 1 primer, a 6-bp barcode, a 10-bp unique molecular identifier (UMI) and an anchored oligo$(dT)_{30}$ for priming, were added to RNA. RT reaction by Maxima H Minus Reverse Transcriptase (Thermo Fisher; EP0753) was used to generate cDNA. Double-stranded cDNA was pooled using DNA Clean & Concentrator-5 columns (Zymo Research; D4013). Excess RT primers were digested using exonuclease I (New England Biolabs; M0293). Full-length cDNAs were amplified by single-primer PCR, cleaned up with magnetic beads, and quantified with the Qubit dsDNA High Sensitivity Assay Kit (Thermo Fisher; 32851). 50 ng of cDNA per sample pool was tagmented using the Tagment DNA Enzyme I (Illumina; 20034197) and amplified using the NEBNext Ultra II Q5 Master Mix (New England BioLabs, M0544L). Libraries were gel purified using 2% E-Gel EX Agarose Gels (Thermo Fisher; G402002), quantified with the Qubit dsDNA High Sensitivity Assay Kit (Thermo Fisher; 32851) and a Tapestation 4200 (Agilent Technologies), and sequenced on the Illumina NextSeq 2000 platform.

mRNA-seq Data Analysis

Raw sequencing reads were first demultiplexed by barcode sequence using Je demultiplex.[175] Read quality was assessed using FastQC.[178] Reads were trimmed using FastP.[179] Post-trimming, quality control was repeated with FastQC to confirm the removal of low-quality bases and adapter sequences. Trimmed reads were aligned to

the mm39 (GRCm39) reference genome using STAR.[180] Once mapped, reads were counted with the RSEM software.[181] Subsequent DE analysis was completed using custom scripts in R. Raw count matrices were normalized across samples using the calcNormFactor function in edgeR.[182] DE genes were further analyzed for functional enrichment using the clusterProfiler package in R.[183] The analysis was conducted for the Biological Process (BP) gene ontology (GO). The hypergeometric test was used to evaluate the overrepresentation of GO terms and multiple testing correction was applied using the Benjamini-Hochberg (BH) method.

Chapter 4 – preQ$_1$ and queuine impact the expression of an immune response mediator in primary dendritic cells

Part of this chapter is derived from a manuscript published in the Journal of Molecular Biology on May 6th, 2025. The Authors are Olivia Zbihley, Kate Johnson, Luke Frietze, Wen Zhang, Marcus Foo, Hoang Anh Tran, Nicolas Chevrier, and Tao Pan. O.Z. and T.P. conceived the project and wrote the paper. O.Z. and K.J. performed BMDC cell and sequencing work under the guidance of N.C. O.Z. analyzed the sequencing data with assistance from L.F., W.Z., and M.F. H.T. performed HEK293T proliferation, mRNA-seq and biochemical characterization.

4.1 Introduction

The innate immune system serves as the first line of defense against pathogens. It is responsible for recognizing a threat in the host, providing a broad defense response, and activating the adaptive immune system.[199] Although the innate immune response requires the coordinated activity of many different cell types, dendritic cells (DCs) are essential for facilitating communication between the innate and adaptive immune systems.[200] DCs are specialized cells that capture, process, and present antigens to T-lymphocytes. Antigen presentation is achieved through major histocompatibility complex class I (MHC-I) and class II (MHC-II) molecules on the DC surface, which interact with and activate $CD8^+$ and $CD4^+$ T-lymphocytes, respectively.[201] Activated T-

lymphocytes play several crucial roles in the finely-tuned adaptive immune response, including the formation of antigen-specific immunological memory.[202]

Unsurprisingly, the immune functions of DCs are tightly regulated and dynamically responsive to external stimuli such as microbial products, inflammatory cytokines, and stress signals.[200,203] DC activation is largely mediated by a family of Toll-like receptors (TLRs) on the cell surface, which recognize and bind a variety of pathogen-derived molecular structures.[204,205] Upon activation, DCs undergo maturation marked by increased expression of co-stimulatory ligands, cytokine secretion, and enhanced MHC-II-mediated antigen presentation.[200,203] The maturation process creates a surge in translational demand resulting in widespread, but orchestrated, changes in both the transcriptome and translatome.[206-208]

Indeed, there is mounting evidence for the role of RNA-based regulatory mechanisms in both DC maturation and their immune activities more broadly. For instance, mRNA stability, N^6-methyladenosine (m^6A) modification levels, and the m^6A writer complex METTL3 are all recognized to play significant roles in dendritic cell maturation.[209-213] In fact, many mRNA modifications and non-coding RNA (ncRNA) modifications have been similarly implicated.[214] Beyond modifications, ncRNAs are involved in the fine-tuned regulation of DC physiology through several mechanisms.[215,216] For example, lnc-DC, a long non-coding RNA expressed exclusively in humans, is required for optimal DC differentiation and regulates DC-mediated activation of T-lymphocytes.[217] tRNA fragments (tRFs) – a class of small RNAs derived from cleavage of mature tRNAs – are also emerging as regulatory elements in immunity. tRFs are involved

in the regulation of many biological processes and have even been shown to interact directly with TLRs.[79,218-220]

Despite this growing body of evidence, the role of queuosine in dendritic cell biology remains unexplored. Here, we investigate the relationship between MHC-II expression, Q, and $preQ_1$ using murine bone marrow-derived dendritic cells (BMDCs), which serve as a widely accepted model for studying the molecular and functional characteristics of DCs.[221] We show that queuine/$preQ_1$ availability in culture medium alters the expression of MHC-II in BMDCs, suggesting a novel connection between these bacterial-derived micronutrients and mammalian immune function.

4.2 Results

4.2.1 Queuine availability regulates MHC-II expression in murine dendritic cells

Our investigation of how Q-modification impacts the BMDC transcriptome revealed that elevated Q-tRNA levels cause upregulation of genes associated with immune cell functions (**Figure 2.4E**). Specifically, the top GO term was “production of a molecular mediator of immune response”, leading us to examine whether Q-modification played a role in dendritic cell function via MHC-II production. To induce DC activation, we utilized lipopolysaccharide (LPS), an outer membrane component of gram-negative bacteria that is recognized by TLR4.[222]

BMDCs were extracted from mice and cultured in queuine-depleted (DFBS) medium for four days. The culture medium was then supplemented with queuine concentrations between 0-1000 nM for 24 hours before data acquisition. On Day 5,

BMDCs were activated with LPS at 100 ng/mL (+LPS) or given normal medium (–LPS) for six hours. Following incubation, cells were fluorescently labeled with anti-CD11b, anti-CD11c, and anti-MHC-II antibodies; stained with DAPI; and analyzed via fluorescence activated cell sorting (FACS) by flow cytometer. Live cells were first selected for expression of surface proteins CD11b and CD11c ($CD11b^{+}CD11c^{+}$), which are dendritic cell markers (**Supplementary Figure S4.1A**). As expected, LPS treatment increased MHC-II expression in $CD11b^{+}CD11c^{+}$ BMDCs (**Figure 4.1A,B**). Varying queuine availability did not significantly alter the magnitude of this change as measured by percent changes in geometric mean (GM) (**Figure 4.1B**). This suggests that BMDC sensitivity to LPS is not dependent on queuine. However, we noticed that the $CD11b^{+}CD11c^{+}$ BMDCs clustered into three MHC-II expression subpopulations: Low ($CD11b^{+}MHC\text{-}II^{Low}$), Medium ("Med"; $CD11b^{+}MHC\text{-}II^{Med}$), and High ($CD11b^{+}MHC\text{-}II^{High}$) MHC-II expression (**Figure 4.1C; Supplementary Figure S4.1B**). We evaluated the relative change of subset sizes within each LPS treatment condition (+/–LPS) and observe a queuine-dependent effect (**Figure 4.1D,E**). In –LPS cells, MHC-II expression was elevated in response to queuine supplementation, except for 1000 nM queuine (**Figure 4.1D**). For 1-300 nM queuine, treatment conditions were not statistically significantly different from one other. However, the queuine-dependent effect appears strongest at intermediate concentrations. For example, $CD11b^{+}MHC\text{-}II^{Med}$ subset population increased by 23%, 26%, and 38% at 1 nM, 3 nM, and 10 nM queuine, respectively, when compared to 0 nM queuine. At queuine concentrations of 30 nM and higher, however, the trend begins to reverse. We observe relative increases of 32%,

24%, and 27% at 30 nM, 100 nM, and 300 nM queuine, respectively. At 1000 nM queuine, the highest tested concentration, subset population sizes had returned to baseline. Generally, the $CD11b^{+}MHC\text{-}II^{Low}$ subset population decreased in queuine-supplemented cells, exhibiting a similar biphasic effect as described.

Given that LPS activation upregulates MHC-II in DCs, we were surprised to observe a queuine-dependent effect in +LPS BMDCs as well, albeit of a slightly lesser magnitude (**Figure 4.1E**). With the exceptions of 3 nM, 300 nM, and 1000 nM, addition of queuine across all concentrations tested resulted in enhanced MHC-II expression.

In –LPS BMDCs, some small changes were observed in the $CD11b^{+}MHC\text{-}II^{High}$ subset across the queuine concentrations tested, while no changes were observed for this group in +LPS BMDCs. However, regardless of LPS treatment, $CD11b^{+}MHC\text{-}II^{High}$ cells accounted for only ~1-2% of all $CD11b^{+}CD11c^{+}$ cells (**Supplementary Figure S4.1C**). Total cell count and cell viability was consistent across conditions and replicates (**Supplementary Figure S4.1D**). These results suggest a queuine-dependent effect on MHC-II expression in murine BMDCs, revealing a previously unknown connection between Q-tRNAs and dendritic cell function.

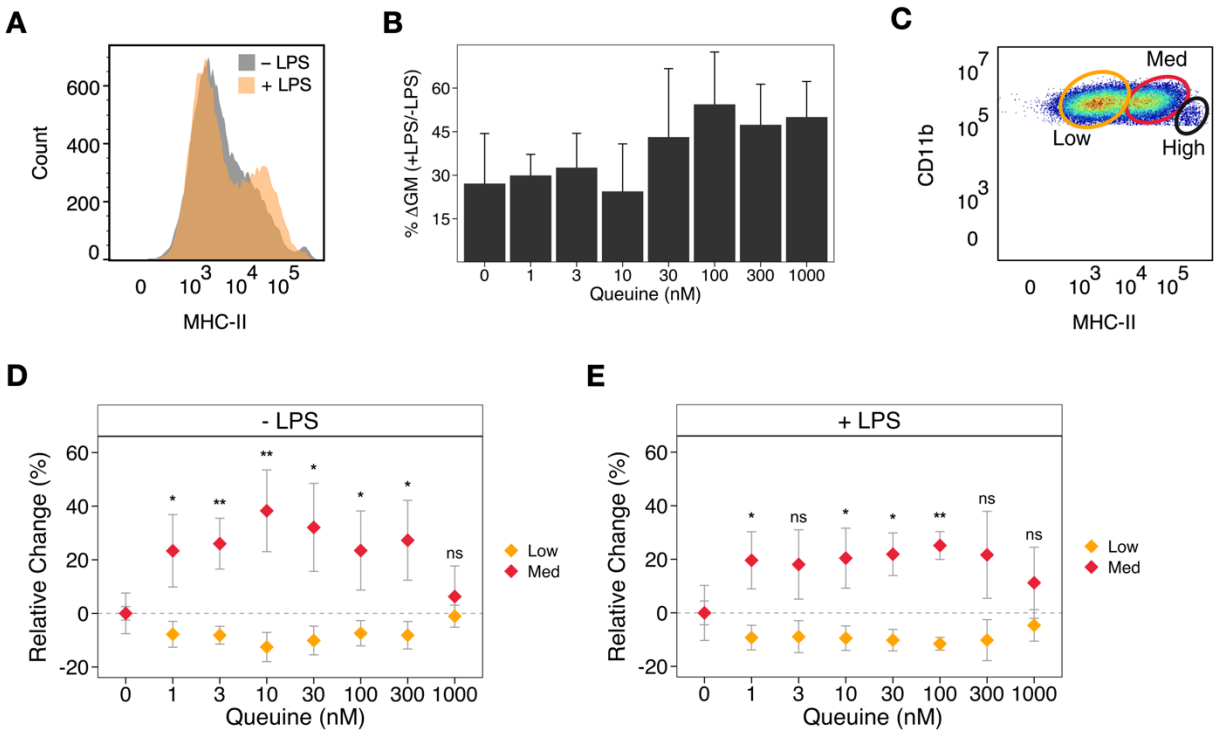

Figure 4.1: MHC-II expression in BMDCs is dependent on queuine.

(A) Representative histogram of MHC-II fluorescence in response to treatment with 100 ng/mL LPS (+LPS) compared to control (–LPS). Data shown is for one replicate of 0 nM queuine.
(B) Bar graph showing the percentage change in geometric mean (GM) of MHC-II fluorescence between +LPS and –LPS BMDCs across queuine concentrations. Bars represent the mean of $n = 4$ biological replicates, and error bars represent one standard deviation.
(C) Representative gating strategy to stratify $CD11b^{+}CD11c^{+}$ BMDCs into Low, Med (Medium), and High MHC-II expression subsets.
(D-E) Changes in $CD11b^{+}MHC\text{-}II^{Low}$ and $CD11b^{+}MHC\text{-}II^{Med}$ populations across queuine supplementation concentrations in (**D**) –LPS and (**E**) +LPS BMDCs. Subset population sizes were measured as a percentage of the parent gate ($CD11b^{+}CD11c^{+}$ cells). Data is displayed as the mean percent change in subset size relative to 0 nM queuine. Error bars represent one standard deviation. Significance was calculated with Welch's *t*-test using 0 nM as the control. $n = 4$ biological replicates. ns: not significant, *: $p < 0.05$, **: $p < 0.01$.

4.2.2 MHC-II levels are also sensitive to $preQ_1$ but only at low concentration

In both our proliferation (**Figure 3.1E**) and mRNA-seq (**Figure 3.2**) studies in BMDCs, we find that Q and $preQ_1$ elicit opposite effects on cell physiology. These results led us to wonder whether the same is true for MHC-II expression.

To assess this phenotype, BMDCs were extracted from mice and treated with 0.1 μM queuine, 0.1 μM $preQ_1$, or 10 μM $preQ_1$ on Day 0 or Day 3 of the differentiation process (**Figure 4.2A**). Two treatment times were evaluated due to the significant attenuation of BMDC proliferation that occurs in response to $preQ_1$. On Day 5, BMDCs were antibody-labeled, stained, and analyzed using the same $CD11b^{+}MHC\text{-}II^{Low/Med/High}$ subpopulation designations as described above (**Figure 4.1C**). For any one condition tested, no significant difference was observed between cells treated on Day 0 and Day 3 (**Figure 4.2B**). As previously observed, addition of 0.1 μM queuine caused an increase in the $CD11b^{+}MHC\text{-}II^{Med}$ subset and a corresponding decrease in the $CD11b^{+}MHC\text{-}II^{Low}$ subset. No difference was observed in the $CD11b^{+}MHC\text{-}II^{High}$ subset population for queuine-treated cells at either timepoint, though it is worth noting that this subset accounted for less than 5% of $CD11b^{+}CD11c^{+}$ cells across all conditions (**Figure S4.1E**). BDMCs treated with 0.1 μM $preQ_1$ exhibit the opposite phenotype. In these cells, the relative $CD11b^{+}MHC\text{-}II^{Low}$ subset population increases by ~20%. Conversely, the $CD11b^{+}MHC\text{-}II^{Med}$ subset decreases, corresponding to an overall attenuation of MHC-II expression. The $CD11b^{+}MHC\text{-}II^{High}$ subset population also decreases significantly. Astoundingly, when the concentration of $preQ_1$ is increased to 10 μM, the observed effect goes away altogether, and MHC-II expression patterns return to that of control

(0Q) cells. The only exception is the CD11b^{+}MHC-II^{High} subset in cells treated at Day 0, which decreases in size from ~3% to ~1% (**Figure S4.1E**). Taken together, our results confirm that queuine and preQ$_1$ cause significant and sustained changes in MHC-II expression in murine BMDCs.

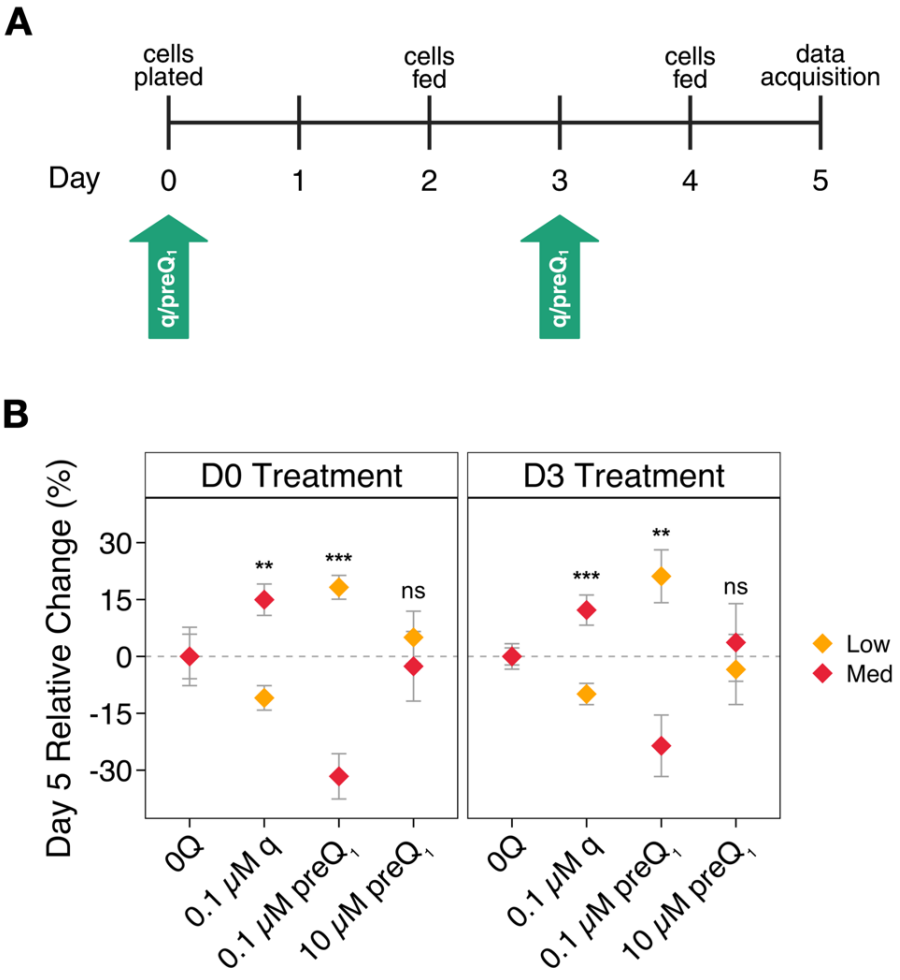

Figure 4.2: MHC-II expression is sensitive to preQ$_1$ at low concentration only.

(A) Experimental schematic used to evaluate preQ$_1$ effect on BMDC MHC-II expression. Extracted cells are cultured with GM-CSF and fed culture medium containing GM-CSF on Days 2 and 4. Queuine or preQ$_1$ was added either on Day 0 or Day 3.
(B) Changes in CD11b^{+}MHC-II^{Low} and CD11b^{+}MHC-II^{Med} populations on Day 5 in –LPS BMDCs treated with queuine or preQ$_1$ on Day 0 (left) or Day 3 (right). Subset population sizes were measured as a percentage of the parent gate (CD11b^{+}CD11c^{+} cells). Data is displayed as the mean percent change in subset size relative to 0Q cells. Error bars represent one standard deviation. Significance was calculated with Welch's *t*-test 0Q as the control. $n = 5$ biological replicates. ns: not significant, **: $p < 0.01$, ***: $p < 0.001$.

4.3 Discussion

In these studies, we demonstrated that both queuine and $preQ_1$ – two microbe-derived metabolites – elicit an effect on MHC-II expression in murine BMDCs. Using antibody labeling and flow cytometry, we show that MHC-II expression generally correlates positively with queuine concentration, whereas it decreases at nanomolar concentrations of $preQ_1$ in culture medium. This result is consistent with our previous proliferation and mRNA-seq experiments (Chapters 2 and 3) in two major ways. Firstly, the two metabolites act in opposite ways on cell culture phenotypes. Secondly, high levels of $preQ_1$ treatment return the observed phenotype to baseline levels. As guanine derivates, queuine and $preQ_1$ are highly structurally similar and share a 7-deazaguanosine core. Considering this, along with the fact that both metabolites are known substrates of eukaryotic QTRT1/QTRT2,[133] it is reasonable to hypothesize that queuine and $preQ_1$ act on the same cellular pathways to up- or down-regulate MHC-II expression.

The mammalian gut microbiome has been extensively studied and is well understood to play a role in host health, particularly in the context of metabolic diseases, mental wellbeing, and immune system function.[223-225] Bacteria in the digestive tract are responsive to the host's environment, ingested food, and psychological state.[226,227] For example, several studies have shown that probiotic consumption, aimed to promote gut microbiome health, can reduce stress-associated and depressive symptoms in humans.[228,229] In turn, metabolites produced by bacteria – including small molecules, fatty

acids, polyamines, vitamins, and more – interact with host cells and elicit on effect on their physiology.[230]

It is unsurprising, then, that dysbiosis of the gut microbiome can perturb host health, and vice versa. Several human pathologies, such as inflammatory bowel disease (IBD), liver cirrhosis, atherosclerosis, and type 2 diabetes, are associated with abnormal composition and function of the gut microbiota.[231-233] Moreover, antibiotic use is known to cause significant perturbations in the composition of the gut microbiome and decrease the presence of several phyla considered important for host homeostasis.[234,235]

However, the roles of Q-tRNA, queuine, $preQ_1$, or related metabolites in host health or immune function remains poorly understood. A recent study in patients with IBD, a gastrointestinal autoimmune disorder, found that QTRT1 expression was reduced and altered QTRT1-related metabolites were present.[146] Moreover, queuine treatment improved cell junction activity and reduced epithelial cell inflammation in *in vitro* and *in vivo* models of IBD. On the other hand, studies of $preQ_1$ and mammalian cell physiology are even more limited, with no published work characterizing any physiological roles of the Q-tRNA precursor *in vivo* (breakthrough Pan lab paper accepted for publication).

Our data reveal a novel connection between queuine, $preQ_1$, and immune signaling pathways in a primary cell model. We report changes in $CD11b^{+}MHC\text{-}II^{Low}$ and $CD11b^{+}MHC\text{-}II^{Med}$ populations in the range of ±30% (**Figure 4.1D,E; Figure 4.2B**). Based on existing immunology literature, these magnitudes are biologically significant and would likely correspond to a meaningful change in DC activity.[236-238] The extent to which

Q-modification and related metabolites play a role in host immune response remains an exciting area for further study and exploration.

4.4 Materials and Methods

Mice

Female C57BL/6J mice were obtained from Jackson Laboratories. Mice were housed under specific pathogen-free and BSL2 conditions at the University of Chicago. All experiments were conducted following the guidelines set by the US National Institutes of Health Guide for the Care and Use of Laboratory Animals and were approved by the Institutional Animal Care and Use Committee at the University of Chicago.

BMDC Cell Culture

Murine BMDCs were generated from 6-8 week-old C57BL/6J female mice. Bone marrow cells were collected from femora and tibiae and cultured at 37°C in RPMI-1640 (Gibco; AM9260G) supplemented with 10% v/v dialyzed fetal bovine serum (Gibco; 26400044), 1% v/v L-glutamine (Gibco; 25030081), 1% v/v penicillin-streptomycin (Gibco; 15140122), 1% v/v MEM non-essential amino acids (Corning; MT25025CI), 1% v/v HEPES (Gibco; 15630080), 1% v/v sodium pyruvate (Corning; MT25000CI), and 0.1% v/v β-mercaptoethanol (Gibco; 21985023). Recombinant murine GM-CSF (Peprotech 315–03-100μg) at 15 ng/mL was added to the complete RPMI medium. Cells were fed at Days 2 and 4 with complete RPMI medium containing GM-CSF.

MHC-II Expression

Murine bone marrow cells were plated at 1×10^5 cells/well in a flat-bottom, non-tissue culture treated 96-well plate (GenClone; 25-104) in 150 µL of complete RPMI-1640, described above. For the queuine screen, cells were fed with 50 µL of complete RPMI medium containing GM-CSF on Day 2. On Day 4, queuine was also added to the GM-CSF-containing RPMI to achieve eight different treatment conditions: 0, 1, 3, 10, 30, 100, 300, and 1000 nM queuine. All conditions were plated in quadruplicate. For the queuine/$preQ_1$ study, cells were treated either immediately (Day 0) or on Day 3. All cells were fed on Days 2 and 4 with 50 µL of complete RPMI medium containing GM-CSF ± queuine ± $preQ_1$. All conditions were plated in quintuplicate.

For the queuine screen, BMDCs were treated with either complete medium containing LPS at a final concentration of 100 ng/mL (+LPS) or complete medium alone (–LPS) on Day 5. Cells were returned to a 37°C incubator for 6 hours. Following activation, BMDCs were resuspended and transferred to a 96-well V-bottom acquisition plate (Sarstedt; NC0068972). For the queuine/$preQ_1$ study, cells were transferred to the V-bottom acquisition plate without LPS-induced activation. To loosen adherent cells, 100 µL of 10 mM EDTA (Invitrogen; AM9260G) in 1× DPBS (Gibco; 14190094) was added to the flat-bottom seeding plate, which was then incubated at 37°C for 10 minutes. After incubation, the cells were again resuspended and transferred to the corresponding well of the acquisition plate. The seeding plate was washed once more with 50 µL 1× DPBS to transfer remaining cells to the acquisition plate. The acquisition plate was centrifuged at 1500 rpm for 5 minutes at 4°C. The supernatant was removed, and pellets were

resuspended with cold FACS buffer (DPBS containing 0.05% v/v dialyzed FBS and 2 mM EDTA) with 10 µg/mL TruStain FcX™ (anti-mouse CD16/32) Antibody (BioLegend; 101320) and incubated on ice for 10 minutes. From this step onward, cells were kept cold and shielded from light.

Cells were then stained with anti-CD11b (BioLegend; 101206), anti-CD11c (BioLegend; 117310), and anti-MHC-II (I-A/I-E) antibodies (BioLegend; 107630) and incubated on ice for 20 minutes. After staining, the plate was centrifuged at 1500 rpm for 5 minutes at 4°C. Cells were resuspended with 100 µL cold FACS buffer with 0.1 µg/mL DAPI (Biotium; 40043) to exclude dead cells. Single-stain controls, fluorescence minus one (FMO) controls, and an unstained control were included. Flow cytometry data were acquired on the NovoCyte Penteon and analyzed using FlowJo and R software. Welch's *t*-test was used to assess pairwise comparisons between treatments and generate *p*-values. Significance levels were annotated on the plots as follows: $p < 0.05$ (*), $p < 0.01$ (**), and $p < 0.001$ (***).

Chapter 5 – preQ$_1$ analog probes reveal a potential new role for microbial metabolites in eukaryotic RNA-protein interactions

5.1 Introduction

Riboswitches are structured RNA elements, typically located in the 5' UTRs of bacterial mRNAs, that regulate gene expression *in cis* by directly binding small molecule metabolites. A typical riboswitch has two functional domains: the aptamer domain, which binds the ligand, and the expression platform, which undergoes conformational changes upon ligand binding.[184] The conformational changes influence transcription termination, translation initiation, or mRNA stability to enable precise gene expression regulation without requiring protein intermediates.[239,240] Importantly, riboswitches allow bacteria to respond efficiently to metabolic shifts or environmental pressures. While very common in bacteria, only one riboswitch class has been described in eukaryotes.[241-243] Nonetheless, the specificity and compact structure of these RNA-based sensors make them attractive models for the study of RNA folding and RNA-ligand interactions.[244]

Among the classes of riboswitches, those responsive to purine analogs – such as guanine, adenine, and their derivatives – are highly prevalent. In fact, half of known riboswitches bind a compound containing a purine or related moiety.[184] The preQ$_1$ riboswitch is particularly noteworthy as the smallest naturally occurring riboswitch, containing as few as 34 nt. PreQ$_1$ riboswitches are grouped into three structurally distinct classes – preQ$_1$-I, II, and III – with preQ$_1$-I being the most prevalent.[245] Several of the genes regulated by preQ$_1$-I riboswitches are involved in the biosynthesis of bacterial Q-tRNA, creating a feedback loop through which Q-modification levels are regulated.[246]

Advances in chemical biology have enabled the development of metabolite analog probes to investigate riboswitch-ligand dynamics *in vitro*. In a landmark study, Balaratnam et al. (2021) presented a series of $preQ_1$ analog probes for covalent labeling of bacterial $preQ_1$-I riboswitches.[247] Their most active probe comprised a $preQ_1$ analog functionalized with a diazirine ring for photoaffinity labeling (**Figure 5.1A**) and exhibited high specificity for the bacterial $preQ_1$ riboswitch aptamer over all other human RNAs *in vitro*. Fascinatingly, in the absence of aptamer, the probe enriched 16 human RNA transcripts: 14 histone mRNAs and 2 ncRNAs of TERC and RMRP, the latter of which form ribonucleoprotein complexes with the human telomerase catalytic subunit (hTERT).[248] All 16 transcripts contain stable RNA secondary structures, suggesting that metabolite-RNA interactions may occur in eukaryotic systems, albeit differently than in a bacterial riboswitch. Despite this exciting *in vitro* result, the potential role of $preQ_1$ or related compounds as binding partners of eukaryotic RNAs has not been explored in a cell culture model.

Here, we evaluated the utility of two $preQ_1$ analog probes as tools in mammalian RNA biology. We conducted proliferation assays to characterize the bioactivity of the probes in human cell culture and identify a candidate probe for further study. Using a modified Northern blot protocol and MSR-seq, we demonstrate that this probe is a substrate of QTRT1/QTRT2 and selectively enriches Q-modifiable tRNAs. Finally, we identify a Q-dependent effect on histone mRNA expression in a liver cancer cell line. Our results provide preliminary support for the model that metabolites – such as guanine, $preQ_1$, and queuine – have specific binding interactions with eukaryotic RNA “aptamers”.

5.2 Results

5.2.1 preQ$_1$ analog probes have queuine-like bioactivity in mammalian cell culture

For this work, we utilized the two most active preQ$_1$ analog photoaffinity probes, probe 11 (p11) and probe 13 (p13), generously provided by the Schneekloth group.[247] Both p11 and p13 are structural analogs of preQ$_1$ (**Figure 5.1A**), contain an alkyne handle to enable further modification, and have high (>30%) UV-activated crosslinking efficiency to the preQ$_1$ riboswitch aptamer domain. Whereas p11 retains the secondary amine group in the endogenous preQ$_1$ metabolite, p13 does not.

We were first interested in evaluating whether, like preQ$_1$, the probes attenuated proliferation of mammalian cell culture. 0Q HEK293T cells were grown in DFBS medium containing preQ$_1$ (1 μM), p11, or p13. Each probe was tested at final concentrations of 0.1 μM, 1 μM, and 10 μM. Proliferation was measured for six days using CCK-8 assay (**Figure 5.1B**). As expected based on our previous experiments, preQ$_1$-treated cells proliferate much less compared to control (0Q). However, neither p11- nor p13-treated cells exhibited any changes in proliferation. At all concentrations tested, probe-treated cell growth was not statistically significantly different from 0Q. These results do suggest that both probes have little to no cytotoxicity in HEK293T cells, even at concentrations up to 10 μM.

Since the probes did not attenuate cell growth, we wondered whether they instead rescue the proliferation of preQ$_1$-treated cells, like queuine. Again, HEK293T cells were grown in DFBS medium for six days in the presence of 1 μM preQ$_1$ ± p11, p13, or queuine for six days (**Figure 5.1C,D**). We observed a concentration-dependent

proliferation rescue effect across 0.1-10 μM for both p11 and p13. Of note, the probes are much less efficacious for proliferation rescue than queuine. Whereas 10 nM queuine is sufficient for a return to control (0Q) proliferation, 10 μM of p11 was required for the same effect. This difference is even greater for 10 μM p13, which rescued proliferation to only ~75% that of control cells. Because p11 displayed more potent bioactivity than p13 and was found to have marginally more crosslinking activity,[247] it was selected for further characterization and subsequent experiments.

We next wished to confirm whether p11 is a suitable substrate for QTRT1/QTRT2 and assess how competitive it is with $preQ_1$ and queuine in cell culture. HEK293T cells were grown in control (0Q) medium, p11 (10 μM), p11 (10 μM) + $preQ_1$ (1 μM), or p11 (10 μM) + queuine (10 nM) for 24 hours before collection of total RNA. To create band separation between p11-tRNA and other tRNA species on an APB gel, we utilized click chemistry to selectively PEGylate the alkyne handle present on p11 (**Figure 5.1E**). The samples were then run on a standard APB gel for Northern blot of $tRNA^{Asp}$ (**Figure 5.1F**). In the presence of 10 μM p11 alone, approximately 32% of $tRNA^{Asp}$ are p11-modified (**Figure 5.1G**). The incorporation rate of p11 is reduced to ~5% when cells are co-treated with 1 μM $preQ_1$ and ~12% when cells are co-treated with 10 nM queuine. The >1,000-fold difference in rescue efficacy between p11 and queuine (**Figure 5.1C,D**) can likely be attributed, in part, to how effectively each molecule serves as a substrate for QTRT1/QTRT2. These results confirm that p11 is internalized by HEK293T cells, utilized by QTRT1/QTRT2 for transglycosylation, and competes with both $preQ_1$ and queuine as a QTRT1/QTRT2 substrate in mammalian cells.

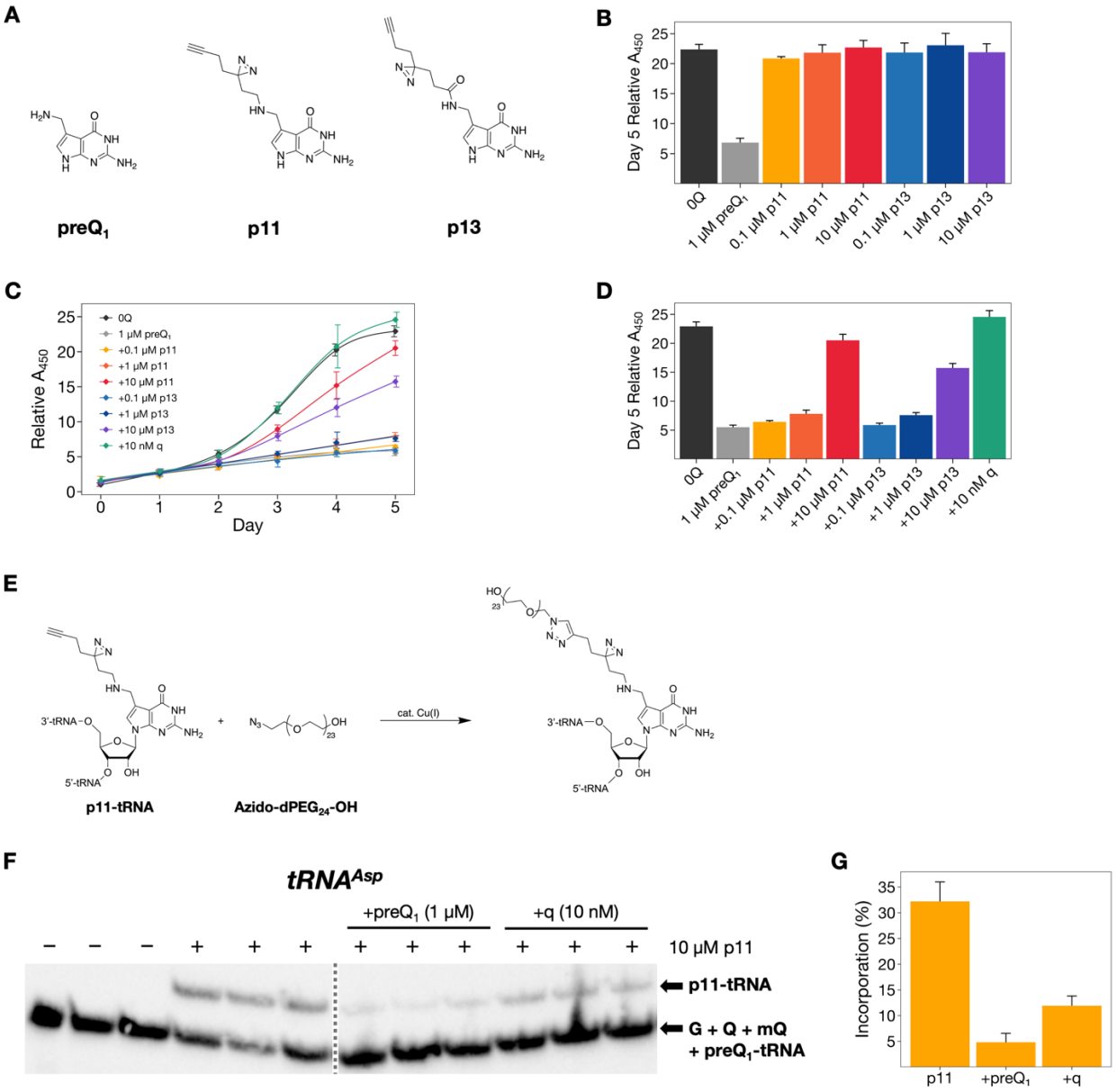

Figure 5.1: preQ$_1$ analog probes exhibit similar bioactivity to queuine.

(A) Chemical structures of preQ$_1$, probe 11 (p11), and probe 13 (p13).
(B) HEK293T cell proliferation, measured by CCK-8 assay, in response to preQ$_1$, p11, or p13. Relative A_{450} was calculated as the sample A_{450} divided by the mean A_{450} for 0Q at Day 0. Bars represent the mean (n = 8) and error bars represent one standard deviation.
(C-D) HEK293T cell proliferation, measured by CCK-8 assay, in response to preQ$_1$ alone or cotreatment with p11, p13, or queuine shown. (**C**) shows data for Days 0-5, while (**D**) shows the same experimental data for Day 5 only. Relative A_{450} was calculated as the sample A_{450} divided by the mean A_{450} for 0Q at Day 0. Bars and points represent the mean (n = 8) and error bars represent one standard deviation.
(E) Reaction schematic for copper-catalyzed PEGylation of p11-tRNA.
(F) Northern blot of tRNA^{Asp} in 0Q HEK293T cells grown in control medium, 10 μM p11, 10 μM p11 + 1 μM preQ$_1$, or 10 μM p11 + 10 nM q for 24 hours; APB gel with biological triplicates. G: unmodified G34-tRNA, Q: Q34-tRNA; mQ: manQ-tRNA.
(G) Quantification of p11 incorporation into tRNA^{Asp} in (**F**) as a percentage of total tRNA.

5.2.2 Q-modifiable tRNAs are selectively enriched by preQ$_1$ analog probes

Having established that p11 has queuine-like bioactivity in cell culture and is incorporated into tRNA, we next wanted to evaluate whether the probe selectively captures Q-modifiable tRNA species. To that end, 0Q HEK293T cells were grown in queuine-free medium and treated with 10 μM p11 for 12 hours. Cells were either UV-crosslinked (+UV) or kept in the dark (–UV) before RNA extraction. To select for probe-labeled RNA species, we used copper-catalyzed click chemistry to covalently and selectively biotinylate at the alkyne handle of p11. Samples were then enriched on streptavidin beads prior to subsequent MSR-seq library preparation. Sequencing library analysis revealed that p11 selectively captures the four Q-modified tRNA isoacceptor families (**Figure 5.2**).

Abundance was evaluated relative to probe-free control (enrichment over bead, **Figure 5.2A**) as well as relative to the 0Q HEK293T tRNAome (enrichment over cell, **Figure 5.2B**). In both comparison methods, we observe enrichment of eight tRNAs (Asn, Asp, His, Tyr, mtAsn, mtAsp, mtHis, and mtTyr) in both +UV and –UV conditions. Enrichment of cytosolic tRNA species was generally stronger than that of mitochondrial tRNA species. Capture of the Q-modifiable tRNAs in UV-free (–UV) conditions can be attributed to covalent insertion of p11 at position 34 by QTRT1/QTRT2. With the exception of tRNA^{Asp}, sample crosslinking (+p11/+UV) resulted in similar or greater enrichment compared to probe alone (+p11/–UV). Taken together, our results indicate that p11 has utility in mammalian cell culture and effectively captures the tRNA interacting partners of queuine.

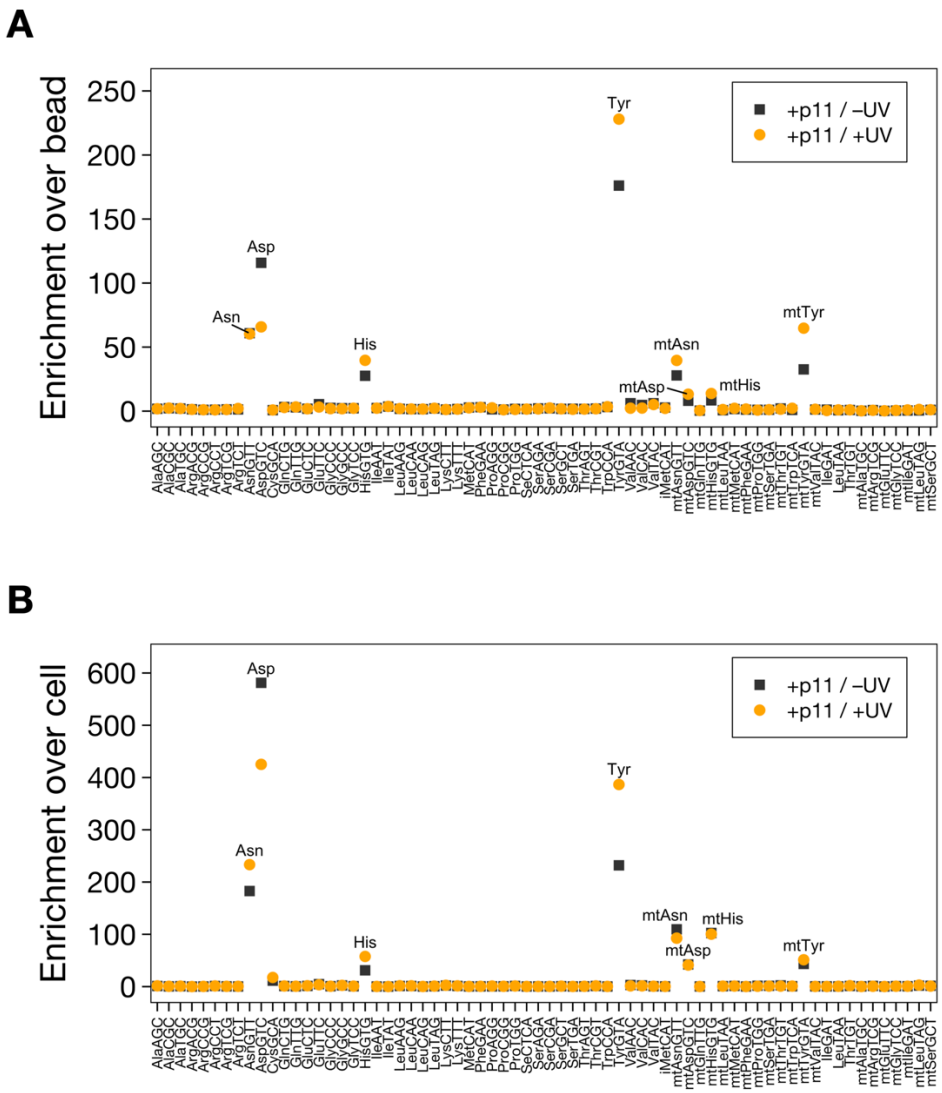

Figure 5.2: p11 selectively enriches Q-modifiable tRNAs in HEK293T cells.

(A) Enrichment of tRNA isodecoders in p11-treated samples relative to untreated control (–p11/+UV) samples. Q-modified tRNAs are labeled. mt: mitochondrial. *n* = 2 replicates.
(B) Enrichment of tRNA isodecoders in p11-treated samples relative to 0Q HEK293T tRNAome. Q-modified tRNAs are labeled. mt: mitochondrial. *n* = 2 replicates.

5.2.3 Histone mRNA expression is responsive to Q levels in liver cancer cells

In their paper, Balaratnam et al. identify 16 human cellular RNAs enriched by p11 *in vitro* in the absence of bacterial $preQ_1$ riboswitch aptamer.[247] Of those RNAs, 14 belong to the histone mRNA family. Moreover, additional sequencing data and competition studies with endogenous $preQ_1$ metabolite demonstrated that the enriched RNAs selectively bind $preQ_1$. These results led us to wonder whether our p11 MSR-seq libraries indicated enrichment of any non-tRNA species. Using the same sequencing libraries as above, we aligned our reads to a modified reference genome which included histone mRNA, ribosomal RNA (rRNA), small nuclear RNA (snRNA), and Y RNA species.

Though they differ broadly in length and function, these RNA classes are alike in that they contain regions with defined secondary structure motifs (e.g., hairpins, loops, and bulges).[249-252] Interestingly, we find that some, but not all, of these RNAs were enriched in p11-treated libraries (**Figure 5.3A**). Generally, capture of rRNAs (5S rRNA, 5.8S rRNA) and Y RNAs (RNY1, RNY3, RNY4, RNY5) was low, and no change in enrichment is observed when comparing +UV and –UV samples. On the other hand, several histone mRNAs and snRNAs (RNU1-1, RNU2-1, RNU4-1, RNU5A-1, and RNU6-1) are enriched in our p11-treated libraries. Among the histone mRNA, enrichment of all but H2BC11 is elevated in crosslinked (+UV) libraries compared to –UV libraries, suggesting successful proximity labeling in our protocol. Like 5S rRNA (~120 nt), 5.8S rRNA (~160 nt), and Y RNAs (83-112 nt), snRNAs are classified as small RNA and are ~150 nucleotides in length.[251] This is in contrast with the histone mRNA transcripts, which comprise hundreds of nucleotides, indicating that the observed proximity labeling

by p11 does not depend on the RNA size. Our results provide additional evidence for $preQ_1$-RNA interaction in human histone mRNAs and indicate that secondary structure may be important, but is not sufficient, for this interaction to occur.

In all metazoans, the majority of histone mRNAs are unique in that they lack a 3' polyadenylation tail. Instead, they contain a 26-nt stem-loop near the 3' end.[253,254] This conserved secondary structure motif is recognized and bound by SLBP (stem-loop binding protein), a factor required for several steps of histone mRNA metabolism: pre-mRNA processing, translation, and mRNA degradation.[255] Histone mRNA transcription is tightly regulated throughout the cell cycle. As cells divide, the rapid production of histone proteins is required to package newly-replicated DNA.[255,256] Consequently, intracellular levels of replication-dependent histone mRNAs increase by about 35-fold as cells enter S (synthesis) phase before returning to baseline levels as mitosis begins.[257] Considering the structural similarities between $preQ_1$, p11, and queuine, our sequencing results led us to wonder whether histone mRNA levels are sensitive to queuine availability. In Chapter 2, we demonstrated that Q-modification levels are positively correlated to proliferation in HEK293T cells (**Figure 2.1B**). It is reasonable to wonder, then, whether elevated histone gene transcription will be observed in 100Q cells due to increased cell division. To investigate, we used RT-qPCR to quantify mRNA transcript levels for several histone genes and SLBP in 0Q and 100Q HEK293T cells but observed no significant changes (**Figure 5.3B**).

Whereas HEK293T cells are stable for months in 0Q conditions, HepG2 cells (an immortalized cell line derived from human hepatocellular carcinoma) have diminished

viability in 0Q conditions after a few weeks (unpublished result from the Pan lab). In fact, Northern blots of $tRNA^{His}$ and $tRNA^{Asp}$ in 0Q and 100Q HepG2 RNA reveal an unidentified tRNA species present only in 0Q samples (**Figure 5.3C**). This may be a tsRNA species associated with stress-induced upregulation of tRNA fragmentation.[258] Given that HepG2 cells are more physiologically sensitive to queuine depletion, we were curious to see how their histone mRNA transcript levels responded to queuine availability. We repeated the RT-qPCR analysis in 0Q and 100Q HepG2 cells and found several significant expression changes (**Figure 5.3D**). Broadly, histone mRNA transcription is upregulated in 100Q HepG2 cells. SLBP mRNA levels are also elevated, which is likely due to the increased cellular demand for histone pre-mRNA processing in 100Q conditions. These exciting preliminary results reveal a potential role for $preQ_1$ and queuine as interacting partners of metazoan histone mRNAs and serve as the basis for our proposed mechanism, described further below.

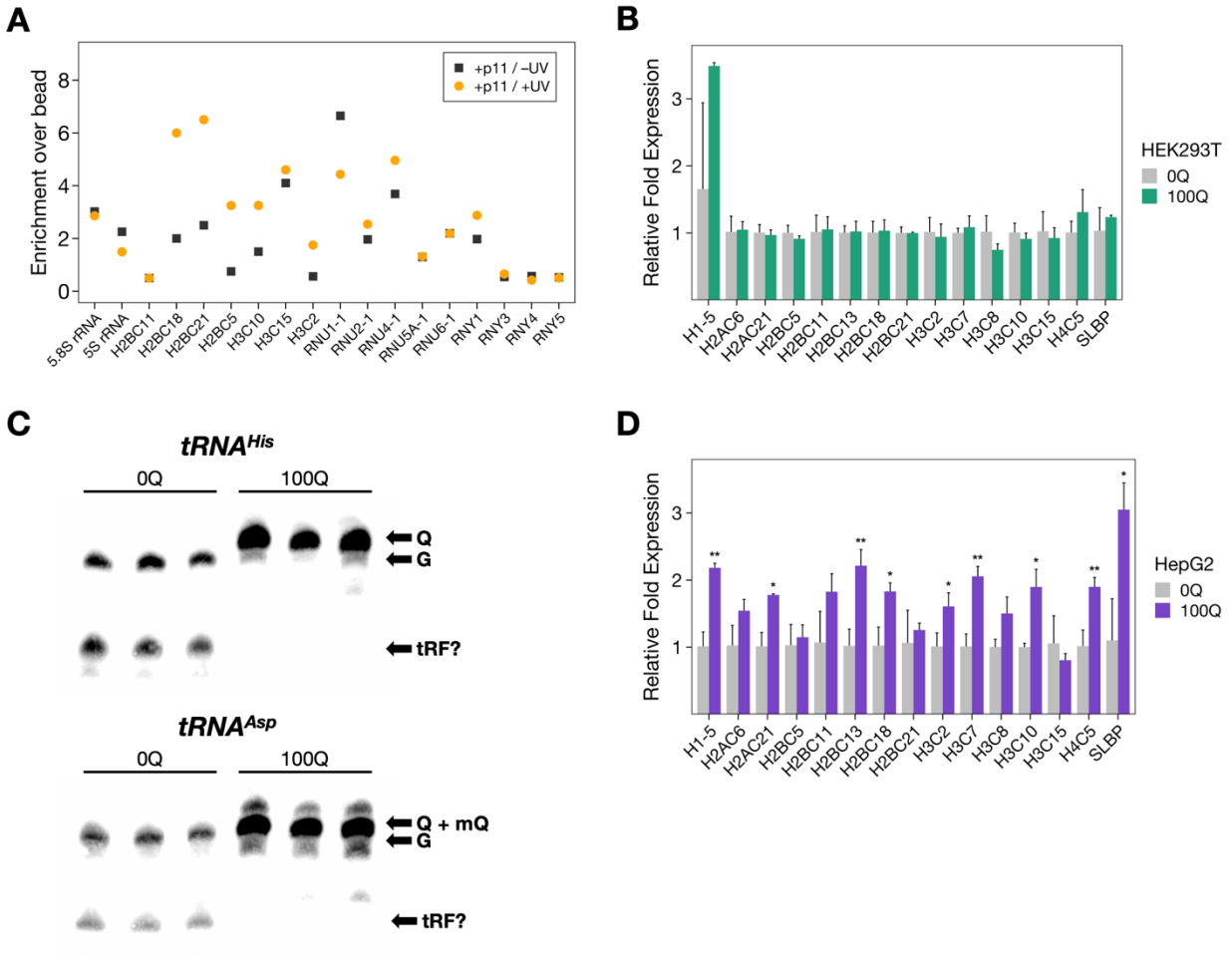

Figure 5.3: Queuine impacts histone mRNA expression in HepG2 cells.

(A) Enrichment of select HEK293T RNAs in p11-treated samples relative to untreated control (–p11/+UV) samples. *n* = 2 replicates.
(B) Levels of various histone mRNA and SLBP mRNA transcripts in 0Q and 100Q HEK293T cells. Bar heights represent the mean of *n* = 3 biological replicates, and error bars represent one standard deviation.
(C) Northern blot of $tRNA^{His}$ (top) and $tRNA^{Asp}$ (bottom) in 0Q and 100Q HepG2 cells, APB gel, biological triplicates. G: unmodified G34-tRNA, Q: Q-modified Q34-tRNA, mQ: manQ-modified tRNA.
(D) Levels of various histone mRNA and SLBP mRNA transcripts in 0Q and 100Q HepG2 cells. Bar heights represent the mean of *n* = 3 biological replicates, and error bars represent one standard deviation.

5.3 Discussion

Here, we characterize the functionality of two photoactivatable $preQ_1$ analog probes – p11 and p13 – in mammalian cell culture. Though they were originally designed for and characterized in *in vitro* work focusing on the bacterial $preQ_1$ riboswitch,[247] we demonstrate that both probes exhibit queuine-like bioactivity in HEK293T cells and rescue $preQ_1$-induced antiproliferative effects. Both probes are less efficacious in this regard than queuine, with p11 having stronger activity than p13. Additionally, we report that p11 is internalized by cells and inserted into Q-modifiable tRNAs by QTRT1/QTRT2. Moreover, p11 competes with both $preQ_1$ and queuine as a substrate for QTRT1/QTRT2. Using MSR-seq, we find that p11 selectively captures Q-modifiable tRNAs (both with and without UV crosslinking) and has some capture affinity for several histone mRNAs and snRNAs.

In their paper, Balaratnam et al. report that p11 enriches human histone mRNAs *in vitro* and that enrichment is diminished with addition of 25 μM and 100 μM of $preQ_1$, suggesting a specific $preQ_1$-RNA binding event.[247] Along with our own capture data, these results led us to wonder whether histone mRNA expression is sensitive to queuine availability in culture medium. Though we found no changes in transcript levels comparing 100Q vs. 0Q HEK293T cells, several histone mRNA transcripts were upregulated in 100Q vs. 0Q HepG2 cells. This is yet another example of the context-dependence of Q-tRNA biology, which has been previously reported.[151-153] Moreover, this result reveals a plausible connection between Q-modification and histone mRNA processing.

The orchestration of histone protein translation is a critical cellular process. Histone mRNA transcription follows a replication-dependent pathway distinct from that of canonical mRNAs (**Figure 5.4**). Lacking introns and a polyadenylation tail, they instead rely on structural and sequence elements – the highly-conserved 3' stem-loop and a downstream histone downstream element (HDE) – that facilitate RNA-binding protein interaction.[255,259] Both histone mRNA levels and SLBP protein levels are tightly coupled to cell cycle progression, increasing rapidly as cells enter S phase and depleting rapidly as cells enter G_2.[254] At the beginning of S phase, SLBP binds the stem-loop of newly-transcribed histone pre-mRNAs in the nucleus. At the same time, U7 small nuclear ribonucleoprotein (U7 snRNP) base-pairs with the HDE and acts as a molecular ruler to position the pre-mRNA cleavage site between the stem-loop and HDE.[259] Other factors are recruited to stabilize the transcript and facilitate mRNA processing. The SLBP-bound mRNA is then exported to the cytoplasm for translation. At the end of S phase, SLBP is degraded, and the histone mRNA stem-loop is bound by 3'hExo, an exonuclease which cleaves the stem-loop to initiate mRNA degradation.[260]

There are RNA-protein interactions at nearly all steps of the histone mRNA life cycle, and RNA structure is relevant for many of those steps: SLBP binding, U7 snRNP formation, translation (i.e., tRNAs), and 3'hExo binding. Similarly, RNA structure is critical for the bacterial $preQ_1$ riboswitch, which comprises two stems and three loops and adopts an H-type pseudoknot form when bound by $preQ_1$.[261] Whereas ligand-binding riboswitches are highly prevalent in bacteria, only one class of eukaryotic riboswitch has been described to date.[241-243] However, there are several reports implicating guanine and

guanine derivatives in RNA-protein interactions.[262,263] It is plausible that $preQ_1$ and queuine interact with RNA structural motifs at the RNA-protein interfaces occurring throughout the histone mRNA life cycle to impact transcript levels. Whether these interacts occur is an area of interest for future study.

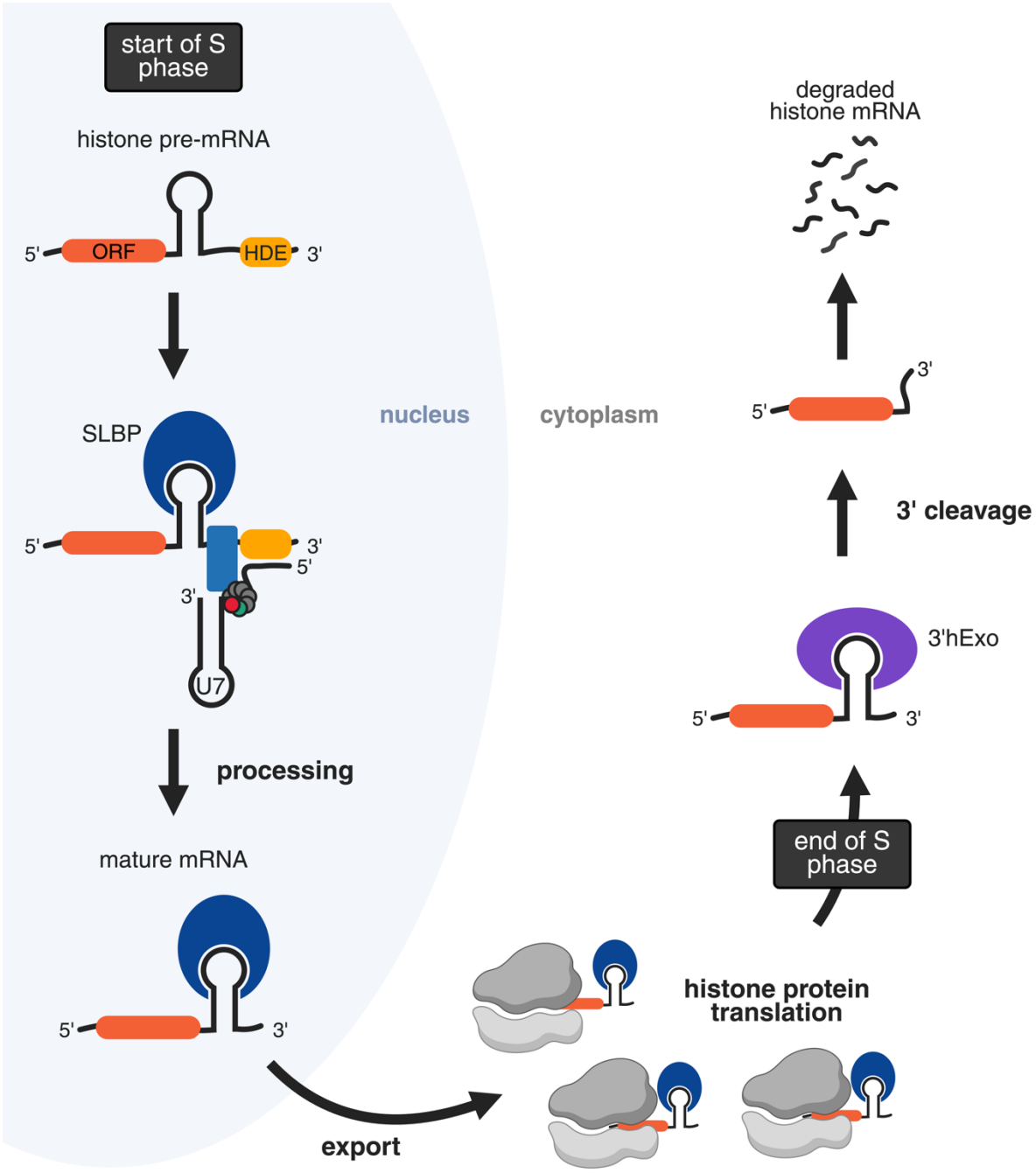

Figure 5.4: Replication-dependent histone mRNA expression.

As S phase begins, histone pre-mRNA is bound by SLBP, U7 snRNP (U7), and other factors to initiate cleavage near the HDE. Mature histone mRNA is exported from the nucleus for translation. At the end of S phase, SLBP is degraded. 3'hExo binds and cleaves the stem-loop to initiate mRNA degradation. HDE: histone downstream element, ORF: open reading frame. Adapted from Jaeger et al. (2005), Marzluff and Duronio (2002).[257,259]

5.4 Materials and Methods

HEK293T and HepG2 Cell Culture and RNA Extraction

Both 0Q and 100Q HEK293T and HepG2 cells were obtained as previously reported.[139,163] Briefly, cells were cultured at 37°C in DMEM (Cytiva; SH30022.01) supplemented with 10% volume/volume (v/v) dialyzed fetal bovine serum (Gibco; 26400044) and 1% v/v Penicillin-Streptomycin (Thermo Fisher; 15070063) to 80% confluency. 100Q cells were obtained by culturing 0Q cells with 1 μM queuine (Toronto Research Chemicals) for 24 hours. TRIzol™ reagent (Thermo Fisher; 15596026) was used to extract total RNA according to the manufacturer's manual.

HEK293T Proliferation Assays

0Q HEK293T cells were plated at 5×10^3 cells/well in a tissue culture treated 96-well plate (Dot Scientific; 667195) in 100 μL of DMEM as described above. Both probe 11 (p11) and probe 13 (p13) were generously provided by the Schneekloth lab.[247] Appropriate volumes of $preQ_1$ (Cayman Chemical), p11, p13, and/or queuine (Toronto Research Chemicals) were added to achieve the treatment conditions, with 0Q cells serving as the untreated control. All conditions were plated with $n = 8$ replicates. Six 96-well plates were prepared – one per measurement time point (0, 1, 2, 3, 4, and 5 days).

HEK293T cell proliferation was measured using the Cell Counting Kit-8 (CCK-8) (Dojindo; CK04-13) according to manufacturer protocol. Briefly, immediately after plating, 10 μL of WST-8 solution was added to each well of the Day 0 plate. The plate was wrapped in aluminum foil and incubated at 37°C for 2 hours. Following incubation, absorbance at 450 nm was measured using a microplate reader to assess cell viability.

WST-8 addition, incubation, and absorbance measurement steps were repeated every 24 hours using the corresponding plate.

The data were visualized using R. Relative A_{450} for each well was calculated as the A_{450} divided by the mean A_{450} for 0Q at Day 0. Data points and bar heights represent the mean of samples, and error bars represent one standard deviation.

Probe 11 Incorporation and Click Chemistry

0Q HEK293T cells were plated at 3×10^5 cells/well in a tissue culture treated 6-well plate (Corning; 353046) in 2 mL of DMEM as described above until 50% confluence. At this time, cells were treated with control medium, 10 μM p11, 10 μM p11 + 1 μM $preQ_1$, or 10 μM p11 + 10 nM q for 24 hours. All conditions were plated in triplicate. To assess only QTRT1/QTRT2-mediated insertion of p11 into substrate tRNAs, cells were protected from light and no UV crosslinking was used. RNA was collected using TRIzol™ reagent (Thermo Fisher; 15596026). Samples were quantified via Nanodrop 2000c (Thermo Scientific) and normalized to 2 μg/μL. Click chemistry was performed to selectively PEGylate p11-tRNAs. First, 10 mM Azido-$dPEG_{24}$-OH (Quanta Biodesign; 10544) in DMSO was added to all samples. The click reaction was catalyzed with L-ascorbic acid (200 mM) and a 2:1 mixture of tris-hydroxypropyltriazolylmethylamine (THPTA, 200 mM):$Cu(II)SO_4$ (100 mM) for one hour at room temperature with periodic vortexing. RNA was purified using glycogen (Invitrogen; AM9510) precipitation. Briefly, 0.1 volume of 3M sodium acetate (pH 5.2), glycogen (100 μg/mL final concentration), and 2.5 volumes of ice-cold 100% ethanol were added to all samples and incubated at -80°C overnight. Samples were spun at max speed for 20 minutes at 4°C. Pellets were

washed with ice-cold 70% ethanol, spun again at max speed for 20 minutes at 4°C, and resuspended in water for analysis by Northern blot (below).

Northern Blots

All Northern blots were performed as previously described[132] using 1-3 µg of total RNA. In $tRNA^{Asp}$ and $tRNA^{Tyr}$, Q34 is glycosylated to form manQ and galQ, respectively. These hypermodified tRNAs require an acid denaturing gel to be distinguishable from G34-tRNAs. To assess p11 incorporation into HEK293T tRNA, we used an APB gel with $tRNA^{Asp}$ probe to provide minimal, if any, resolution between G34-tRNAs, Q34-tRNAs, $preQ_1$-tRNAs, and manQ-tRNAs. Only PEGylated $dPEG_{24}$-p11-tRNAs, prepared as described above, would be distinguishable. For Northern blots of 0Q and 100Q HepG2 RNA, an APB gel was used for $tRNA^{His}$, while an acid denaturing gel was used for $tRNA^{Asp}$. All blots were visualized with Clarity Western ECL Substrate (Bio-Rad; 1705061) using a Bio-Rad Chemi-Doc MP and analyzed using ImageJ (1.53t).

The oligonucleotide probe sequences used here are:

$tRNA^{Asp}$:

5′-biotin-

CTCCCCGTCGGGGAATCGAACCCCGGTCTCCCGCGTGACAGGCGGGGATAC

TCACCACTATACTAACGAGGA

$tRNA^{His}$:

5′-biotin-

TGCCGTGACTCGGATTCGAACCGAGGTTGCTGCGGCCACAACGCAGAGTACT

AACCACTATACGATCACGGC

MSR-seq Library Preparation

0Q HEK293T cells were plated in tissue culture treated 100mm plates (CELLTREAT; 229690) in 10 mL of DMEM as described above to 90% confluence. At this time, medium was swapped for serum-free control medium (–p11) or medium containing 10 μM p11 (+p11) for 12 hours. Plates were then irradiated under a 365 nm UV lamp (UV Stratalinker 2400, Stratagene) for 10 min (+UV). A UV-free (–UV) control was also used and protected from all light. All conditions (–p11/+UV; +p11/–UV; +p11/+UV) were plated in duplicate. TRIzol™ reagent (Thermo Fisher; 15596026) was used to extract total RNA from crosslinked cells.

Following RNA isolation, biotin was clicked onto p11-modified RNA as described above. Briefly, 10 mM biotin-disulfide-azide (Vector Laboratories; CCT-1168) in DMSO was added to all samples. The click reaction was catalyzed with L-ascorbic acid and 2:1 THPTA:Cu(II)SO_4. RNA was purified using glycogen as described above. At this point, 10% of each sample was stored for an input (**I**) control. The remaining sample volume was used for enrichment using Dynabeads™ MyOne™ Streptavidin C1 beads (Thermo Fisher; 65001) per standard manufacturer protocol. Briefly, prepared Dynabeads™ were combined with biotinylated RNA sample, rotated at room temperature for 15 minutes, and washed four times to remove unbound sample. After the final wash, biotinylated RNAs were eluted using a 1:1 mixture of tris(2-carboxyethyl)phosphine (TCEP, 200 mM):K_2CO_3 (600 mM) with shaking at 37°C for 30 minutes to reduce disulfide bonds. The reaction was quenched with 1.0 volume of iodoacetamide (400 mM) with shaking at room temperature for 30 minutes.[264] The eluted samples were placed on a magnetic tube rack

to separate Dynabeads™, and the enriched (**E**) supernatant was prepared for library building using a Zymo RNA Clean & Concentrator™ Kit. Separate MSR-seq libraries using both **I** (input) and **E** (enriched) RNA from each sample were prepared as described by Watkins et al.[96]

MSR-seq Data Analysis

Data processing followed the MSR-seq analysis pipeline as previously reported.[96] The analysis pipeline is available at GitHub (https://github.com/ckatanski/CHRIS-seq). Paired-end reads were demultiplexed by barcode sequence using Je demultiplex.[175] Barcode sequences are as previously described.[96] The following parameters were used, optimized for samples where the barcode is located in read 2: BPOS = BOTH BM = READ_2 LEN = 6:4 FORCE = true C = false. Following demultiplexing, data were aligned to the GtRNAdb hg38 reference genome using bowtie2[176] (version 2.3.3.1) with the following parameters: -q -p 10 --local --no-unal.

Bowtie2 output sam files were converted to bam files, then sorted using samtools.[177] IGVtools count was used to collapse reads into a 1nt window using the following parameters: -z 5 -w 1 -e 250 —bases. The resulting IGV output.wig files were reformatted using custom Python scripts to obtain mutation rate, read coverage, and fragmentation information[165] compatible with R for data visualization and analysis. To find enrichment levels, all library sizes and read counts were normalized. For each sample, counts for all isodecoders within an isodecoder family were summed together. To find enrichment over bead, the counts for **E** libraries of p11-treated samples (+p11/±UV) were divided by the counts of **E** libraries of untreated samples (–p11/+UV).

To find enrichment over cell, we divided **E** library counts by the counts of total 0Q HEK293T as found by our MSR-seq analysis (Chapter 2).

RT-qPCR

Total RNA was isolated using TRIzol™ reagent (Thermo Fisher; 15596026). DNA was digested using the DNA-*free*™ DNA Removal Kit (Thermo Fisher; AM1906) and cDNA was reverse-transcribed with the High-Capacity cDNA Reverse Transcription Kit (Thermo Fisher; 4368813) according to manufacturer protocol. The RT thermocycler protocol was as follows: 25°C for 10 minutes, 37°C for 120 minutes, and 85°C for 5 minutes. RT-qPCR was performed using LightCycler 480 SYBR Green I Master (Roche; 04707516001) and the Azure Cielo system (Azure Biosystems). The PCR thermocycler protocol was as follows: 95°C for 5 minutes; followed by 45 cycles of 95°C for 10 seconds, 57°C for 20 seconds, and 72°C for 8 seconds. Following the PCR run, amplicon quality was confirmed using melting curves generated by a 0.5°C temperature ramp to 95°C. Cq (quantification cycle) values were extracted using the Cielo Manager software (Azure Biosystems). Relative mRNA levels of target genes were normalized to GAPDH mRNA levels and analyzed with the $2^{-\Delta\Delta Cq}$ method.[265] Primer pairs used for this study are listed in **Supplementary Table S5.1**.

Chapter 6 – Future Directions and Perspectives

6.1 Queuosine, Immunity, and the Gut Microbiome

Despite the fact that queuosine was discovered in the late 1960s,[8] the full extent of its role in eukaryotic physiology is still being elucidated. The entirety of this thesis explores the role of Q and its derivatives in mammalian cells. In Chapters 2 and 3, I demonstrate that queuine and $preQ_1$ up- and down-regulate proliferation, respectively, and induce cell-type-specific responses in the transcriptome. For BMDCs, genes upregulated in response to queuine were associated with immune response activities. This result was further explored in Chapter 4, where I identified a novel queuine- and $preQ_1$-dependent effect on MHC-II expression in BMDCs. These results suggest that Q and its derivatives may play a role in facilitating crosstalk between the gut microbiome and host immunity.

Simply put, the role of the gut microbiome in host health cannot be overstated, and its interconnectedness with the host immune system is very well established.[197,198,223,266] Under normal conditions, the gut microbiome confers protection against pathogens and tolerance to innocuous antigens. Commensal bacteria dynamically interact with host epithelial and innate immune cells, including through the production of metabolites, directly influencing their activity.[223] Conversely, intestinal microbes are sensitive to host antibiotic use, diet, and other environmental cues.[227,235] These and other aberrations to the gut microbiome have been associated with various cancers, metabolic diseases, and IBD.[266]

The hypothesis that Q (and related metabolites) mediates host-microbiome crosstalk is rooted in several facts and findings. Firstly, Q-tRNA has already been implicated in IBD[146] and colon parasite virulence,[102] suggesting a role in gut homeostasis. Secondly, upon bacterial turnover in the gut, local availability of queuine/Q/preQ$_1$ would be acutely altered for nearby epithelial or immune cells. Importantly, our observation that MHC-II expression in BMDCs is queuine- and preQ$_1$-dependent (Chapter 4) provides a plausible mechanism underlying the hypothesized crosstalk. Finally, Q is the only microbe-derived tRNA modification described in eukaryotes to date, although our lab recently discovered that preQ$_1$ is also naturally incorporated into mammalian tRNAs (manuscript accepted for publication). Consequently, queuine and preQ$_1$ would have the unique capability to act as immune response modulators through canonical (Q-tRNA mediated) or non-canonical pathways (e.g., adjuvant, signaling molecule, etc.).

The results in Chapter 4 present a novel connection between Q-tRNA derivatives and primary immune cell activity. Canonically, MHC-II enables DC-mediated activation of CD4$^+$ T-lymphocytes. Thus, it would be informative to understand whether queuine or preQ$_1$ ultimately impact the activation of CD4$^+$ cells using coculture experiments.

Because the studies in this work were conducted in cell culture, it is important to contextualize queuosine biology at the organismal level. In mice, for example, Q-modification levels have been shown to vary by tissue type.[143] This is in agreement with our observations that BMDCs require higher queuine supplementation (100 nM) than HEK293T cells (10 nM) to achieve saturation of Q-modification (**Figure 2.1**). In humans, it is estimated that typical circulating levels of queuine are in the range of 1-10 nM.[8] It is

not unreasonable to imagine, then, that physiological levels of queuine are sufficient for fine-tuned regulatory signaling, whether via canonical or non-canonical pathways.

On the other hand, the role of $preQ_1$ outside of bacterial systems is virtually unexplored. In considering the anti-proliferative effects of $preQ_1$, it would be valuable to explore its therapeutic potentially, particularly in the context of oncology.

6.2 Non-Canonical Roles of Queuosine and its Derivatives

In Chapter 5, I presented preliminary support of the hypothesis that $preQ_1$ selectively binds to human histone mRNA transcripts, first posed by Balaratnam et al. following a series of *in vitro* experiments.[247] Using photoactivatable $preQ_1$ analog probes for proximity labeling of HEK293T cells in culture, we observe enrichment of histone mRNA transcripts (**Figure 5.3A**). Though we do not see a queuine-dependent effect on histone mRNA or SLBP mRNA transcription in HEK293T cells (**Figure 5.3B**), we do report a queuine-dependent upregulation of these transcripts in HepG2 cells (**Figure 5.3D**), which are more sensitive to queuine depletion (**Figure 5.3C**).

Given that p11 capture of HEK293T histone mRNA transcripts was elevated in +UV compared to –UV conditions (**Figure 5.3A**), our results point to a model where the nucleobases, rather than modified tRNA itself, play a role in the histone mRNA life cycle. Further biochemical studies, such as binding assays and structural analyses, are needed to validate this model and elucidate the role of $preQ_1$ and queuine in the context of histone mRNA. Importantly, the use of a QTRT1 KD/KO model will be required to distinguish the effects of modified tRNAs (i.e., Q-tRNA and $preQ_1$-tRNA) from the effects

of the nucleobases themselves. Additionally, the proteomic application of p11 would reveal whether $preQ_1$ has protein interacting partners in eukaryotic cells.

In a similar vein, it is fascinating to wonder whether Q-modification is deposited onto other RNA species. It is well established that the eukaryotic QTRT1 enzyme has high specificity for (mt-)tRNAs for Asn, Asp, His, and Tyr, enabled by the recognition of anticodon loop nucleotides $Y_{32}U_{33}G_{34}U_{35}$ (Y = C or U). However, Fergus et al. reported that QTRT1/QTRT2 could modify a 9-nt $tRNA^{Asp}$ stem loop *in vitro*.[133] Given the plethora of ncRNA transcribed by the human genome,[267] it would be valuable to search for other endogenous, non-tRNA substrates of QTRT1/QTRT2 that share the $Y_{32}U_{33}G_{34}U_{35}$ sequence.

Appendix: Supplementary Data

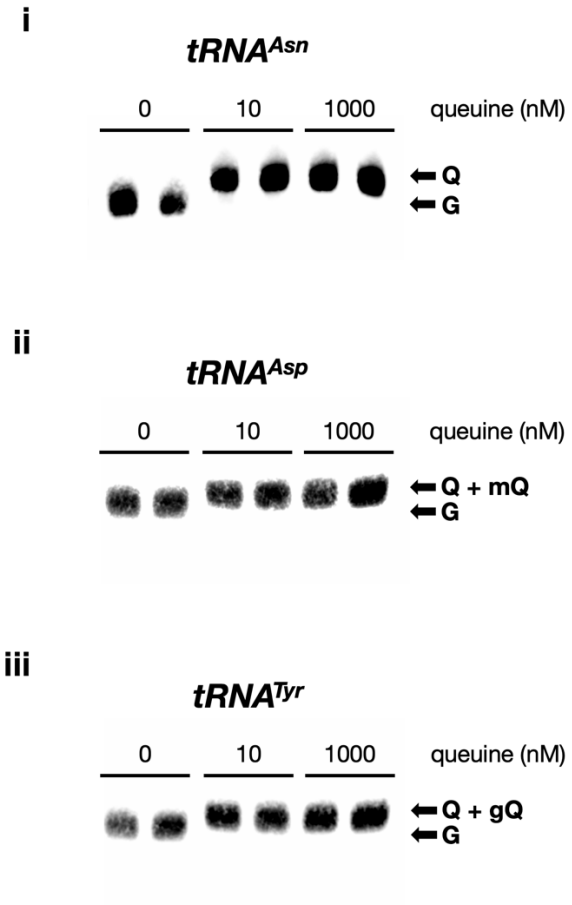

Figure S2.1A: Additional data for Figure 2.1A: Northern blots of Q-modifiable tRNAs in HEK293T cells.

Northern blot of (**i**) $tRNA^{Asn}$ (APB gel), (**ii**) $tRNA^{Asp}$ (acid denaturing gel), and (**iii**) $tRNA^{Tyr}$ (acid denaturing gel) in 0Q HEK293T cells grown in medium supplemented with 0, 10, or 1000 nM queuine, all biological duplicates. Total RNA was extracted from HEK293T cells 24 hours after queuine reintroduction. G: unmodified G34-tRNA, Q: Q-modified Q34-tRNA, mQ: manQ-modified tRNA, gQ: galQ-modified tRNA.

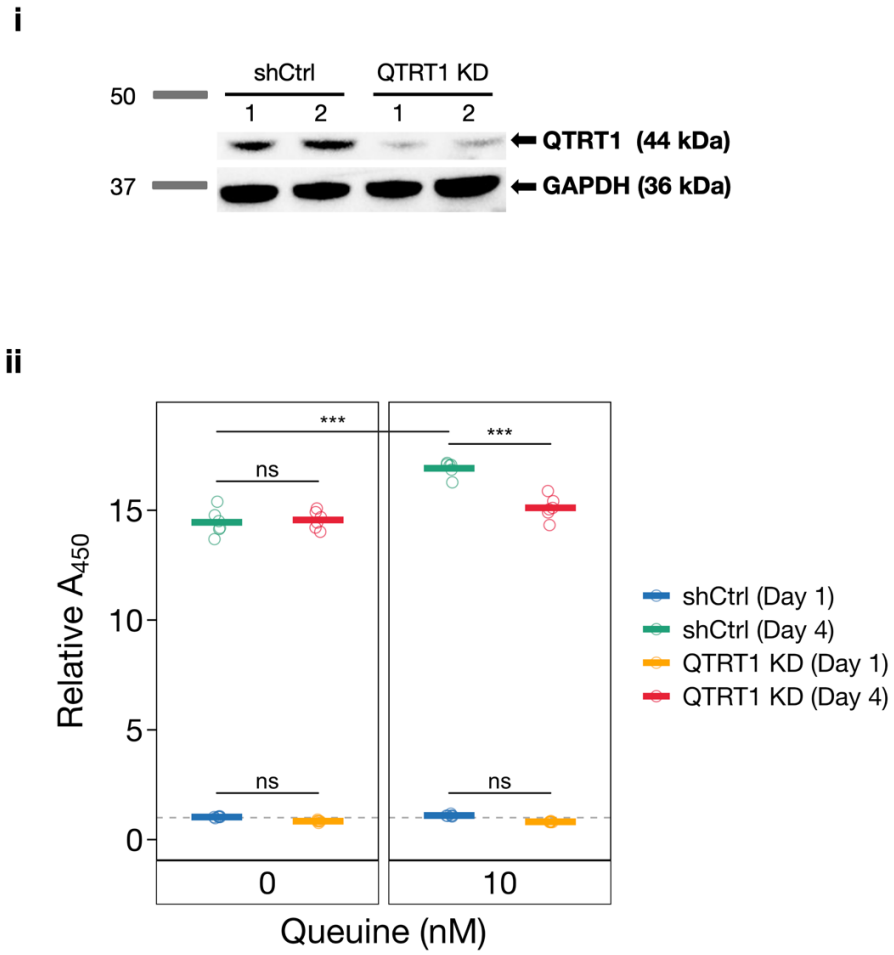

Figure S2.1B: Additional data for Figure 2.1B: Proliferation analysis in QTRT1 KD HEK293T cells.

(i) Western blots showing successful QTRT1 knockdown in 0Q QTRT1 KD HEK293T cells (top) using GAPDH as a loading control (bottom). Each lane contains 50 µg of lysate. $n = 2$ biological replicates.
(ii) Proliferation of QTRT1 stable knockdown (QTRT1 KD) and Control shRNA (shCtrl) HEK293T cells was assessed by CCK-8 assay, which reports absorbance at 450nm (A_{450}). Relative A_{450} for each well was calculated as the A_{450} divided by the mean A_{450} for 0 nM queuine at Day 1. Horizontal bars represent the group mean, while points correspond to individual wells. $n = 8$ biological replicates. Adjusted p-values from Tukey's Honest Significant Difference (HSD) test are reported. ns: not significant, ***: $p < 0.001$.

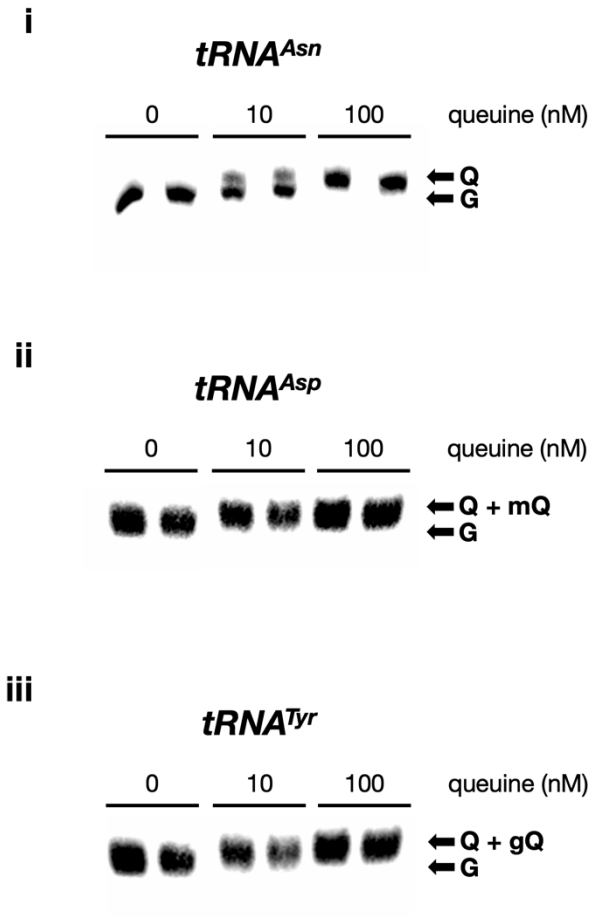

Figure S2.1C: Additional data for Figure 2.1C: Northern blots of Q-modifiable tRNAs in BMDCs.

Northern blot of (**i**) $tRNA^{Asn}$ (APB gel) (**ii**) $tRNA^{Asp}$ (acid denaturing gel) and (**iii**) $tRNA^{Tyr}$ (acid denaturing gel) in 0Q BMDCs grown in medium supplemented with 0, 10, or 100 nM queuine, all biological duplicates. Total RNA was collected from BMDCs 5 days after retrieval from mouse and plating. G: unmodified G34-tRNA, Q: Q-modified Q34-tRNA, mQ: manQ-modified tRNA, gQ: galQ-modified tRNA.

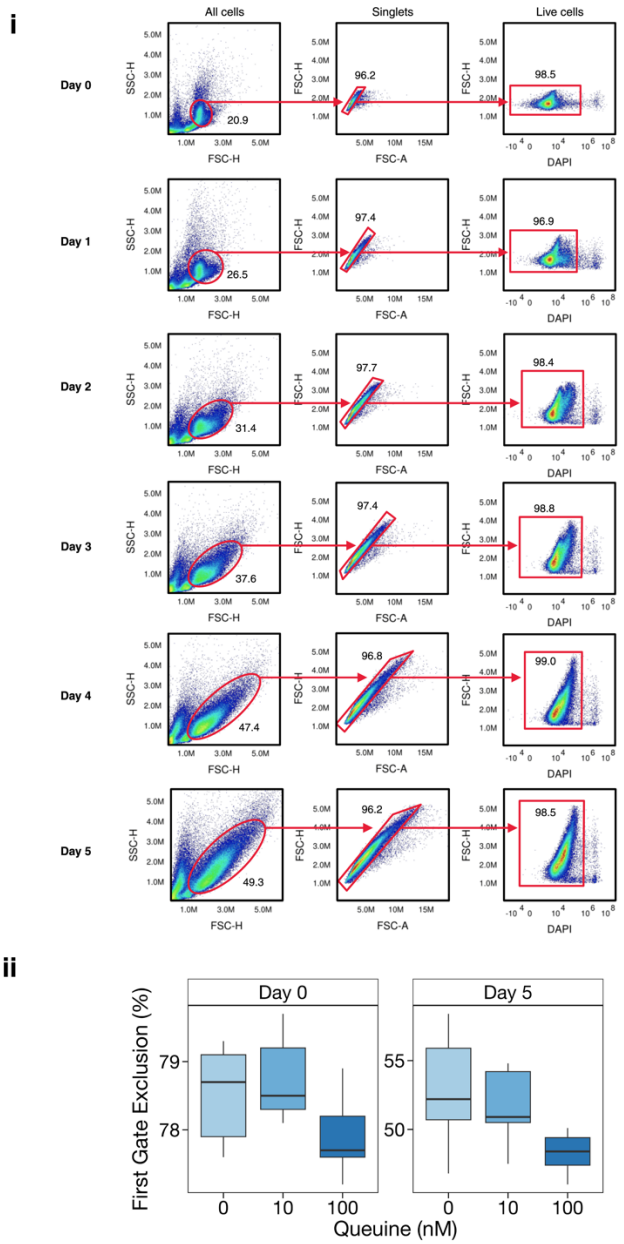

Figure S2.1D: Additional data for Figure 2.1D: BMDC proliferation analysis.

(i) Representative FlowJo gating strategy for obtaining live BMDC counts. Data shown is 0 nM queuine, replicate 1. Numbers represent the percentage (%) of cells captured by the gate.
(ii) Boxplot of the percentage of flow cytometry events at Day 0 and Day 5 that were excluded from the first gate ("All cells") in each queuine concentration. For each day, no comparisons were statistically significant ($p > 0.05$). $n = 5$ biological replicates.

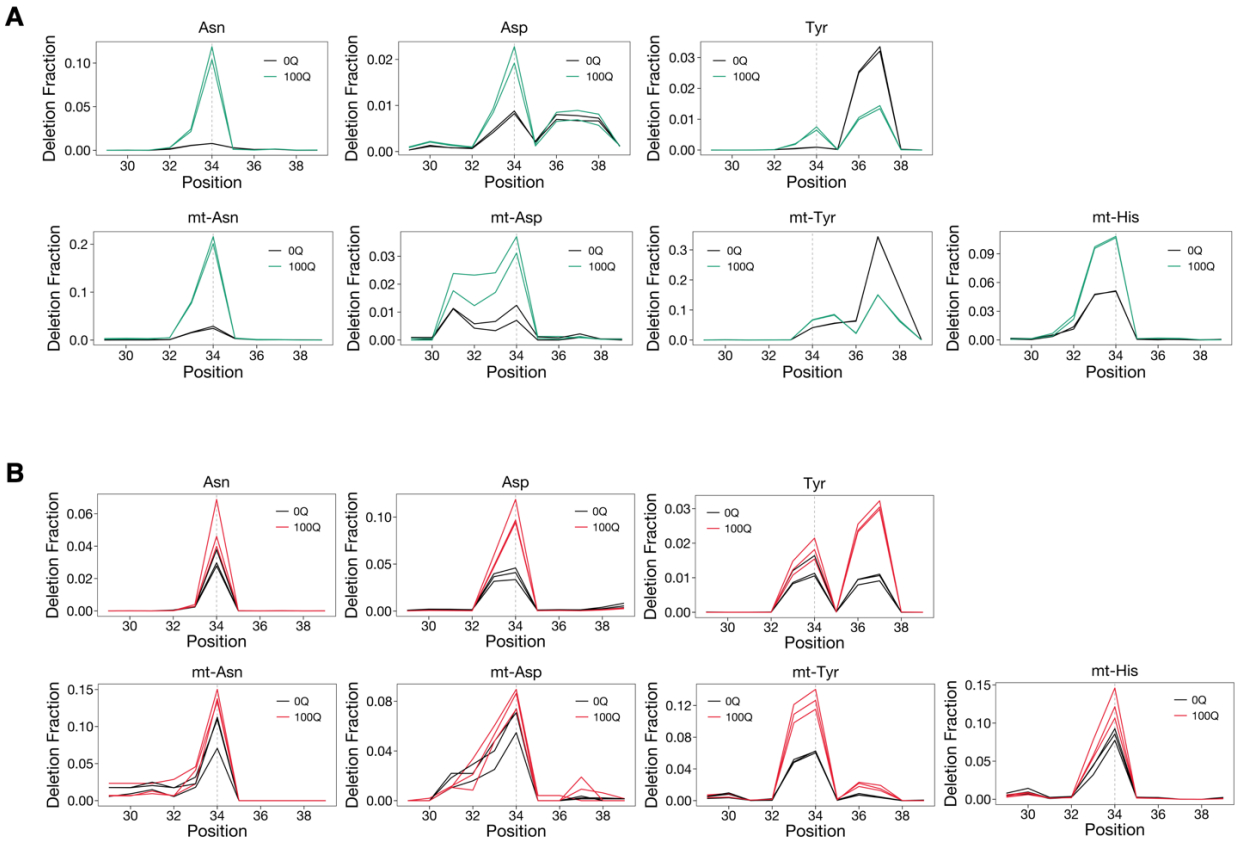

Figure S2.2: Additional data for Figure 2.2: Q-modification signatures detected by MSR-seq.

Deletion signatures in other tRNAs containing Q-modification in (**A**) HEK293T cells and (**B**) murine BMDCs. Regions shown are ±5 nucleotides to the Q34 residue (dashed line) in each tRNA. Biological replicates are overlaid in each graph. For cytosolic tRNAs, only the most abundant isodecoder for Asn/Asp/Tyr is shown. Known modifications that also produce a deletion signature at position 37 are m^1G in $tRNA^{Tyr}$ (Tyr) and ms^2i^6A in mitochondrial $tRNA^{Tyr}$ (mt-Tyr).

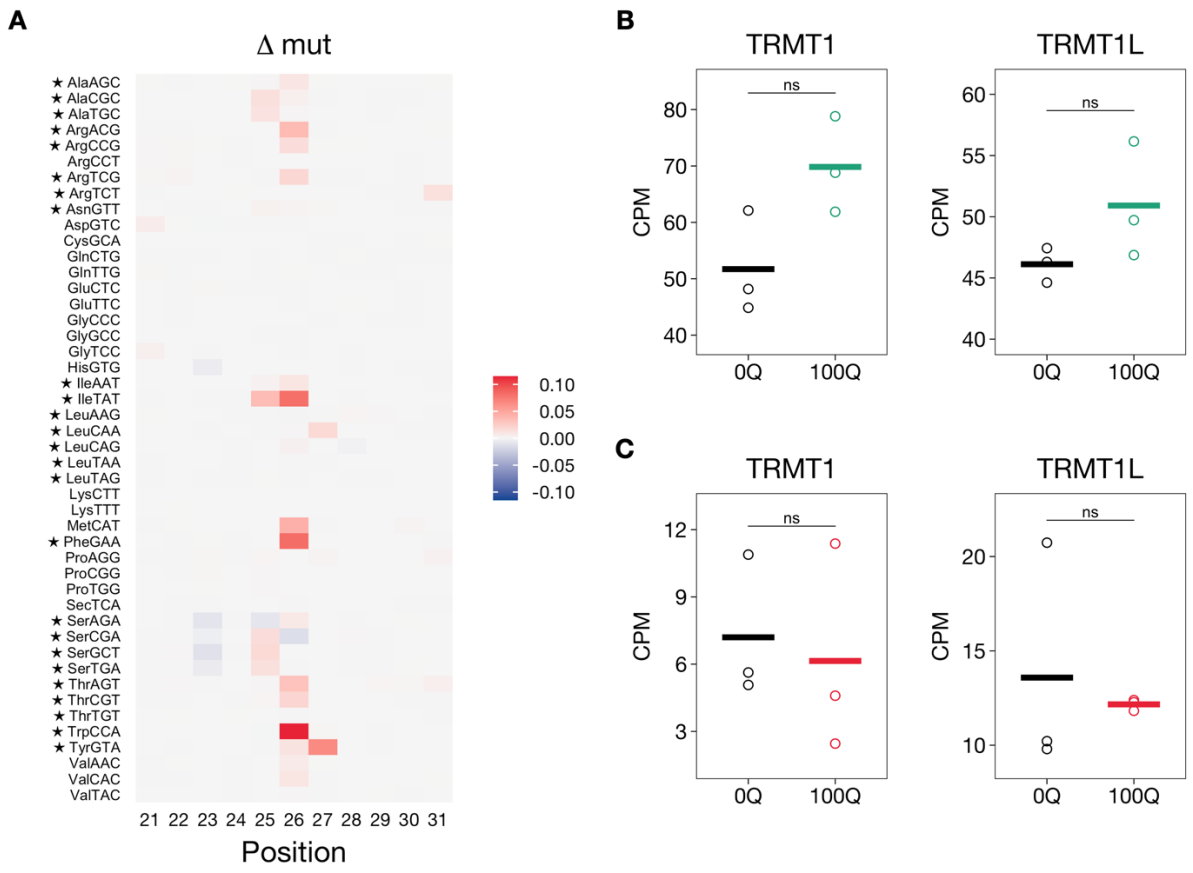

Figure S2.3: Additional data for Figure 2.3: Q-modification is correlated with $m^2{}_2G$ modification.

(A) Heatmap of $\Delta\, mut$ in 100Q BMDCs near position 26 of cytosolic tRNA species, corresponding to the $m^2{}_2G26$ modification. Region shown is ± 5 nucleotides to the $m^2{}_2G26$ residue. Data is expressed as the difference between the mean mutation fractions of n = 3 replicates for 100Q and 0Q samples. Only the most abundant isodecoder of each tRNA anticodon family is shown. tRNA species with known $m^2{}_2G26$ modification are marked with a star (★).
(B) Counts per million (CPM) values from HEK293T mRNA-seq data for *TRMT1* (left) and *TRMT1L* (right). Horizontal bars represent the group mean and points correspond to individual replicates *(n* = 3 per condition). ns: not significant.
(C) Counts per million (CPM) values from BMDC mRNA-seq data for *TRMT1* (left) and *TRMT1L* (right). Horizontal bars represent the group mean and points correspond to individual replicates *(n* = 3 per condition). ns: not significant.

i

0Q	r1	r2	r3
r1	1	0.989	0.977
r2	0.989	1	0.952
r3	0.977	0.953	1

ii

100Q	r1	r2	r3
r1	1	0.986	0.900
r2	0.986	1	0.846
r3	0.900	0.846	1

iii

0Q	r1	r2	r3
r1	1	0.992	0.991
r2	0.992	1	0.997
r3	0.991	0.997	1

iv

100Q	r1	r2	r3
r1	1	0.990	0.995
r2	0.990	1	0.994
r3	0.995	0.994	1

Figure S2.4A: Additional data for Figure 2.4: mRNA-seq replicate correlations.

Pearson correlation coefficients between mRNA-seq replicates 1-3 of (**i**) HEK293T 0Q, (**ii**) HEK293T 100Q, (**iii**) BMDC 0Q, and (**iv**) BMDC 100Q samples. Coefficients were calculated using $\log_{10}$-transformed count matrices.

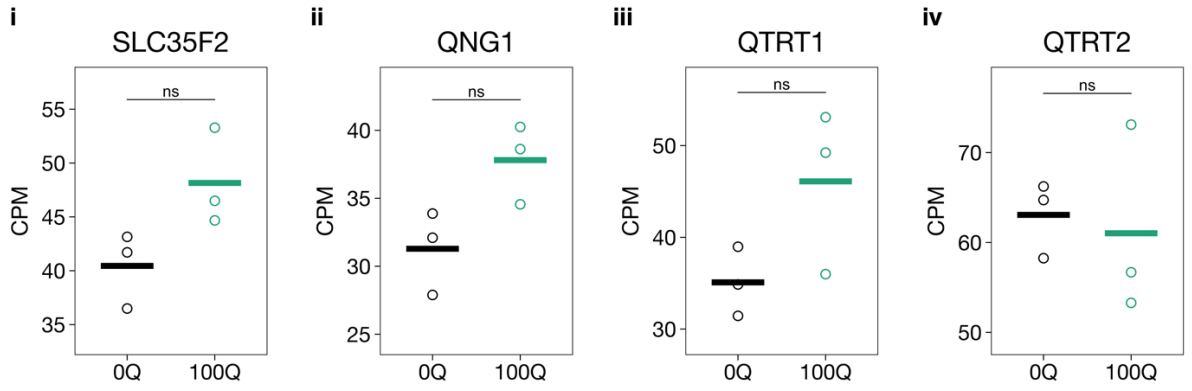

Figure S2.4B: Additional data for Figure 2.4: HEK293T CPM values for select Q-tRNA metabolism genes.

Counts per million (CPM) values from HEK293T mRNA-seq data for (**i**) *SLC35F2*, (**ii**) *QNG1*, (**iii**) *QTRT1*, and (**iv**) *QTRT2*. Horizontal bars represent the group mean and points correspond to individual replicates (*n* = 3 per condition). ns: not significant.

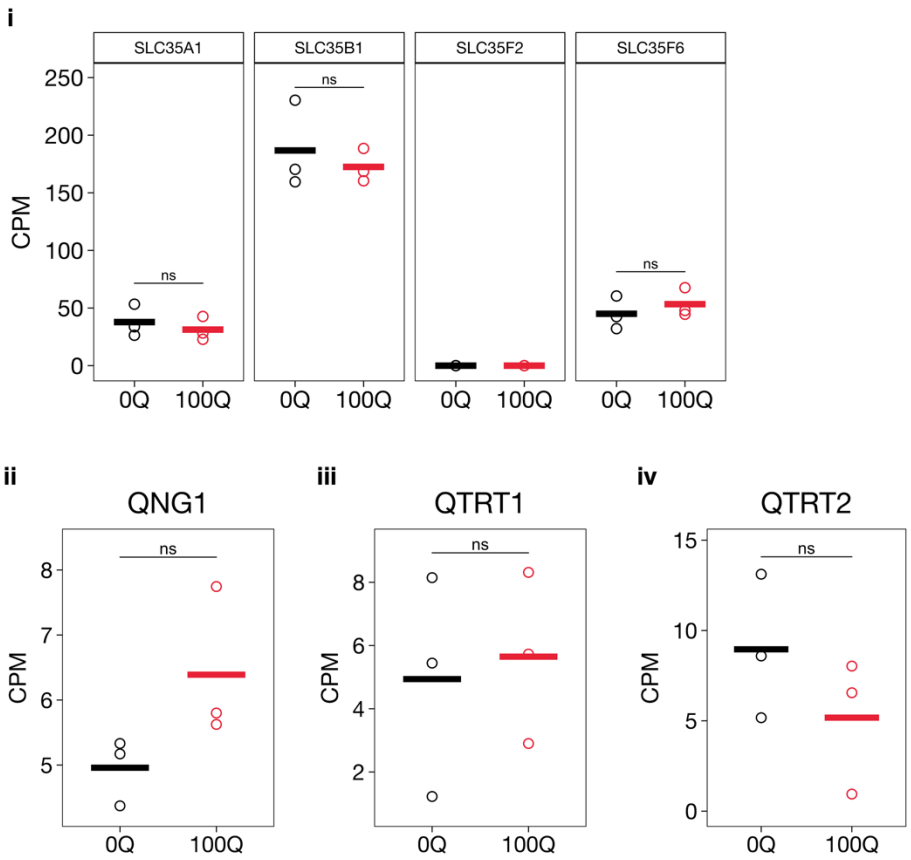

Figure S2.4C: Additional data for Figure 2.4: BMDC CPM values for select Q-tRNA metabolism genes.

Counts per million (CPM) values from BMDC mRNA-seq data for (**i**) the three most highly expressed SLC35 family genes and *SLC35F2,* (**ii**) *QNG1*, (**iii**) *QTRT1*, and (**iv**) *QTRT2*. Horizontal bars represent the group mean and points correspond to individual replicates *(n* = 3 per condition). ns: not significant.

A

preQ$_1$	r1	r2	r3
r1	1	0.999	0.997
r2	0.999	1	0.995
r3	0.997	0.995	1

B

Both	r1	r2	r3
r1	1	0.996	0.998
r2	0.996	1	0.994
r3	0.998	0.994	1

Figure S3.1: Additional data for Figure 3.3: BMDC mRNA-seq replicate correlations.

Pearson correlation coefficients between BMDC mRNA-seq replicates 1-3 of (**A**) **"**preQ$_1$" and (**B**) **"**Both" (preQ$_1$ and queuine co-treatment) samples. Coefficients were calculated using $\log_{10}$-transformed count matrices.

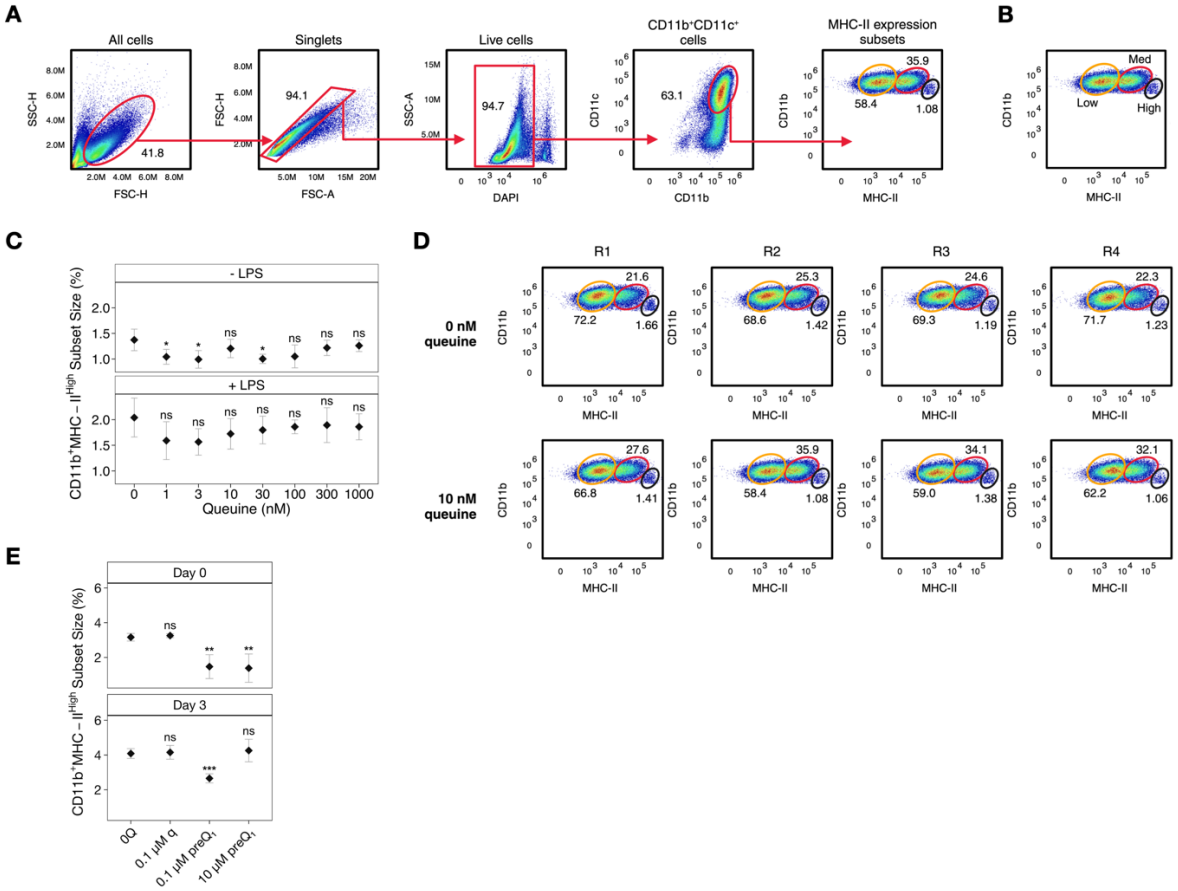

Figure S4.1: Additional data for Figure 4.1: MHC-II expression in mouse BMDCs is both queuine- and preQ$_1$-dependent.

(A) Gating strategy for FACS of the three subpopulations present in GM-CSF-induced BMDC cultures: CD11b$^+$MHC-II^{Low} (yellow), CD11b$^+$MHC-II^{Med} (red), CD11b$^+$MHC-II^{High} (black) cells. Numbers represent the percentage of cells captured by the gate.
(B) Representative gating strategy to stratify CD11b$^+$CD11c$^+$ BMDCs into Low, Med (Medium), and High MHC-II expression subsets.
(C) CD11b$^+$MHC-II^{High} subset sizes in –LPS (top) and +LPS (bottom) BMDCs. Data is displayed as the mean subset size as a percentage of the parent gate (CD11b$^+$CD11c$^+$). Error bars represent one standard deviation. Significance was calculated with Welch's *t*-test using 0 nM as the control. n = 4 biological replicates. ns: not significant, *: $p < 0.05$.
(D) MHC-II expression data for replicates 1-4 of –LPS BMDCs cultured with 0 nM q (top) or 10 nM q (bottom). Numbers represent the percentage of cells captured by the gate.
(E) CD11b$^+$MHC-II^{High} subset sizes of –LPS BMDCs treated with q/preQ$_1$ on Day 0 (top) or Day 3 (bottom) of the expansion protocol. Data is displayed as the mean subset size as a percentage of the parent gate (CD11b$^+$CD11c$^+$). Error bars represent one standard deviation. Significance was calculated with Welch's *t*-test using 0Q as the control. n = 5 biological replicates. ns: not significant, **: $p < 0.01$; ***: $p < 0.001$.

Target	Forward Primer (5'-3')	Reverse Primer (5'-3')
GAPDH	CATCACTGCCACCCAGAAGACTG	ATGCCAGTGAGCTTCCCGTTCAG
H1-5	GCTACGACGTGGAGAAGAATAA	GTTGAGTTTAAAGGAGCCAGAAG
H2AC6	CTGCTCCGTAAAGGCAACTA	GGGATGATGCGAGTCTTCTT
H2AC21	GCTCGGGACAACAAGAAGA	AACAGGACAGCCTGGATATTG
H2BC5	CAGAAGAAGGACGGGAAGAAG	CCCATTGCCTTGGAAGAGAT
H2BC11	GCAGAAGAAAGACGGCAAGA	CCATGGCCTTGGACGAAAT
H2BC13	CCAGAAGAAGGATGGCAAGAA	GATTCCCATGGCCTTAGAAGAG
H2BC18	CCCAAGAAGGGCTCCAAA	CCTTGTACACGTAAACGGAGTAG
H2BC21	CAAGAAAGCCGTCACCAAAG	CCTTGTACACGTAGATGGAGTAG
H3C2	AGGCTTGTGAGGCCTACTT	GCTGGATGTCTTTGGGCATAAT
H3C7	ATCCGCCGCTATCAGAAATC	GCAGGTCGGTCTTGAAGT
H3C8	ATCTGCGCTTTCAGAGTTCC	GGCATGATAGTCACTCGCTTAG
H3C10	AAGACCGACTTGCGCTTC	CATGATAGTCACCCGCTTGG
H3C15	CAGGACTTTAAGACGGACCTG	CTGGATGTCCTTGGGCATAA
H4C5	CGGAAAGGGACTGGGTAAAG	CCTCGTAGATGAGACCAGAAATG
SLBP	CACCCTGTAGACCTTGAATCTG	TCAAACTCATCCTCCACTTGAC

Table S5.1: Additional data for Figure 5.3: Primers used for RT-qPCR.

All primers were designed with the help of the IDT PrimerQuest™ Tool.

Cell Type	Experiment	Sample	Bowtie Total Reads	Bowtie Alignment Rate
BMDC	mRNA-seq	0Q r1	6714561	69.82%
BMDC	mRNA-seq	0Q r2	8064489	70.48%
BMDC	mRNA-seq	0Q r3	4420069	69.10%
BMDC	mRNA-seq	100Q r1	6243048	70.80%
BMDC	mRNA-seq	100Q r2	5607673	68.19%
BMDC	mRNA-seq	100Q r3	23078271	69.83%
BMDC	mRNA-seq	preQ1 r1	10546424	70.94%
BMDC	mRNA-seq	preQ1 r2	4806953	67.30%
BMDC	mRNA-seq	preQ1 r3	9696665	60.53%
BMDC	mRNA-seq	Both r1	9364861	69.71%
BMDC	mRNA-seq	Both r2	5965237	68.93%
BMDC	mRNA-seq	Both r3	6966897	67.75%
BMDC	MSR-seq	0Q r1	29754456	58.99%
BMDC	MSR-seq	0Q r2	27244132	65.55%
BMDC	MSR-seq	0Q r3	20801555	59.56%
BMDC	MSR-seq	100Q r1	24882442	64.46%
BMDC	MSR-seq	100Q r2	26821474	58.96%
BMDC	MSR-seq	100Q r3	23906936	54.43%
HEK293T	mRNA-seq	0Q r1	50618064	66.44%
HEK293T	mRNA-seq	0Q r2	54376345	66.59%
HEK293T	mRNA-seq	0Q r3	52730031	67.61%
HEK293T	mRNA-seq	100Q r1	36327527	67.79%
HEK293T	mRNA-seq	100Q r2	25655337	70.26%
HEK293T	mRNA-seq	100Q r3	82487850	68.05%
HEK293T	MSR-seq	0Q r1	19291602	34.04%
HEK293T	MSR-seq	0Q r2	15109087	39.73%
HEK293T	MSR-seq	100Q r1	18261587	30.02%
HEK293T	MSR-seq	100Q r2	24106924	38.65%
HEK293T	p11 crosslinking (MSR-seq)	–p11/+UV r1 (enriched)	515441	0.75%
HEK293T	p11 crosslinking (MSR-seq)	–p11/+UV r2 (enriched)	22325480	0.40%
HEK293T	p11 crosslinking (MSR-seq)	+p11/–UV r1 (enriched)	9569893	18.01%
HEK293T	p11 crosslinking (MSR-seq)	+p11/–UV r2 (enriched)	10805976	14.56%
HEK293T	p11 crosslinking (MSR-seq)	+p11/+UV r1 (enriched)	265632	18.24%
HEK293T	p11 crosslinking (MSR-seq)	+p11/+UV r2 (enriched)	11162299	21.54%

Table S6.1: Mapping statistics for all sequencing samples.

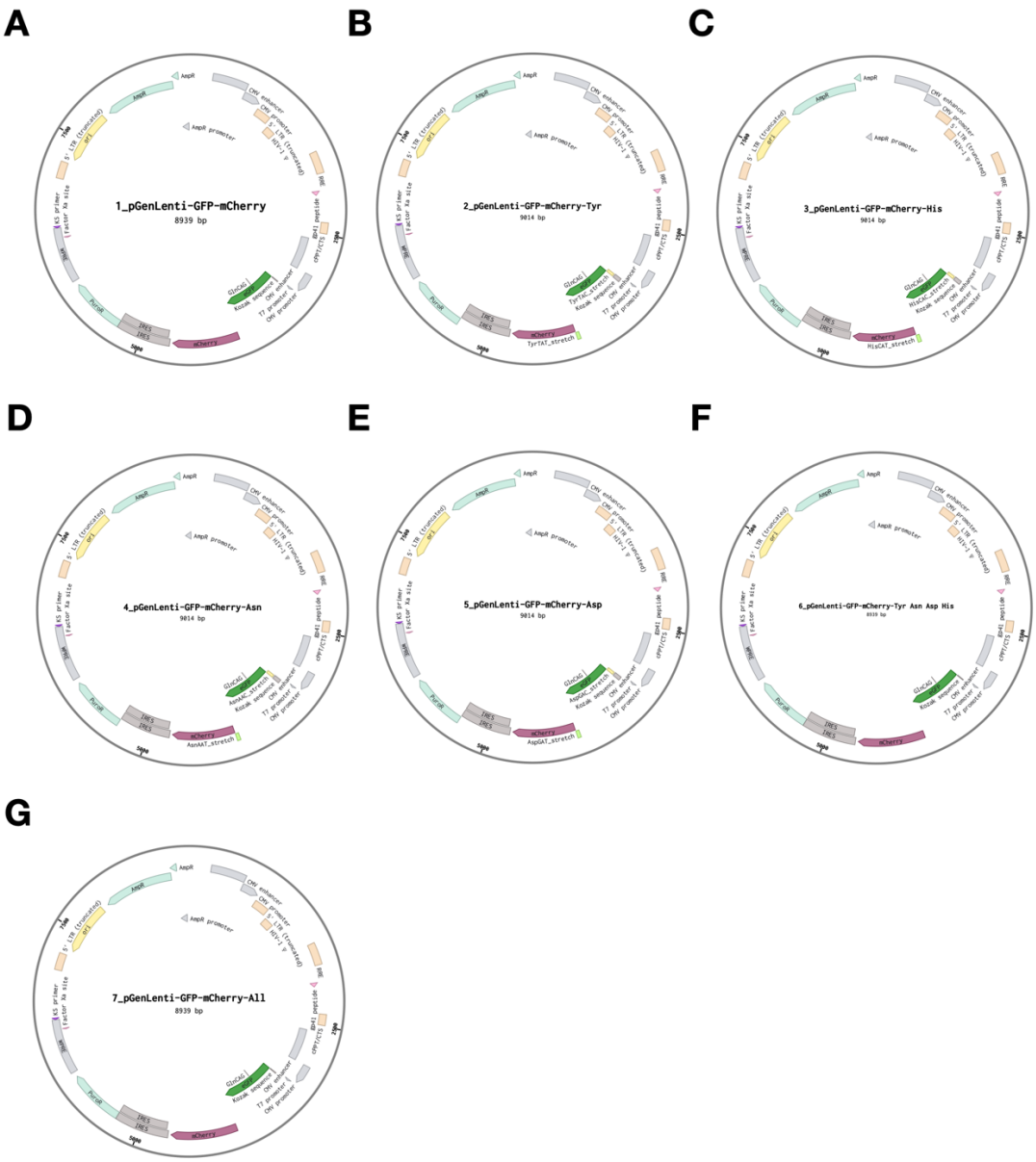

Figure S6.1: Dual fluorescence Q-tRNA reporter constructs.

(A) Wild-type (WT) eGFP-mCherry
(B-E) eGFP-mCherry constructs with twelve C-ending codons for (**B**) Tyr, (**C**) His, (**D**) Asn, or (**E**) Asp inserted before eGFP and twelve U-ending codons for (**B**) Tyr, (**C**) His, (**D**) Asn, or (**E**) Asp inserted before mCherry.
(F) eGFP-mCherry construct with all codons for Tyr, His, Asn, and Asp converted to C-ending codons in eGFP and U-ending codons in mCherry.
(G) eGFP-mCherry construct with all synonymous NNC/U codons converted to C-ending codons in eGFP and U-ending codons in mCherry.

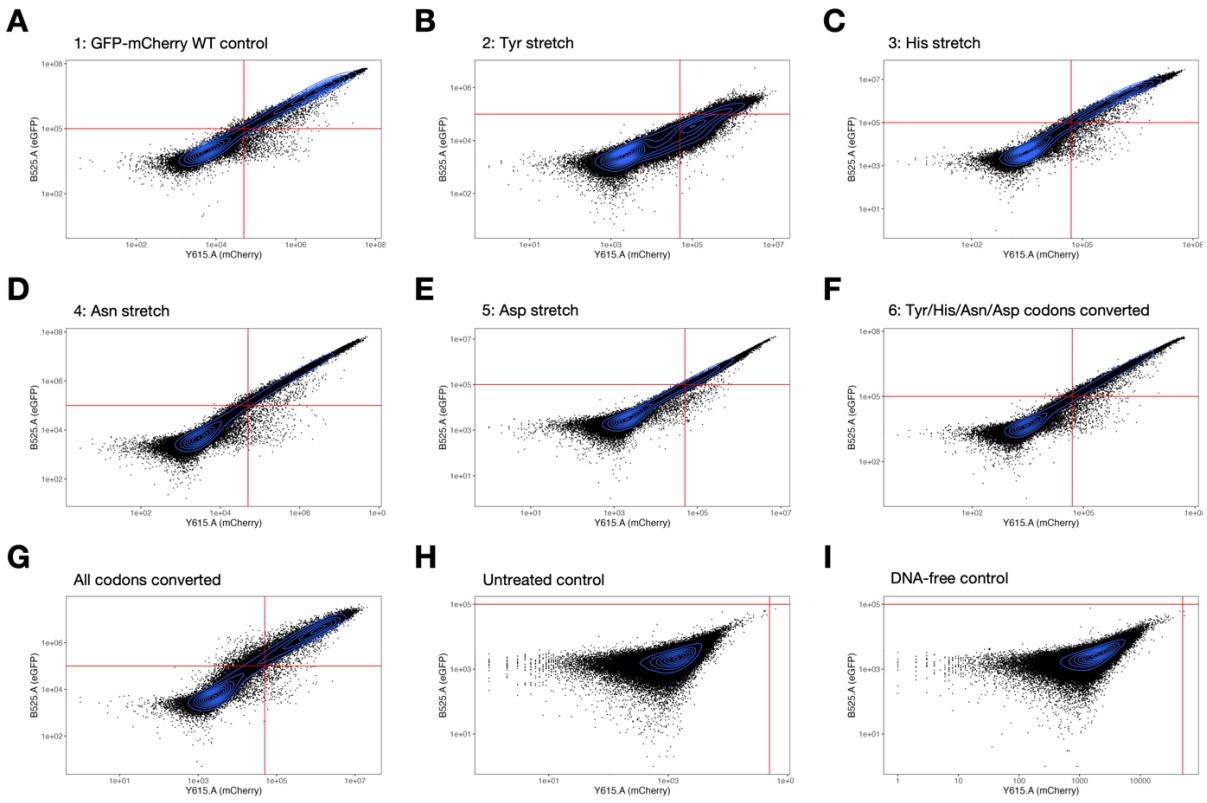

Figure S6.2: Fluorescence of HEK293T cells transfected with Q reporter constructs.

eGFP and mCherry fluorescence of HEK293T cells transfected with the plasmids in **Figure S6.1** for 48 hours prior to measurement.
(A-G) Cells transfected with plasmids corresponding to (**A-G**) in **Figure S6.1**.
(H) Untreated control receiving no transfection reagents.
(I) DNA-free control treated with transfection reagents but no plasmid.

Plasmid	Queuine	GFP	mCherry	G:M Ratio	GFP (norm to WT 0Q)	mCherry (norm to WT 0Q)	Normalized G:M Ratio
1 (WT)	0Q	3061847	1850782	1.654	1	1	1
1 (WT)	100Q	2967550	1843633	1.610	0.969	0.996	0.973
2 (Tyr)	0Q	40919	158018	0.259	0.013	0.085	0.157
2 (Tyr)	100Q	41843	163221	0.256	0.014	0.088	0.155
3 (His)	0Q	1228974	747947	1.643	0.401	0.404	0.993
3 (His)	100Q	1211703	780591	1.552	0.396	0.422	0.938
4 (Asn)	0Q	1456776	650043	2.241	0.476	0.351	1.355
4 (Asn)	100Q	1560707	733619	2.127	0.510	0.396	1.286
5 (Asp)	0Q	292632	162879	1.797	0.096	0.088	1.086
5 (Asp)	100Q	287016	170342	1.685	0.094	0.092	1.018
6 (Tyr/His/Asn/Asp)	0Q	1134845	685284	1.656	0.371	0.370	1.001
6 (Tyr/His/Asn/Asp)	100Q	1068550	671253	1.592	0.349	0.363	0.962
7 (All)	0Q	2100024	618194	3.397	0.686	0.334	2.053
7 (All)	100Q	1964497	590272	3.328	0.642	0.319	2.013

Table S6.2: Quantitative results for Figure S6.2.

Different constructs result in different G:M ratios, though variation of Q-tRNA levels does not appear to significantly change the G:M ratio in any construct tested here.

Bibliography

1. Crick, F.H., *On protein synthesis.* Symp Soc Exp Biol, 1958. **12**: p. 138-63.
2. Hoagland MB, S.M., Scott JF, Hecht LI, and Zamecnik PC *A soluble ribonucleic acid intermediate in protein synthesis.* J Biol Chem, 1958(231): p. 241–257.
3. Holley, R.W., et al., *Structure of a Ribonucleic Acid.* Science, 1965. **147**(3664): p. 1462-1465.
4. Kim, S.H., et al., *Three-Dimensional Tertiary Structure of Yeast Phenylalanine Transfer RNA.* Science, 1974. **185**(4149): p. 435-440.
5. Brennan, T. and M. Sundaralingam, *Structure, of transfer RNA molecules containing the long variable loop.* Nucleic Acids Research, 1976. **3**(11): p. 3235-3252.
6. Pan, T., *Modifications and functional genomics of human transfer RNA.* Cell Research, 2018. **28**(4): p. 395-404.
7. Schauss, J., et al., *Magnesium Contact Ions Stabilize the Tertiary Structure of Transfer RNA: Electrostatics Mapped by Two-Dimensional Infrared Spectra and Theoretical Simulations.* The Journal of Physical Chemistry B, 2021. **125**(3): p. 740-747.
8. Fergus, C., et al., *The Queuine Micronutrient: Charting a Course from Microbe to Man.* Nutrients, 2015. **7**(4): p. 2897-2929.
9. Rubio Gomez, M.A. and M. Ibba, *Aminoacyl-tRNA synthetases.* RNA, 2020. **26**(8): p. 910-936.
10. Tamura, K., *Origins and Early Evolution of the tRNA Molecule.* Life, 2015. **5**(4): p. 1687-1699.
11. Giegé, R., et al., *Structure of transfer RNAs: similarity and variability.* WIREs RNA, 2012. **3**(1): p. 37-61.
12. Beuning, P.J. and K. Musier-Forsyth, *Transfer RNA recognition by aminoacyl-tRNA synthetases.* Biopolymers, 1999. **52**(1): p. 1-28.
13. Chan, P.P. and T.M. Lowe, *GtRNAdb 2.0: an expanded database of transfer RNA genes identified in complete and draft genomes.* Nucleic Acids Research, 2016. **44**(D1): p. D184-D189.
14. Tamaki, S., et al., *Systematic Analysis of the Binding Surfaces between tRNAs and Their Respective Aminoacyl tRNA Synthetase Based on Structural and Evolutionary Data.* Frontiers in Genetics, 2018. **8**.
15. Goodenbour, J.M. and T. Pan, *Diversity of tRNA genes in eukaryotes.* Nucleic Acids Research, 2006. **34**(21): p. 6137-6146.
16. Fredrick, K. and M. Ibba, *How the Sequence of a Gene Can Tune Its Translation.* Cell, 2010. **141**(2): p. 227-229.
17. Parvathy, S.T., V. Udayasuriyan, and V. Bhadana, *Codon usage bias.* Molecular Biology Reports, 2022. **49**(1): p. 539-565.
18. Tuller, T., et al., *An Evolutionarily Conserved Mechanism for Controlling the Efficiency of Protein Translation.* Cell, 2010. **141**(2): p. 344-354.

19. Cannarozzi, G., et al., *A role for codon order in translation dynamics.* Cell, 2010. **141**(2): p. 355-67.
20. Geslain, R. and T. Pan, *Functional Analysis of Human tRNA Isodecoders.* Journal of Molecular Biology, 2010. **396**(3): p. 821-831.
21. Crick, F.H., *Codon--anticodon pairing: the wobble hypothesis.* J Mol Biol, 1966. **19**(2): p. 548-55.
22. Agris, P.F., et al., *Celebrating wobble decoding: Half a century and still much is new.* RNA Biology, 2018. **15**(4-5): p. 537-553.
23. Ranjan, N. and M.V. Rodnina, *tRNA wobble modifications and protein homeostasis.* Translation, 2016. **4**(1): p. e1143076.
24. Bruce Alberts, A.J., Julian Lewis, Martin Raff, Keith Roberts, and Peter Walter, *Molecular Biology of the Cell. 4th edition.* 2002, Garland Science: New York.
25. Anderson, S., et al., *Sequence and organization of the human mitochondrial genome.* Nature, 1981. **290**(5806): p. 457-465.
26. Suzuki, T., et al., *Complete chemical structures of human mitochondrial tRNAs.* Nature Communications, 2020. **11**(1).
27. Suzuki, T., A. Nagao, and T. Suzuki, *Human Mitochondrial tRNAs: Biogenesis, Function, Structural Aspects, and Diseases.* Annual Review of Genetics, 2011. **45**(1): p. 299-329.
28. Schimmel, P., *The emerging complexity of the tRNA world: mammalian tRNAs beyond protein synthesis.* Nat Rev Mol Cell Biol, 2018. **19**(1): p. 45-58.
29. De Bruijn, M.H.L., et al., *A mammalian mitochondrial serine transfer RNA lacking the "dihydrouridine" loop and stem.* Nucleic Acids Research, 1980. **8**(22): p. 5213-5222.
30. Belostotsky, R., Y. Frishberg, and N. Entelis, *Human mitochondrial tRNA quality control in health and disease.* RNA Biology, 2012. **9**(1): p. 33-39.
31. Bykhovskaya, Y., et al., *Missense Mutation in Pseudouridine Synthase 1 (PUS1) Causes Mitochondrial Myopathy and Sideroblastic Anemia (MLASA).* The American Journal of Human Genetics, 2004. **74**(6): p. 1303-1308.
32. Kirino, Y., et al., *Specific correlation between the wobble modification deficiency in mutant tRNAs and the clinical features of a human mitochondrial disease.* Proceedings of the National Academy of Sciences, 2005. **102**(20): p. 7127-7132.
33. Kelley, S.O., P. Schimmel, and S.V. Steinberg, *Functional defects of pathogenic human mitochondrial tRNAs related to structural fragility.* Nature Structural Biology, 2000. **7**(10): p. 862-865.
34. Kelley, S.O., S.V. Steinberg, and P. Schimmel, *Fragile T-stem in Disease-associated Human Mitochondrial tRNA Sensitizes Structure to Local and Distant Mutations.* Journal of Biological Chemistry, 2001. **276**(14): p. 10607-10611.
35. Su, Z., et al., *Noncanonical Roles of tRNAs: tRNA Fragments and Beyond.* Annual Review of Genetics, 2020. **54**(1): p. 47-69.
36. Kumar, P., C. Kuscu, and A. Dutta, *Biogenesis and Function of Transfer RNA-Related Fragments (tRFs).* Trends in Biochemical Sciences, 2016. **41**(8): p. 679-689.

37. Anderson, P. and P. Ivanov, *tRNA fragments in human health and disease.* FEBS Letters, 2014. **588**(23): p. 4297-4304.
38. Lee, Y.S., et al., *A novel class of small RNAs: tRNA-derived RNA fragments (tRFs).* Genes & Development, 2009. **23**(22): p. 2639-2649.
39. Maraia, R.J. and T.N. Lamichhane, *3′ processing of eukaryotic precursor tRNAs.* WIREs RNA, 2011. **2**(3): p. 362-375.
40. Cole, C., et al., *Filtering of deep sequencing data reveals the existence of abundant Dicer-dependent small RNAs derived from tRNAs.* RNA, 2009. **15**(12): p. 2147-2160.
41. Kumar, P., et al., *Meta-analysis of tRNA derived RNA fragments reveals that they are evolutionarily conserved and associate with AGO proteins to recognize specific RNA targets.* BMC Biology, 2014. **12**(1).
42. Goodarzi, H., et al., *Endogenous tRNA-Derived Fragments Suppress Breast Cancer Progression via YBX1 Displacement.* Cell, 2015. **161**(4): p. 790-802.
43. Li, S., Z. Xu, and J. Sheng, *tRNA-Derived Small RNA: A Novel Regulatory Small Non-Coding RNA.* Genes, 2018. **9**(5): p. 246.
44. Thompson, D.M. and R. Parker, *Stressing Out over tRNA Cleavage.* Cell, 2009. **138**(2): p. 215-219.
45. Dhahbi, J.M., *5' tRNA Halves: The Next Generation of Immune Signaling Molecules.* Frontiers in Immunology, 2015. **6**.
46. Su, Z., et al., *Angiogenin generates specific stress-induced tRNA halves and is not involved in tRF-3–mediated gene silencing.* Journal of Biological Chemistry, 2019. **294**(45): p. 16930-16941.
47. Xie, Y., et al., *Action mechanisms and research methods of tRNA-derived small RNAs.* Signal Transduction and Targeted Therapy, 2020. **5**(1).
48. Luo, S., et al., *Drosophila tsRNAs preferentially suppress general translation machinery via antisense pairing and participate in cellular starvation response.* Nucleic Acids Research, 2018. **46**(10): p. 5250-5268.
49. Maute, R.L., et al., *tRNA-derived microRNA modulates proliferation and the DNA damage response and is down-regulated in B cell lymphoma.* Proceedings of the National Academy of Sciences, 2013. **110**(4): p. 1404-1409.
50. Haussecker, D., et al., *Human tRNA-derived small RNAs in the global regulation of RNA silencing.* RNA, 2010. **16**(4): p. 673-695.
51. Lyons, S.M., et al., *Identification of functional tetramolecular RNA G-quadruplexes derived from transfer RNAs.* Nature Communications, 2017. **8**(1).
52. Ivanov, P., et al., *Angiogenin-Induced tRNA Fragments Inhibit Translation Initiation.* Molecular Cell, 2011. **43**(4): p. 613-623.
53. Ivanov, P., et al., *G-quadruplex structures contribute to the neuroprotective effects of angiogenin-induced tRNA fragments.* Proceedings of the National Academy of Sciences, 2014. **111**(51): p. 18201-18206.
54. Gonskikh, Y., et al., *Modulation of mammalian translation by a ribosome-associated tRNA half.* RNA Biology, 2020. **17**(8): p. 1125-1136.

55. Lyons, S.M., et al., *YB-1 regulates tiRNA-induced Stress Granule formation but not translational repression.* Nucleic Acids Research, 2016. **44**(14): p. 6949-6960.
56. Emara, M.M., et al., *Angiogenin-induced tRNA-derived Stress-induced RNAs Promote Stress-induced Stress Granule Assembly.* Journal of Biological Chemistry, 2010. **285**(14): p. 10959-10968.
57. Saikia, M., et al., *Angiogenin-Cleaved tRNA Halves Interact with Cytochrome c, Protecting Cells from Apoptosis during Osmotic Stress.* Molecular and Cellular Biology, 2014. **34**(13): p. 2450-2463.
58. Chen, Z., et al., *Transfer RNA demethylase ALKBH3 promotes cancer progression via induction of tRNA-derived small RNAs.* Nucleic Acids Research, 2019. **47**(5): p. 2533-2545.
59. Dhahbi, J.M., et al., *5′ tRNA halves are present as abundant complexes in serum, concentrated in blood cells, and modulated by aging and calorie restriction.* BMC Genomics, 2013. **14**(1): p. 298.
60. Zhang, Y., et al., *Identification and characterization of an ancient class of small RNAs enriched in serum associating with active infection.* Journal of Molecular Cell Biology, 2014. **6**(2): p. 172-174.
61. Wang, Z., et al., *The 3′ CCACCA Sequence of tRNA^{Ala}(UGC) Is the Motif That Is Important in Inducing Th1-Like Immune Response, and This Motif Can Be Recognized by Toll-Like Receptor 3.* Clinical and Vaccine Immunology, 2006. **13**(7): p. 733-739.
62. Pawar, K., et al., *Infection-induced 5′-half molecules of tRNA^{HisGUG} activate Toll-like receptor 7.* PLOS Biology, 2020. **18**(12): p. e3000982.
63. Chiou, N.-T., R. Kageyama, and K.M. Ansel, *Selective Export into Extracellular Vesicles and Function of tRNA Fragments during T Cell Activation.* Cell Reports, 2018. **25**(12): p. 3356-3370.e4.
64. Chen, Q., et al., *Sperm tsRNAs contribute to intergenerational inheritance of an acquired metabolic disorder.* Science, 2016. **351**(6271): p. 397-400.
65. Huypens, P., et al., *Epigenetic germline inheritance of diet-induced obesity and insulin resistance.* Nature Genetics, 2016. **48**(5): p. 497-499.
66. Schuster, A., M.K. Skinner, and W. Yan, *Ancestral vinclozolin exposure alters the epigenetic transgenerational inheritance of sperm small noncoding RNAs.* Environmental Epigenetics, 2016. **2**(1): p. dvw001.
67. Donkin, I., et al., *Obesity and Bariatric Surgery Drive Epigenetic Variation of Spermatozoa in Humans.* Cell Metabolism, 2016. **23**(2): p. 369-378.
68. Hou, J., et al., *tRFs and tRNA Halves: Novel Cellular Defenders in Multiple Biological Processes.* Current Issues in Molecular Biology, 2022. **44**(12): p. 5949-5962.
69. Anderson, P. and P. Ivanov, *tRNA fragments in human health and disease.* FEBS Lett, 2014. **588**(23): p. 4297-304.
70. Mao, C., et al., *Transfer RNA-derived small RNAs: A class of potential biomarkers in multiple cancers (Review).* Oncology Letters, 2024. **28**(1).

71. Zhang, M., et al., *tRNA-derived fragment tRF-03357 promotes cell proliferation, migration and invasion in high-grade serous ovarian cancer.* OncoTargets and Therapy, 2019. **Volume 12**: p. 6371-6383.
72. Huang, B., et al., *tRF/miR-1280 Suppresses Stem Cell–like Cells and Metastasis in Colorectal Cancer.* Cancer Research, 2017. **77**(12): p. 3194-3206.
73. Shao, Y., et al., *tRF-Leu-CAG promotes cell proliferation and cell cycle in non-small cell lung cancer.* Chemical Biology & Drug Design, 2017. **90**(5): p. 730-738.
74. Dong, X., et al., *Comprehensively Identifying the Key tRNA-Derived Fragments and Investigating Their Function in Gastric Cancer Processes.* OncoTargets and Therapy, 2020. **Volume 13**: p. 10931-10943.
75. Veneziano, D., et al., *Dysregulation of different classes of tRNA fragments in chronic lymphocytic leukemia.* Proceedings of the National Academy of Sciences, 2019. **116**(48): p. 24252-24258.
76. Shen, Y., et al., *Clinical diagnostic values of transfer RNA-derived fragment tRF-19-3L7L73JD and its effects on the growth of gastric cancer cells.* Journal of Cancer, 2021. **12**(11): p. 3230-3238.
77. Xiong, W., et al., *Identification of tRNA-derived fragments in colon cancer by comprehensive small RNA sequencing.* Oncology Reports, 2019.
78. Oberbauer, V. and M.R. Schaefer, *tRNA-Derived Small RNAs: Biogenesis, Modification, Function and Potential Impact on Human Disease Development.* Genes (Basel), 2018. **9**(12).
79. Jia, H. and L. Zhang, *tRNA-derived small RNAs in disease immunity.* Theranostics, 2025. **15**(1): p. 245-257.
80. Katanski, C.D., et al., *tRNA abundance, modification and fragmentation in nasopharyngeal swabs as biomarkers for COVID-19 severity.* Front Cell Dev Biol, 2022. **10**: p. 999351.
81. Cappannini, A., et al., *MODOMICS: a database of RNA modifications and related information. 2023 update.* Nucleic Acids Research, 2024. **52**(D1): p. D239-D244.
82. Zhang, M. and Z. Lu, *tRNA modifications: greasing the wheels of translation and beyond.* RNA Biology, 2025. **22**(1): p. 1-25.
83. Hou, Y.M., H. Gamper, and W. Yang, *Post-transcriptional modifications to tRNA--a response to the genetic code degeneracy.* RNA, 2015. **21**(4): p. 642-4.
84. Suzuki, T., *The expanding world of tRNA modifications and their disease relevance.* Nature Reviews Molecular Cell Biology, 2021. **22**(6): p. 375-392.
85. Motorin, Y. and M. Helm, *tRNA Stabilization by Modified Nucleotides.* Biochemistry, 2010. **49**(24): p. 4934-4944.
86. Clark, W.C., et al., *tRNA base methylation identification and quantification via high-throughput sequencing.* RNA, 2016. **22**(11): p. 1771-1784.
87. Cozen, A.E., et al., *ARM-seq: AlkB-facilitated RNA methylation sequencing reveals a complex landscape of modified tRNA fragments.* Nature Methods, 2015. **12**(9): p. 879-884.
88. Ozanick, S., et al., *The bipartite structure of the tRNA m^1A58 methyltransferase from S. cerevisiae is conserved in humans.* RNA, 2005. **11**(8): p. 1281-1290.

89. Alexandrov, A., et al., *Rapid tRNA Decay Can Result from Lack of Nonessential Modifications.* Molecular Cell, 2006. **21**(1): p. 87-96.
90. Kotelawala, L., E.J. Grayhack, and E.M. Phizicky, *Identification of yeast tRNA Um_{44} 2′-O-methyltransferase (Trm44) and demonstration of a Trm44 role in sustaining levels of specific $tRNA^{Ser}$ species.* RNA, 2008. **14**(1): p. 158-169.
91. Anderson, J., et al., *The essential Gcd10p–Gcd14p nuclear complex is required for 1-methyladenosine modification and maturation of initiator methionyl-tRNA.* Genes & Development, 1998. **12**(23): p. 3650-3662.
92. Murphy, F.V., et al., *The role of modifications in codon discrimination by $tRNA^{Lys}UUU$.* Nature Structural & Molecular Biology, 2004. **11**(12): p. 1186-1191.
93. Gustilo, E.M., F.A. Vendeix, and P.F. Agris, *tRNA's modifications bring order to gene expression.* Current Opinion in Microbiology, 2008. **11**(2): p. 134-140.
94. Liang, Y., et al., *tsRNA modifications: An emerging layer of biological regulation in disease.* Journal of Advanced Research, 2024.
95. Guzzi, N., et al., *Pseudouridylation of tRNA-Derived Fragments Steers Translational Control in Stem Cells.* Cell, 2018. **173**(5): p. 1204-1216.e26.
96. Watkins, C.P., et al., *A multiplex platform for small RNA sequencing elucidates multifaceted tRNA stress response and translational regulation.* Nat Commun, 2022. **13**(1): p. 2491.
97. Zhang, W., et al., *tRNA modification dynamics from individual organisms to metaepitranscriptomics of microbiomes.* Molecular Cell, 2022. **82**(5): p. 891-906.
98. Chan, C.T.Y., et al., *A Quantitative Systems Approach Reveals Dynamic Control of tRNA Modifications during Cellular Stress.* PLoS Genetics, 2010. **6**(12): p. e1001247.
99. Liu, F., et al., *ALKBH1-Mediated tRNA Demethylation Regulates Translation.* Cell, 2016. **167**(3): p. 816-828 e16.
100. Wei, J., et al., *Differential m6A, m6Am, and m1A Demethylation Mediated by FTO in the Cell Nucleus and Cytoplasm.* Molecular Cell, 2018. **71**(6): p. 973-985.e5.
101. Müller, M., et al., *Dynamic modulation of Dnmt2-dependent tRNA methylation by the micronutrient queuine.* Nucleic Acids Research, 2015. **43**(22): p. 10952-10962.
102. Nagaraja, S., et al., *Queuine Is a Nutritional Regulator of Entamoeba histolytica Response to Oxidative Stress and a Virulence Attenuator.* mBio, 2021. **12**(2).
103. Tuorto, F., et al., *Queuosine-modified tRNAs confer nutritional control of protein translation.* The EMBO Journal, 2018. **37**(18): p. e99777.
104. Kimura, S., P.C. Dedon, and M.K. Waldor, *Comparative tRNA sequencing and RNA mass spectrometry for surveying tRNA modifications.* Nature Chemical Biology, 2020. **16**(9): p. 964-972.
105. Reichle, V.F., et al., *NAIL-MS reveals the repair of 2-methylthiocytidine by AlkB in E. coli.* Nature Communications, 2019. **10**(1).
106. Asano, K., et al., *Metabolic and chemical regulation of tRNA modification associated with taurine deficiency and human disease.* Nucleic Acids Research, 2018. **46**(4): p. 1565-1583.

107. Suzuki, T., *Taurine as a constituent of mitochondrial tRNAs: new insights into the functions of taurine and human mitochondrial diseases.* The EMBO Journal, 2002. **21**(23): p. 6581-6589.
108. Sasarman, F., et al., *The 2-thiouridylase function of the human MTU1 (TRMU) enzyme is dispensable for mitochondrial translation.* Human Molecular Genetics, 2011. **20**(23): p. 4634-4643.
109. Mandal, D., et al., *Identification and codon reading properties of 5-cyanomethyl uridine, a new modified nucleoside found in the anticodon wobble position of mutant haloarchaeal isoleucine tRNAs.* RNA, 2014. **20**(2): p. 177-188.
110. Sakai, Y., et al., *Biogenesis and growth phase-dependent alteration of 5-methoxycarbonylmethoxyuridine in tRNA anticodons.* Nucleic Acids Research, 2016. **44**(2): p. 509-523.
111. Sierant, M., et al., *Escherichia coli tRNA 2-selenouridine synthase (SelU) converts S2U-RNA to Se2U-RNA via S-geranylated-intermediate.* FEBS Letters, 2018. **592**(13): p. 2248-2258.
112. Dumelin, C.E., et al., *Discovery and biological characterization of geranylated RNA in bacteria.* Nature Chemical Biology, 2012. **8**(11): p. 913-919.
113. Jäger, G., P. Chen, and G.R. Björk, *Transfer RNA Bound to MnmH Protein Is Enriched with Geranylated tRNA – A Possible Intermediate in Its Selenation?* PLOS ONE, 2016. **11**(4): p. e0153488.
114. Ikeuchi, Y., et al., *Agmatine-conjugated cytidine in a tRNA anticodon is essential for AUA decoding in archaea.* Nature Chemical Biology, 2010. **6**(4): p. 277-282.
115. Zhao, X., et al., *Glycosylated queuosines in tRNAs optimize translational rate and post-embryonic growth.* Cell, 2023. **186**(25): p. 5517-5535.e24.
116. Salazar, J.C., et al., *A truncated aminoacyl–tRNA synthetase modifies RNA.* Proceedings of the National Academy of Sciences, 2004. **101**(20): p. 7536-7541.
117. Miyauchi, K., S. Kimura, and T. Suzuki, *A cyclic form of N6-threonylcarbamoyladenosine as a widely distributed tRNA hypermodification.* Nature Chemical Biology, 2013. **9**(2): p. 105-111.
118. Nagao, A., et al., *Hydroxylation of a conserved tRNA modification establishes non-universal genetic code in echinoderm mitochondria.* Nature Structural & Molecular Biology, 2017. **24**(9): p. 778-782.
119. Kang, B.-I., et al., *Identification of 2-methylthio cyclic N6-threonylcarbamoyladenosine (ms2ct6A) as a novel RNA modification at position 37 of tRNAs.* Nucleic Acids Research, 2017. **45**(4): p. 2124-2136.
120. Dal Magro, C., et al., *A Vastly Increased Chemical Variety of RNA Modifications Containing a Thioacetal Structure.* Angewandte Chemie International Edition, 2018. **57**(26): p. 7893-7897.
121. Krog, J.S., et al., *3-(3-amino-3-carboxypropyl)-5,6-Dihydrouridine is one of two novel post-transcriptional modifications in tRNA^{Lys}(UUU) from Trypanosoma brucei.* The FEBS Journal, 2011. **278**(24): p. 4782-4796.
122. Rose, S., et al., *The hyperthermophilic partners Nanoarchaeum and Ignicoccus stabilize their tRNA T-loops via different but structurally equivalent modifications.* Nucleic Acids Research, 2020. **48**(12): p. 6906-6918.

123. Harada, F. and S. Nishimura, *Possible anticodon sequences of tRNA^{His}, tRNA^{Asn}, and tRNA^{Asp} from Escherichia coli B. Universal presence of nucleoside O in the first position of the anticodons of these transfer ribonucleic acids.* Biochemistry, 1972. **11**(2): p. 301-308.
124. Goodman, H.M., et al., *Amber Suppression: a Nucleotide Change in the Anticodon of a Tyrosine Transfer RNA.* Nature, 1968. **217**(5133): p. 1019-1024.
125. Suzuki, T., et al., *Biogenesis and roles of tRNA queuosine modification and its glycosylated derivatives in human health and diseases.* Cell Chemical Biology, 2025. **32**(2): p. 227-238.
126. Zallot, R., Y. Yuan, and V. De Crécy-Lagard, *The Escherichia coli COG1738 Member YhhQ Is Involved in 7-Cyanodeazaguanine (preQ0) Transport.* Biomolecules, 2017. **7**(1): p. 12.
127. Zallot, R., et al., *Identification of a Novel Epoxyqueuosine Reductase Family by Comparative Genomics.* ACS Chemical Biology, 2017. **12**(3): p. 844-851.
128. Adeleye, S.A. and S.S. Yadavalli, *Queuosine biosynthetic enzyme, QueE moonlights as a cell division regulator.* PLOS Genetics, 2024. **20**(5): p. e1011287.
129. Yuan, Y., et al., *Discovery of novel bacterial queuine salvage enzymes and pathways in human pathogens.* Proceedings of the National Academy of Sciences, 2019. **116**(38): p. 19126-19135.
130. Burtnyak, L., et al., *The oncogene SLC35F2 is a high-specificity transporter for the micronutrients queuine and queuosine*. 2024, Cold Spring Harbor Laboratory.
131. Sievers, K., et al., *Structural and functional insights into human tRNA guanine transglycosylase.* RNA Biology, 2021. **18**(sup1): p. 382-396.
132. Zhang, W., et al., *Detection and quantification of glycosylated queuosine modified tRNAs by acid denaturing and APB gels.* RNA, 2020. **26**(9): p. 1291-1298.
133. Fergus, C., et al., *The human tRNA-guanine transglycosylase displays promiscuous nucleobase preference but strict tRNA specificity.* Nucleic Acids Research, 2021. **49**(9): p. 4877-4890.
134. Hung, S.-H., et al., *Structural basis of Qng1-mediated salvage of the micronutrient queuine from queuosine-5′-monophosphate as the biological substrate.* Nucleic Acids Research, 2023. **51**(2): p. 935-951.
135. Patel, B.I., et al., *Queuosine salvage in fission yeast by Qng1-mediated hydrolysis to queuine.* Biochemical and Biophysical Research Communications, 2022. **624**: p. 146-150.
136. Rashad, S., *Queuosine tRNA Modification: Connecting the Microbiome to the Translatome.* BioEssays, 2025. **47**(2).
137. Müller, M., et al., *Queuine links translational control in eukaryotes to a micronutrient from bacteria.* Nucleic Acids Research, 2019. **47**(7): p. 3711-3727.
138. Ehrenhofer-Murray, A.E., *Queuine: A Bacterial Nucleobase Shaping Translation in Eukaryotes.* Journal of Molecular Biology, 2025: p. 168985.
139. Wang, X., et al., *Queuosine modification protects cognate tRNAs against ribonuclease cleavage.* RNA, 2018. **24**(10): p. 1305-1313.
140. Rashad, S., et al., *Translational response to mitochondrial stresses is orchestrated by tRNA modifications*. 2024, Cold Spring Harbor Laboratory.

141. Reyniers, J.P., et al., *Administration of exogenous queuine is essential for the biosynthesis of the queuosine-containing transfer RNAs in the mouse.* J Biol Chem, 1981. **256**(22): p. 11591-4.
142. Farkas, W.R., *Effect of diet on the queuosine family of tRNAs of germ-free mice.* J Biol Chem, 1980. **255**(14): p. 6832-5.
143. Cirzi, C., et al., *Queuosine-tRNA promotes sex-dependent learning and memory formation by maintaining codon-biased translation elongation speed.* The EMBO Journal, 2023. **42**(19).
144. Richard, P., et al., *Queuine, a bacterial-derived hypermodified nucleobase, shows protection in in vitro models of neurodegeneration.* PLOS ONE, 2021. **16**(8): p. e0253216.
145. Hayes, P., et al., *Queuine Micronutrient Deficiency Promotes Warburg Metabolism and Reversal of the Mitochondrial ATP Synthase in Hela Cells.* Nutrients, 2020. **12**(3): p. 871.
146. Zhang, J., et al., *Disruption to tRNA Modification by Queuine Contributes to Inflammatory Bowel Disease.* Cellular and Molecular Gastroenterology and Hepatology, 2023. **15**(6): p. 1371-1389.
147. Pinkard, O., et al., *Quantitative tRNA-sequencing uncovers metazoan tissue-specific tRNA regulation.* Nature Communications, 2020. **11**(1).
148. Lin, H., et al., *CO2-sensitive tRNA modification associated with human mitochondrial disease.* Nature Communications, 2018. **9**(1).
149. Grosjean, H., V. De Crécy-Lagard, and C. Marck, *Deciphering synonymous codons in the three domains of life: Co-evolution with specific tRNA modification enzymes.* FEBS Letters, 2010. **584**(2): p. 252-264.
150. Meier, F., et al., *Queuosine modification of the wobble base in tRNA^{His} influences 'in vivo' decoding properties.* The EMBO Journal, 1985. **4**(3): p. 823-827.
151. Ostrov, N., et al., *Design, synthesis, and testing toward a 57-codon genome.* Science, 2016. **353**(6301): p. 819-822.
152. Manickam, N., et al., *Effects of tRNA modification on translational accuracy depend on intrinsic codon–anticodon strength.* Nucleic Acids Research, 2016. **44**(4): p. 1871-1881.
153. Manickam, N., et al., *Studies of translational misreading in vivo show that the ribosome very efficiently discriminates against most potential errors.* RNA, 2014. **20**(1): p. 9-15.
154. Vinayak, M. and C. Pathak, *Queuosine modification of tRNA: its divergent role in cellular machinery.* Bioscience Reports, 2010. **30**(2): p. 135-148.
155. McCarty, R.M., et al., *The deazapurine biosynthetic pathway revealed: in vitro enzymatic synthesis of PreQ(0) from guanosine 5'-triphosphate in four steps.* Biochemistry, 2009. **48**(18): p. 3847-52.
156. Hutinet, G., M.A. Swarjo, and V. De Crécy-Lagard, *Deazaguanine derivatives, examples of crosstalk between RNA and DNA modification pathways.* RNA Biology, 2017. **14**(9): p. 1175-1184.

157. Slany, R.K., et al., *A new function of S-adenosylmethionine: the ribosyl moiety of AdoMet is the precursor of the cyclopentenediol moiety of the tRNA wobble base queuine.* Biochemistry, 1993. **32**(30): p. 7811-7.
158. Chen, Y.-C., et al., *Characterization of the human tRNA-guanine transglycosylase: Confirmation of the heterodimeric subunit structure.* RNA, 2010. **16**(5): p. 958-968.
159. Siard, T.J., K.B. Jacobson, and W.R. Farkas, *Queuine metabolism and cadmium toxicity in Drosophila melanogaster.* Biofactors, 1991. **3**(1): p. 41-7.
160. Kasai, H., et al., *Distribution of the modified nucleoside Q and its derivatives in animal and plant transfer RNA's.* Nucleic Acids Research, 1975. **2**(10): p. 1931-1940.
161. Kasai, H., et al., *Letter: The structure of Q* nucleoside isolated from rabbit liver transfer ribonucleic acid.* J Am Chem Soc, 1976. **98**(16): p. 5044-6.
162. Marks, T. and W.R. Farkas, *Effects of a Diet Deficient in Tyrosine and Queuine on Germfree Mice.* Biochemical and Biophysical Research Communications, 1997. **230**(2): p. 233-237.
163. Rakovich, T., et al., *Queuosine Deficiency in Eukaryotes Compromises Tyrosine Production through Increased Tetrahydrobiopterin Oxidation.* Journal of Biological Chemistry, 2011. **286**(22): p. 19354-19363.
164. Katanski, C.D., et al., *Analysis of queuosine and 2-thio tRNA modifications by high throughput sequencing.* Nucleic Acids Research, 2022. **50**(17): p. e99-e99.
165. Frietze, L.R. and T. Pan, *Bioinformatics of simultaneous, quantitative measurements of full-length tRNA and tRNA fragments by MSR sequencing*. 2024, Elsevier.
166. Liu, J., *The human tRNA(m^2_2G26)dimethyltransferase: functional expression and characterization of a cloned hTRM1 gene.* Nucleic Acids Research, 2000. **28**(18): p. 3445-3451.
167. Zhang, K., et al., *Human TRMT1 and TRMT1L paralogs ensure the proper modification state, stability, and function of tRNAs.* Cell Reports, 2025. **44**(1): p. 115092.
168. Hwang, S.-P., et al., *TRMT1L-catalyzed m^2_2G27 on tyrosine tRNA is required for efficient mRNA translation and cell survival under oxidative stress.* Cell Reports, 2025. **44**(1): p. 115167.
169. Dewe, J.M., et al., *TRMT1-Catalyzed tRNA Modifications Are Required for Redox Homeostasis To Ensure Proper Cellular Proliferation and Oxidative Stress Survival.* Molecular and Cellular Biology, 2017. **37**(21).
170. Pathak, C., Y.K. Jaiswal, and M. Vinayak, *Queuine promotes antioxidant defence system by activating cellular antioxidant enzyme activities in cancer.* Bioscience Reports, 2008. **28**(2): p. 73-81.
171. Zaborske, J.M., et al., *A Nutrient-Driven tRNA Modification Alters Translational Fidelity and Genome-wide Protein Coding across an Animal Genus.* PLoS Biology, 2014. **12**(12): p. e1002015.
172. Kadoki, M., et al., *Organism-Level Analysis of Vaccination Reveals Networks of Protection across Tissues.* Cell, 2017. **171**(2): p. 398-413.e21.

173. Pandey, S., et al., *Pairwise Stimulations of Pathogen-Sensing Pathways Predict Immune Responses to Multi-adjuvant Combinations.* Cell Systems, 2020. **11**(5): p. 495-508.e10.
174. Takahama, M., et al., *A pairwise cytokine code explains the organism-wide response to sepsis.* Nature Immunology, 2024. **25**(2): p. 226-239.
175. Girardot, C., et al., *Je, a versatile suite to handle multiplexed NGS libraries with unique molecular identifiers.* BMC Bioinformatics, 2016. **17**(1).
176. Langmead, B., et al., *Ultrafast and memory-efficient alignment of short DNA sequences to the human genome.* Genome Biology, 2009. **10**(3): p. R25.
177. Li, H., et al., *The Sequence Alignment/Map format and SAMtools.* Bioinformatics, 2009. **25**(16): p. 2078-2079.
178. Andrews, S. *FastQC: a quality control tool for high throughput sequence data.* 2010; Available from: http://www.bioinformatics.babraham.ac.uk/projects/fastqc.
179. Chen, S., et al., *fastp: an ultra-fast all-in-one FASTQ preprocessor.* Bioinformatics, 2018. **34**(17): p. i884-i890.
180. Dobin, A., et al., *STAR: ultrafast universal RNA-seq aligner.* Bioinformatics, 2013. **29**(1): p. 15-21.
181. Li, B. and C.N. Dewey, *RSEM: accurate transcript quantification from RNA-Seq data with or without a reference genome.* BMC Bioinformatics, 2011. **12**(1): p. 323.
182. Robinson, M.D., D.J. McCarthy, and G.K. Smyth, *edgeR: a Bioconductor package for differential expression analysis of digital gene expression data.* Bioinformatics, 2010. **26**(1): p. 139-140.
183. Yu, G., et al., *clusterProfiler: an R Package for Comparing Biological Themes Among Gene Clusters.* OMICS: A Journal of Integrative Biology, 2012. **16**(5): p. 284-287.
184. Batey, R.T., *Structure and mechanism of purine-binding riboswitches.* Quarterly Reviews of Biophysics, 2012. **45**(3): p. 345-381.
185. Bessler, L., et al., *Functional integration of a semi-synthetic azido-queuosine derivative into translation and a tRNA modification circuit.* Nucleic Acids Research, 2022. **50**(18): p. 10785-10800.
186. Chen, D.W. and N.R. Garud, *Rapid evolution and strain turnover in the infant gut microbiome.* Genome Research, 2022. **32**(6): p. 1124-1136.
187. Garud, N.R., et al., *Evolutionary dynamics of bacteria in the gut microbiome within and across hosts.* PLOS Biology, 2019. **17**(1): p. e3000102.
188. Zhao, S., et al., *Adaptive Evolution within Gut Microbiomes of Healthy People.* Cell Host & Microbe, 2019. **25**(5): p. 656-667.e8.
189. Jiang, X., et al., *Invertible promoters mediate bacterial phase variation, antibiotic resistance, and host adaptation in the gut.* Science, 2019. **363**(6423): p. 181-187.
190. Sebastiani, M., et al., *Structural and Biochemical Investigation of the Heterodimeric Murine tRNA-Guanine Transglycosylase.* ACS Chemical Biology, 2022. **17**(8): p. 2229-2247.
191. Wang, Z., *Cell Cycle Progression and Synchronization: An Overview*. 2022, Springer US. p. 3-23.

192. Liu, J., et al., *Dendritic cell migration in inflammation and immunity.* Cellular & Molecular Immunology, 2021. **18**(11): p. 2461-2471.
193. Tiberio, L., et al., *Chemokine and chemotactic signals in dendritic cell migration.* Cellular & Molecular Immunology, 2018. **15**(4): p. 346-352.
194. McGettrick, A.F. and L.A.J. O'Neill, *How Metabolism Generates Signals during Innate Immunity and Inflammation.* Journal of Biological Chemistry, 2013. **288**(32): p. 22893-22898.
195. Pearce, E.J. and B. Everts, *Dendritic cell metabolism.* Nature Reviews Immunology, 2015. **15**(1): p. 18-29.
196. Gao, J., et al., *Impact of the Gut Microbiota on Intestinal Immunity Mediated by Tryptophan Metabolism.* Frontiers in Cellular and Infection Microbiology, 2018. **8**.
197. Zheng, D., T. Liwinski, and E. Elinav, *Interaction between microbiota and immunity in health and disease.* Cell Research, 2020. **30**(6): p. 492-506.
198. Wiertsema, S.P., et al., *The Interplay between the Gut Microbiome and the Immune System in the Context of Infectious Diseases throughout Life and the Role of Nutrition in Optimizing Treatment Strategies.* Nutrients, 2021. **13**(3): p. 886.
199. Kaur, B.P. and E. Secord, *Innate Immunity.* Pediatric Clinics of North America, 2019. **66**(5): p. 905-911.
200. Banchereau, J. and R.M. Steinman, *Dendritic cells and the control of immunity.* Nature, 1998. **392**(6673): p. 245-252.
201. Holling, T.M., E. Schooten, and P.J. Van Den Elsen, *Function and regulation of MHC class II molecules in T-lymphocytes: of mice and men.* Human Immunology, 2004. **65**(4): p. 282-290.
202. Lam, N., Y. Lee, and D.L. Farber, *A guide to adaptive immune memory.* Nature Reviews Immunology, 2024. **24**(11): p. 810-829.
203. Trombetta, E.S. and I. Mellman, *CELL BIOLOGY OF ANTIGEN PROCESSING IN VITRO AND IN VIVO.* Annual Review of Immunology, 2005. **23**(1): p. 975-1028.
204. Reis E Sousa, C., *Toll-like receptors and dendritic cells: for whom the bug tolls.* Seminars in Immunology, 2004. **16**(1): p. 27-34.
205. Kaisho, T. and S. Akira, *Regulation of Dendritic Cell Function Through Toll-like Receptors.* Current Molecular Medicine, 2003. **3**(4): p. 373-385.
206. Amon, L., et al., *Transcriptional control of dendritic cell development and functions*. 2019, Elsevier. p. 55-151.
207. Lelouard, H., et al., *Regulation of translation is required for dendritic cell function and survival during activation.* The Journal of Cell Biology, 2007. **179**(7): p. 1427-1439.
208. Zhang, S., et al., *Transcriptional regulation of dendritic cell development and function.* Frontiers in Immunology, 2023. **14**.
209. Deng, Y., et al., *Regulation of mRNA stability contributes to the function of innate lymphoid cells in various diseases.* Frontiers in Immunology, 2023. **14**.
210. Zhang, Y., et al., *TTP-mediated regulation of mRNA stability in immune cells contributes to adaptive immunity, immune tolerance and clinical applications.* RNA Biology, 2021. **18**(12): p. 2150-2156.

211. Kumagai, Y., et al., *Genome-wide map of RNA degradation kinetics patterns in dendritic cells after LPS stimulation facilitates identification of primary sequence and secondary structure motifs in mRNAs.* BMC Genomics, 2016. **17**(S13): p. 127-140.
212. Winkler, R., et al., *m^6A modification controls the innate immune response to infection by targeting type I interferons.* Nature Immunology, 2019. **20**(2): p. 173-182.
213. Shulman, Z. and N. Stern-Ginossar, *The RNA modification N6-methyladenosine as a novel regulator of the immune system.* Nature Immunology, 2020. **21**(5): p. 501-512.
214. Cui, L., et al., *RNA modifications: importance in immune cell biology and related diseases.* Signal Transduction and Targeted Therapy, 2022. **7**(1).
215. Bocchetti, M., et al., *LncRNAs and Immunity: Coding the Immune System with Noncoding Oligonucleotides.* International Journal of Molecular Sciences, 2021. **22**(4): p. 1741.
216. Hu, W., et al., *Long noncoding RNA-mediated anti-apoptotic activity in murine erythroid terminal differentiation.* Genes & Development, 2011. **25**(24): p. 2573-2578.
217. Wang, P., et al., *The STAT3-Binding Long Noncoding RNA lnc-DC Controls Human Dendritic Cell Differentiation.* Science, 2014. **344**(6181): p. 310-313.
218. Jöckel, S., et al., *The 2′-O-methylation status of a single guanosine controls transfer RNA–mediated Toll-like receptor 7 activation or inhibition.* Journal of Experimental Medicine, 2012. **209**(2): p. 235-241.
219. Wang, Z., et al., *The 3′ CCACCA Sequence of $tRNA^{Ala}$ (UGC) Is the Motif That Is Important in Inducing Th1-Like Immune Response, and This Motif Can Be Recognized by Toll-Like Receptor 3.* Clinical and Vaccine Immunology, 2006. **13**(7): p. 733-739.
220. Pandey, K.K., et al., *Regulatory roles of tRNA-derived RNA fragments in human pathophysiology.* Molecular Therapy - Nucleic Acids, 2021. **26**: p. 161-173.
221. Inaba, K., et al., *Generation of large numbers of dendritic cells from mouse bone marrow cultures supplemented with granulocyte/macrophage colony-stimulating factor.* The Journal of experimental medicine, 1992. **176**(6): p. 1693-1702.
222. Farhana, A. and Y.S. Khan, *Biochemistry, Lipopolysaccharide*, in *StatPearls*. 2025: Treasure Island (FL).
223. Gomaa, E.Z., *Human gut microbiota/microbiome in health and diseases: a review.* Antonie van Leeuwenhoek, 2020. **113**(12): p. 2019-2040.
224. Fan, Y. and O. Pedersen, *Gut microbiota in human metabolic health and disease.* Nature Reviews Microbiology, 2021. **19**(1): p. 55-71.
225. D'Amelio, P. and F. Sassi, *Gut Microbiota, Immune System, and Bone.* Calcified Tissue International, 2018. **102**(4): p. 415-425.
226. Madison, A. and J.K. Kiecolt-Glaser, *Stress, depression, diet, and the gut microbiota: human–bacteria interactions at the core of psychoneuroimmunology and nutrition.* Current Opinion in Behavioral Sciences, 2019. **28**: p. 105-110.

227. Zhang, P., *Influence of Foods and Nutrition on the Gut Microbiome and Implications for Intestinal Health.* International Journal of Molecular Sciences, 2022. **23**(17): p. 9588.
228. Nishida, K., et al., *Daily administration of paraprobiotic Lactobacillus gasseri CP2305 ameliorates chronic stress-associated symptoms in Japanese medical students.* Journal of Functional Foods, 2017. **36**: p. 112-121.
229. Park, C., et al., *Probiotics for the treatment of depressive symptoms: An anti-inflammatory mechanism?* Brain, Behavior, and Immunity, 2018. **73**: p. 115-124.
230. Rahman, S., *Gut microbial metabolites and its impact on human health.* Annals of Gastroenterology, 2023.
231. Qin, N., et al., *Alterations of the human gut microbiome in liver cirrhosis.* Nature, 2014. **513**(7516): p. 59-64.
232. Qin, J., et al., *A metagenome-wide association study of gut microbiota in type 2 diabetes.* Nature, 2012. **490**(7418): p. 55-60.
233. Koeth, R.A., et al., *Intestinal microbiota metabolism of l-carnitine, a nutrient in red meat, promotes atherosclerosis.* Nature Medicine, 2013. **19**(5): p. 576-585.
234. Fishbein, S.R.S., B. Mahmud, and G. Dantas, *Antibiotic perturbations to the gut microbiome.* Nature Reviews Microbiology, 2023. **21**(12): p. 772-788.
235. Iizumi, T., et al., *Gut Microbiome and Antibiotics.* Archives of Medical Research, 2017. **48**(8): p. 727-734.
236. Olguín-Alor, R., et al., *A Key Role for Inhibins in Dendritic Cell Maturation and Function.* PLOS ONE, 2016. **11**(12): p. e0167813.
237. Meng, J., et al., *Maturation of mouse bone marrow dendritic cells (BMDCs) induced by Laminaria japonica polysaccharides (LJP).* International Journal of Biological Macromolecules, 2014. **69**: p. 388-392.
238. Sun, Y., et al., *Modulation of dendritic cell function and immune response by cysteine protease inhibitor from murine nematode parasite Heligmosomoides polygyrus.* Immunology, 2013. **138**(4): p. 370-381.
239. Breaker, R.R., *Riboswitches and the RNA World.* Cold Spring Harbor Perspectives in Biology, 2012. **4**(2): p. a003566-a003566.
240. Serganov, A. and E. Nudler, *A Decade of Riboswitches.* Cell, 2013. **152**(1-2): p. 17-24.
241. Sudarsan, N., J.E. Barrick, and R.R. Breaker, *Metabolite-binding RNA domains are present in the genes of eukaryotes.* RNA, 2003. **9**(6): p. 644-647.
242. Yadav, S., D. Swati, and H. Chandrasekharan, *Thiamine Pyrophosphate Riboswitch in Some Representative Plant Species: A Bioinformatics Study.* Journal of Computational Biology, 2015. **22**(1): p. 1-9.
243. Mukherjee, S., et al., *Phylogenomic and comparative analysis of the distribution and regulatory patterns of TPP riboswitches in fungi.* Scientific Reports, 2018. **8**(1).
244. Roth, A. and R.R. Breaker, *The Structural and Functional Diversity of Metabolite-Binding Riboswitches.* Annual Review of Biochemistry, 2009. **78**(1): p. 305-334.
245. Phillip, et al., *Structural, Functional, and Taxonomic Diversity of Three PreQ1 Riboswitch Classes.* Chemistry & Biology, 2014. **21**(7): p. 880-889.

246. Roth, A., et al., *A riboswitch selective for the queuosine precursor preQ1 contains an unusually small aptamer domain.* Nature Structural & Molecular Biology, 2007. **14**(4): p. 308-317.
247. Balaratnam, S., et al., *A chemical probe based on the PreQ1 metabolite enables transcriptome-wide mapping of binding sites.* Nature Communications, 2021. **12**(1).
248. Maida, Y., et al., *An RNA-dependent RNA polymerase formed by TERT and the RMRP RNA.* Nature, 2009. **461**(7261): p. 230-235.
249. Maroteaux, L., M. Herzog, and M.-O. Soyer-Gobillard, *Molecular organization of dinoflagellate ribosomal DNA: evolutionary implications of the deduced 5.8 S rRNA secondary structure.* Biosystems, 1985. **18**(3-4): p. 307-319.
250. Dominski, Z. and W.F. Marzluff, *Formation of the 3′ end of histone mRNA.* Gene, 1999. **239**(1): p. 1-14.
251. Matera, A.G., R.M. Terns, and M.P. Terns, *Non-coding RNAs: lessons from the small nuclear and small nucleolar RNAs.* Nature Reviews Molecular Cell Biology, 2007. **8**(3): p. 209-220.
252. Kowalski, M.P. and T. Krude, *Functional roles of non-coding Y RNAs.* The International Journal of Biochemistry & Cell Biology, 2015. **66**: p. 20-29.
253. Marzluff, W.F. and K.P. Koreski, *Birth and Death of Histone mRNAs.* Trends in Genetics, 2017. **33**(10): p. 745-759.
254. Marzluff, W.F., E.J. Wagner, and R.J. Duronio, *Metabolism and regulation of canonical histone mRNAs: life without a poly(A) tail.* Nature Reviews Genetics, 2008. **9**(11): p. 843-854.
255. Marzluff, W.F., *Metazoan replication-dependent histone mRNAs: a distinct set of RNA polymerase II transcripts.* Current Opinion in Cell Biology, 2005. **17**(3): p. 274-280.
256. Singh, R., et al., *Replication-dependent histone isoforms: a new source of complexity in chromatin structure and function.* Nucleic Acids Research, 2018. **46**(17): p. 8665-8678.
257. Marzluff, W.F. and R.J. Duronio, *Histone mRNA expression: multiple levels of cell cycle regulation and important developmental consequences.* Current Opinion in Cell Biology, 2002. **14**(6): p. 692-699.
258. Huang, H.Y. and A.K. Hopper, *Multiple Layers of Stress-Induced Regulation in tRNA Biology.* Life (Basel), 2016. **6**(2).
259. Jaeger, S., et al., *Expression of metazoan replication-dependent histone genes.* Biochimie, 2005. **87**(9-10): p. 827-834.
260. Yang, X.-C., et al., *Characterization of 3′hExo, a 3′ Exonuclease Specifically Interacting with the 3′ End of Histone mRNA.* Journal of Biological Chemistry, 2006. **281**(41): p. 30447-30454.
261. Connelly, C.M., et al., *Synthetic ligands for PreQ1 riboswitches provide structural and mechanistic insights into targeting RNA tertiary structure.* Nature Communications, 2019. **10**(1).

262. Elfiky, A.A., et al., *Molecular dynamics simulations and MM-GBSA reveal novel guanosine derivatives against SARS-CoV-2 RNA dependent RNA polymerase.* RSC Advances, 2022. **12**(5): p. 2741-2750.
263. Chen, X., et al., *Structure-Guided Design, Synthesis, and Evaluation of Guanine-Derived Inhibitors of the eIF4E mRNA–Cap Interaction.* Journal of Medicinal Chemistry, 2012. **55**(8): p. 3837-3851.
264. Chen, J.L., et al., *Design, Optimization, and Study of Small Molecules That Target Tau Pre-mRNA and Affect Splicing.* Journal of the American Chemical Society, 2020. **142**(19): p. 8706-8727.
265. Livak, K.J. and T.D. Schmittgen, *Analysis of Relative Gene Expression Data Using Real-Time Quantitative PCR and the 2−ΔΔCT Method.* Methods, 2001. **25**(4): p. 402-408.
266. Belkaid, Y. and Timothy, *Role of the Microbiota in Immunity and Inflammation.* Cell, 2014. **157**(1): p. 121-141.
267. Geng, J., Z. Sun, and H. Li, *The Roles of tRNA-Derived Fragments in Cancer: Updates and Perspectives.* International Journal of Molecular Sciences, 2025. **26**(12): p. 5822.